

**New strategies for the electrochemical detection of zinc-related biomarkers in  
cancer diagnosis**

By Daniela Vieira

April, 2023



Faculty of Medicine

Department of Experimental Surgery

McGill University, Montreal, QC

A thesis submitted to McGill University in partial fulfillment of the requirements for the degree  
of Doctor of Philosophy

©Daniela Vieira 2023

## Table of contents

Abstract.....	3
Résumé.....	5
Acknowledgements.....	8
Author contributions and contributions to original knowledge.....	9
List of Figures.....	13
List of Supplementary Figures.....	16
List of Tables.....	18
List of Abbreviations.....	19
Introduction.....	22
Chapter 1. A review on the electrochemical detection of Zinc-related biomarkers observed in cancer.....	29
Chapter 2. Zincon-Modified CNTs Electrochemical Tool for Salivary and Urinary Zinc Detection.....	87
Chapter 3. Stripping metalloprotein with bismuth nanomaterials tethered on carbon surface. ....	115
Chapter 4. Detecting the PEX Like Domain of Matrix Metalloproteinase-14 (MMP-14) with Therapeutic Conjugated CNTs.....	143
Conclusions and Future Perspective.....	172

## Abstract

Biomarkers are powerful tools that can be used to detect early stages of diseases, monitor disease progression, assess treatment efficacy, and predict treatment outcomes. Defined as measurable variations in biological media, as such as tissues, cells, or biofluids, they are key indicators of abnormal bioprocess. In cancer, biomarkers have been used as predictors of stage, initiation, development, and progression; and most important, they provide an early indication of disease, allowing a better guidance of treatments. Zinc (Zn) has been highlighted as a promise biomarker due to its key role in many biological processes, including catalytic and structural functions of ~3000 proteins. Although the monitoring of Zn and Zn-related biomarkers is significant to understand the development of cancer, there is a lack of reliable, accessible, and specific diagnostic methods for their detection. Analysis of free Zn are usually accomplished via atomic absorption and mass spectrometry techniques, while Zn-containing proteins are usually monitored by ELISA. These techniques provide high sensitivity and accuracy, but they are expensive, use complex equipment and require qualified personnel. In this context, electrochemical methods are fast, portable, and accessible tools, representing an interesting way to replace these costly time-consuming methods. Combined with nanotechnology, electrochemical sensors are becoming more competitive in terms of sensitivity, allowing very low limit of detection (LOD); however, the specificity remains challenging since biofluids are complex with many interferents reducing the accuracy of the sensor. Current strategies combine the use of nanostructures with, in most of the cases, recognition bioelements, as such as enzymes, antibody and aptamers to allow a better specificity. Although these recognition bioelements allow high specificity, their short shelf-life, instability, and high cost limit their one time use and/or potential continuous monitoring in clinical applications. To overcome these limitations, we hypothesized that simple inorganic and organic

molecules could be used as recognition elements, interacting exclusively with Zn-related biomarkers while providing electrical signals. We carefully selected 3 Zn-related biomarkers: urinary and salivary mobile Zn due its abnormal behavior in a variety of cancer; carbonic anhydrase (CA), the most investigated Zn-enzyme, presents in 85% of all hypoxic tumors; and MMP-14, a Zn-protein that significant contributes to tumor angiogenesis. For each biomarker, we used low cost functionalized carbon-based nanostructures as nanocarbons offer chemical inertness, wide potential window, low background current, low cost, and versatility. In chapter 1, we well discussed the importance of zinc-related biomarkers and the current strategies applied on their detection. In chapter 2, we developed a zincon-carbon system to detect urinary and salivary mobile Zn. Carbon nanotubes (CNTs) were covalently functionalized with zincon, a metal chelator that allows electron transfer by complexing and de-complexing with Zn. The system quantified mobile Zn in salivary and urinary matrices with a sensitivity of  $100 \text{ ng.ml}^{-1}$  and a LOD of  $20 \text{ ng.ml}^{-1}$ . In chapter 3, we designed a sensor based on bismuth and mesoporous carbon through a conductive spacer arm, aiming to reach the redox center of CA. The bismuth-carbon sensor successfully tunnels Zn within the catalytic domain showing LOD of  $11 \text{ ng.ml}^{-1}$ . In chapter 4, we designed a sensor based on the detection of the hemopexin (PEX) domain of the MMP-14 with a stable and low-cost commercial molecule. This molecule, called NSC-405020, is specific of the PEX domain of MMP-14. Through the covalent grafting of the molecule on CNT, the system was able to detect and quantify MMP-14 with a linear range of detection of  $10 \text{ ng.ml}^{-1}$  to  $100 \text{ ng.ml}^{-1}$ , and LOD of  $7.5 \text{ ng.ml}^{-1}$ . Over chapters 2,3 and 4, we well demonstrated through different strategies the ability of simple molecules on the interaction with the Zn-related biomarkers, presenting very low limit and range of detection compatible with cancerous samples.

## Résumé

Les biomarqueurs sont des outils puissants qui peuvent être utilisés pour détecter les stades précoces des maladies, surveiller la progression de la maladie, évaluer l'efficacité du traitement et prédire les résultats du traitement. Définis comme des variations mesurables dans les milieux biologiques, tels que les tissus, les cellules ou les biofluides, ils sont des indicateurs clés d'un bioprocessus anormal. Dans le cancer, les biomarqueurs ont été utilisés comme prédicteurs du stade, de l'initiation, du développement et de la progression ; et surtout, ils fournissent une indication précoce de la maladie, permettant une meilleure orientation des traitements. Le zinc (Zn) a été mis en évidence comme un biomarqueur prometteur en raison de son rôle clé dans de nombreux processus biologiques, y compris les fonctions catalytiques et structurelles d'environ 3000 protéines. Bien que le suivi des biomarqueurs Zn et liés au Zn soit important pour comprendre le développement du cancer, il existe un manque de méthodes de diagnostic fiables, accessibles et spécifiques pour leur détection. L'analyse du Zn libre est généralement réalisée via des techniques d'absorption atomique et de spectrométrie de masse, tandis que les protéines contenant du Zn sont généralement contrôlées par ELISA. Ces techniques offrent une sensibilité et une précision élevées, mais elles sont coûteuses, utilisent un équipement complexe et nécessitent un personnel qualifié. Dans ce contexte, les méthodes électrochimiques sont des outils rapides, portables et accessibles, représentant une voie intéressante pour remplacer ces méthodes coûteuses et chronophages. Associés aux nanotechnologies, les capteurs électrochimiques deviennent de plus en plus compétitifs en termes de sensibilité, permettant une limite de détection (LOD) très basse ; cependant, la spécificité reste difficile car les biofluides sont complexes avec de nombreux interférents réduisant la précision du capteur. Les stratégies actuelles combinent l'utilisation de nanostructures avec, dans la plupart des cas, des bioéléments de reconnaissance, tels que des

enzymes, des anticorps et des aptamères pour permettre une meilleure spécificité. Bien que ces bioéléments de reconnaissance permettent une spécificité élevée, leur courte durée de conservation, leur instabilité et leur coût élevé limitent leur utilisation unique et/ou leur surveillance continue potentielle dans les applications cliniques. Pour surmonter ces limitations, nous avons émis l'hypothèse que de simples molécules inorganiques et organiques pourraient être utilisées comme éléments de reconnaissance, interagissant exclusivement avec des biomarqueurs liés au Zn tout en fournissant des signaux électriques. Nous avons soigneusement sélectionné 3 biomarqueurs liés au Zn : Zn mobile urinaire et salivaire en raison de son comportement anormal dans une variété de cancers ; l'anhydrase carbonique (CA), l'enzyme Zn la plus étudiée, est présente dans 85 % de toutes les tumeurs hypoxiques ; et MMP-14, une protéine Zn qui contribue de manière significative à l'angiogenèse tumorale. Pour chaque biomarqueur, nous avons utilisé des nanostructures à base de carbone fonctionnalisées à faible coût, car les nanocarbones offrent une inertie chimique, une large fenêtre de potentiel, un faible courant de fond, un faible coût et une polyvalence. Dans le chapitre 1, nous avons bien discuté de l'importance des biomarqueurs liés au zinc et des stratégies actuelles appliquées à leur détection. Dans le chapitre 2, nous avons développé un système zincon-carbone pour détecter le Zn mobile urinaire et salivaire. Des nanotubes de carbone (NTC) ont été fonctionnalisés de manière covalente avec du zincon, un chélateur métallique qui permet le transfert d'électrons par complexation et décomplexation avec Zn. Le système a quantifié le Zn mobile dans les matrices salivaires et urinaires avec une sensibilité de 100 ng.ml<sup>-1</sup> et une LOD de 20 ng.ml<sup>-1</sup>. Dans le chapitre 3, nous avons conçu un capteur à base de bismuth et de carbone mésoporeux à travers un bras espaceur conducteur, visant à atteindre le centre redox de CA. Le capteur de bismuth-carbone tunnelise avec succès le Zn dans le domaine catalytique montrant une limite de détection de 11 ng.ml<sup>-1</sup>. Dans le chapitre 4, nous avons conçu

un capteur basé sur la détection du domaine hémapexine (PEX) de la MMP-14 avec une molécule commerciale stable et peu coûteuse. Cette molécule, appelée NSC-405020, est spécifique du domaine PEX de la MMP-14. Grâce au greffage covalent de la molécule sur les NTC, le système a pu détecter et quantifier la MMP-14 avec une gamme linéaire de détection de 10 ng.ml<sup>-1</sup> à 100 ng.ml<sup>-1</sup>, et une LOD de 7,5 ng.ml<sup>-1</sup>. Au cours des chapitres 2,3 et 4, nous avons bien démontré à travers différentes stratégies la capacité de molécules simples sur l'interaction avec les biomarqueurs liés au Zn, présentant une limite très basse et une plage de détection compatible avec des échantillons cancéreux.

## **Acknowledgements**

I would like to thank my admired supervisors – Dr Geraldine Merle and Dr Edward Harvey for their valuable supervision, support, and tutelage during my PhD degree. My gratitude extends to the Faculty of Medicine and Fonds de Recherche du Québec for the funding opportunity to undertake my studies at the Department of Experimental Surgery, McGill University.

Additionally, I would like to express gratitude to Dr. Jake Barralet for his support which was really influential in shaping my critical thinking. I would like to thank Prof. Uwe Gbureck for inviting me to work at his lab in Germany. I also thank my graduator advisor Dr. Louis-Nicolas Veilleux and my internship supervisor Nektaria Markoglou for their mentorship. I would like to thank all staff at McGill University, especially Sharon Turner and Yu Ling for their lovely support.

I would like to thank my friends, lab mates, colleagues, and research team – Bill, Ben, Baptiste, Nazhat, Aslan, Andrew, Francis, Yazan, Drew, Lina, Rachel, Matthew, and Justin for a cherished time spent together. I also thank the polytechnic team, Graziela, Jerome, and Zahra, and all interns during my PhD path.

My gratitude also goes out to my family, Mãe, Pai, Bruno, Hugo e Caio for their encouragement and support all through my studies. I also thank my Canadian family, Ba, Silvio, Stella, Gu, Re, Vini, Ca, and Henrique for all support.

Finally, I would like to thank my lovely husband, Gui. It would never be possible without your support. This thesis is dedicated to you and our little one, Lucca.

## **Author contributions and contributions to original knowledge**

### **Chapter I: A review on the electrochemical detection of Zinc-related biomarkers observed in cancer**

*Daniela Vieira, Edward J Harvey, Geraldine Merle*

- Daniela Vieira: Design and implementation; Data collection and analysis; Preparation of the manuscript.
- Edward Harvey and Geraldine Merle conceived the ideas and supervised the project.

#### **Contribution to original knowledge:**

- Explored the recent developments on electrochemical sensors for the detection of zinc ions and zinc-containing proteins.
- An easy and complete guide for the strategies applied on the detection of zinc-related biomarkers.

### **Chapter II: Zincon-Modified CNTs Electrochemical Tool for Salivary and Urinary Zinc Detection**

*Daniela Vieira, Jérôme Allard, Kathleen Taylor, Edward J Harvey, Geraldine Merle*

Published in: Nanomaterials 2022, 12(24), 4431; <https://doi.org/10.3390/nano12244431>

- Daniela Vieira: Experimental design, implementation, and performance; Data collection and analysis; Preparation of the manuscript.

- Jérôme Allard: Performance of the experiment with different ions in buffer solution (reviewer suggestion)
- Kathleen Taylor: wrote part of the introduction.
- Edward Harvey and Geraldine Merle conceived the ideas and supervised the project.

**Contribution to original knowledge:**

- Explored the covalent binding of the zincon molecule and carbon nanotube structure, assuring a better stability.
- Explored a facile and selective electrochemical detection of zinc ions using a non bio recognition element in urine and saliva fluids.
- The zincon-CNT system could specifically quantify mobile  $Zn^{2+}$  in salivary and urinary fluids with a sensitivity of  $100 \text{ ng}\cdot\text{ml}^{-1}$  and a limit of detection (LOD) of  $20 \text{ ng}\cdot\text{ml}^{-1}$ .

**Chapter III: Stripping metalloprotein with bismuth nanomaterials tethered on carbon surface**

*Daniela Vieira, Edward J Harvey, Geraldine Merle*

Submitted: Applied Surface Science (*in review -Manuscript Number: APSUSC-D-23-02673*)

- Daniela Vieira: Experimental design, implementation, and performance; Data collection and analysis; Preparation of the manuscript.
- Edward Harvey and Geraldine Merle conceived the ideas and supervised the project.

**Contribution to original knowledge:**

- Explored a facile and selective electrochemical detection of carbonic anhydrase, a zinc-containing protein overexpressed in a variety of cancer, using bismuth nanoparticles deposited on sulfonated-carbon structure (S-CN-Bi) electrode.
- Explored the use of a non bio recognition element, e.g., bismuth metal, on the detection of zinc-containing proteins.
- Explored the theory of inhibitory molecules, e.g., sulfonated group, as a mechanism of electrochemical detection of metalloproteins.
- Explored the electrochemical detection of carbonic anhydrase by detecting its catalytic domain.
- The S-CN-Bi system could specifically quantify carbonic anhydrase showing limit of detection (LOD) of 11 ng.ml<sup>-1</sup>. The system was also evaluated in artificial saliva.

#### **Chapter IV: Detecting the PEX Like Domain of Matrix Metalloproteinase-14 (MMP-14) with Therapeutic Conjugated CNTs**

*Daniela Vieira, Jake Barralet, Edward J Harvey, Geraldine Merle*

Published: Biosensors 2022, 12(10), 884; <https://doi.org/10.3390/bios12100884>

- Daniela Vieira: Experimental design, implementation, and performance; Data collection and analysis; Preparation of the manuscript.
- Jake Barralet, Edward Harvey and Geraldine Merle conceived the ideas and supervised the project.

**Contribution to original knowledge:**

- Explored the covalent binding of inhibitory drug on carbon nanotube structure, assuring a better stability.
- Explored a facile and selective electrochemical detection of MMP-14, a zinc-containing protein overexpressed in a variety of cancer, using a functionalized-carbon nanotube electrode.
- Explored the theory of inhibitory molecules, e.g., NSC-405020 drug, as a mechanism of electrochemical detection of metalloproteins.
- Explored the electrochemical detection of MMP-14 by detecting its hemopexin domain.
- The inhibitory drug functionalized-CNT system could specifically quantify MMP-14 showing limit of detection (LOD) of  $7.5 \text{ ng.ml}^{-1}$ .

## List of Figures

- Figure 1.1** Expected outcomes from (A) amperometry and (B) voltammetry techniques..... 46
- Figure 1.2** - Schematic of EIS detection where the target specie interact with the electrode surface and an increase in the resistance flow is noted as an outcome ..... 47
- Figure 1.3** - Strategies to improve sensitivity and specificity of electrochemical sensors in biosensing, including (A) the use of nanostructures, (B) the use of recognition elements and (C) the combined nanostructure and recognition elements strategies..... 49
- Figure 2.1** - (A) Suggested mechanism of covalent grafting facilitated by KPS and, schematic of (B) CNT and (C) zincon-modified CNT followed by SEM images (low and high magnitude), where hexagon, gray dots, blue dots, red dots, and star represent aromatic group, oxygen element, carbon element, nitrogen element and Sulfonic acid, respectively. .... 99
- Figure 2.2** - (A) FTIR spectrum of CNT and zincon–modified CNT, where black arrows show the zincon peaks. (B) CV showing the reduction and oxidation peaks of zincon present on CNT after grafting process. The zincon–modified CNT showed good stability after (C) 10 CVs on tris–HCl (pH 7.5), scan rate 10 mV/s. The blue arrows mean the direction of the CV from + to -. .... 100
- Figure 2.3** - CVs for GCE, CNT and zincon–modified CNT in (A) 1 mM  $K_4Fe(CN)_6$  in a 0.1 M KCl and (B) tris HCl (pH 7.5) containing  $0.5\text{ mg}\cdot\text{ml}^{-1}$  of zinc. The blue arrows mean the direction of the CV from + to -. .... 101
- Figure 2.4** - Schematic of complexation mechanism of zincon–modified CNT and  $Zn^{+2}$ ; (I) adsorption, (II) reduction and (III) stripping step. The hexagon, gray dots, blue dots, red dots, and star represent aromatic group, oxygen element, carbon element, nitrogen element and sulfonic acid, respectively..... 103
- Figure 2.5** - . Study of the electrochemical detection of  $Zn^{+2}$  on 0.1 M Tris–HCl (pH 7.5) solution. (A) CV in absence and presence of  $0.5\text{ mg}\cdot\text{ml}^{-1}$  of  $Zn^{+2}$ . (B) SWV showing the increase of current after grafting of zincon on CNT in Tris–HCl solution containing concentration of  $Zn^{+2} = 1\text{ }\mu\text{g}\cdot\text{ml}^{-1}$ , and (C) SWV of zincon–modified CNT varying  $Zn^{+2}$  concentration from 0 to  $1000\text{ ng}\cdot\text{ml}^{-1}$  and its linear fit ( $n = 3$ ). .... 104
- Figure 2.6** - CV in absence and presence of  $0.5\text{ mg}\cdot\text{ml}^{-1}$  of bivalent metals in 0.1 M Tris–HCl (pH 7.5) solution. SWV showing the increase of current after grafting of zincon on CNT in Tris–HCl solution containing concentration of  $Zn^{+2}$  and other metals at a concentration of  $0.5\text{ mg}\cdot\text{ml}^{-1}$ . 106
- Figure 2.7** - Salivary and urinary zinc quantification using zincon–modified CNT electrode. CV in absence and presence of zinc and SWV varying zinc concentration from 0 to  $1000\text{ ng}\cdot\text{ml}^{-1}$  in artificial (A) urine and (B) saliva, respectively ( $n = 3$ ). .... 107
- Figure 3.1**- Schematic of particles on GCE surface and SEM pictures (low and high magnification) showing particles distribution for carbon nanoparticles (CN), sulfonated-carbon nanoparticles (S-

CN) and bismuth deposited on sulfonated-carbon nanoparticles (S-CN-Bi), respectively. .... **Erro! Indicador não definido.**

**Figure 3.2** – TEM images of (A) CN, (B) S-CN and (C) S-CN-Bi materials. The contrast and size of Bi nanoparticles was determined via STEM at low and high magnification (D). XRD patterns (E) of GCE, CN, S-CN and S-CN-Bi electrodes. Bi rhombohedral structure was identified without any impurities or oxides..... **Erro! Indicador não definido.**

**Figure 3.3** - (A) SWV response for S-CN-Bi electrodes in different concentrations of zinc solutions, from 0 ng.ml<sup>-1</sup> to 1000 ng.ml<sup>-1</sup>, using potential of deposition of zinc at -1.40V (vs SCE), for 300s and (B) linear function of zinc concentration and the current response, showing LOD of ~8.5 ng.ml<sup>-1</sup>, (n=3)..... **Erro! Indicador não definido.**

**Figure 3.4** – (A) CVs showing the ability of S-CN-Bi electrode to detect CA in 0.5 mg.ml<sup>-1</sup> CA/PBS, pH=6, scan rate 5 mV/s) and (B) current response of S-CN-Bi electrode in function of CA concentration at -1.7V (vs SCE), from 0 ng.ml<sup>-1</sup> to 500 ng.ml<sup>-1</sup>. (n=2, *p-value* < 0.05), significant difference between current response for respective concentrations. **Erro! Indicador não definido.**

**Figure 3.5** - CVs of S-CN-Bi electrode in absence and presence of CA, collagenase, and both proteins (0.5 mg.ml<sup>-1</sup> of each protein in PBS, pH=6, scan rate 5 mV/s) and (B) current response of S-CN-Bi electrode in function of CA concentration at -1.7V (vs SCE), from 0 ng.ml<sup>-1</sup> to 500 ng.ml<sup>-1</sup> when collagenase was present in the solution (n=2, *p-value* < 0.05), significant difference between current response for respective concentrations. No peak could be detected in absence of protein. Note there was no significant difference when compared to only CA, meaning the collagenase did not interfere in the CA detection. .... **Erro! Indicador não definido.**

**Figure 3.6** – (A) CVs of S-CN-Bi electrodes in artificial saliva in presence and absence of CA, from -1V to -1.7V (vs SCE) at scan rate of 5mV/s and (B) Concentration of CA in a healthy and cancerous saliva. .... **Erro! Indicador não definido.**

**Figure 4.1** - (A) Schematic representation of NSC-405020 molecule grafted onto CNTs surface followed by (B) SEM images for pristine, acylated, and inhibitor loaded CNTs (low and high magnification). ..... 154

**Figure 4.2** - (A) FTIR spectrum (top) of pristine, acylated, and inhibitor loaded CNTs, respectively. The spectrum (down) of NSC-405020 molecule is also demonstrated. (B) CVs for GCE, pristine, acylated, and inhibitor loaded CNTs in PBS (pH 7.40) containing 10 mmol.ml<sup>-1</sup> of K<sub>4</sub>[Fe (CN)<sub>6</sub>]<sup>-</sup>, 10 mmol.ml<sup>-1</sup> of K<sub>3</sub>[Fe (CN)<sub>6</sub>]<sup>-</sup> and 10 mmol.ml<sup>-1</sup> of NaCl, scan rate 10 mV/s..... 156

**Figure 4.3** - (A) Nyquist plots of inhibitor loaded CNTs before and after interaction with different concentrations of MMP-14 for 10 minutes in PBS (pH 7.40) containing 10 mmol.ml<sup>-1</sup> of K<sub>3</sub>[Fe (CN)<sub>6</sub>]<sup>-</sup> and 10 mmol.ml<sup>-1</sup> of NaCl. (B) Linear fit of EIS response for different concentrations of MMP-14, presenting LOD of 7.5 ng.ml<sup>-1</sup>. Significant difference between measurements was obtained at *p-value* < 0.05 (n = 2). Protein concentration varying from 10 ng.ml<sup>-1</sup> to 100 ng.ml<sup>-1</sup>, applied potential of +0.20 V, from 50 kHz to 500 Hz, amplitude 50 mV. .... 158

**Figure 4.4** - (A) The inhibitor/protein interaction between small molecule NSC-405020 and the binding pocket of MMP-14 and (B) Schematic of the MMP-14 detection through the binding mechanism of protein and inhibitory small molecule as the recognition element..... 163

**Figure 4.5** - EIS response for the inhibitor loaded CNT after individual interaction with 50 ng.ml<sup>-1</sup> of MMP-1 and MMP-14 in PBS (pH 7.40) containing 10 mmol.ml<sup>-1</sup> of K<sub>4</sub>[Fe (CN)<sub>6</sub>]<sup>-</sup> 10 mmol.ml<sup>-1</sup> of K<sub>3</sub>[Fe (CN)<sub>6</sub>]<sup>-</sup> and 10 mmol.ml<sup>-1</sup> of NaCl. The inhibitor loaded CNT showed specificity to MMP-14 (applied potential of +0.20 V, from 50 kHz to 500 Hz, amplitude 50 mV).  
..... 164

## List of Supplementary Figures

- Figure S 3.1** - CN and S-CN in ultrapure water. Clearly S-CN presented better dispersion of particles in water when compared with CN..... 133
- Figure S 3.2 - EDS patterns for (A) CN, (B) S-CN and (C) S-CN-Bi..... 134
- Figure S 3.3** - Cyclic voltammograms in 1 mM  $K_4Fe(CN)_6$  in a 0.1 M KCl at 10 mV/s for GCE (dashed line), (A) CN, (B) S-CN and (C) S-CN-Bi, respectively..... 135
- Figure S 3.4** - Study of different parameters to electroreduced Bi ions in 0.5  $\mu g.ml^{-1}$  of Zinc + 0.1M tris HCL. (A) The potential of deposition was varied from -0.4V to -0.6V (vs SCE), setting  $t=400s$ , and (B) the time of reduction was analysed from 300s to 600s, setting  $U= -0.6V$  (vs SCE). The best condition found to electroreduce Bi ions was -0.6V (vs SCE) for 400s. .... 135
- Figure S 3.5** – Study of different parameters to detect Zn ions in 0.5  $\mu g.ml^{-1}$  of Zinc + 0.1M tris HCL. (A) CV of S-CN-Bi electrode in 1  $mg.ml^{-1}$  Zn Acetate + 0.1M ABS (pH=4.5) aqueous solution, from -0.8V to -1.3V (vs SCE) at scan rate 10mV/s. (B) The potential of deposition was varied from -1.2V to -1.5V (vs SCE), setting  $t=300s$ , and (C) The time of reduction was analysed from 50s to 600s, setting  $U= -1.4 V$  (vs SCE). The best condition found to detect Zn ions was -1.4V (vs SCE) for 300s. .... 136
- Figure S 3.6** - Study of the best pH in PBS to detect CA..... 136
- Figure S 3.7** - Incoherent current response of CN and S-CN electrode in function of CA concentration at -1.7V (vs SCE), from 0  $ng.ml^{-1}$  to 500  $ng.ml^{-1}$ , respectively (PBS, pH 6). ..... 137
- Figure S 3.8** - Schematic of (A) CA and (B) Structural length of S-CN-Bi and C-Bi structures. .... 137
- Figure S 3.9 - Incoherent current response of S-CN-Bi electrode in function of collagenase concentration at -1.7V (vs SCE), from 0  $ng.ml^{-1}$  to 500  $ng.ml^{-1}$  (PBS, pH 6)..... 138
- Figure S 4.1** - Circuit fit for inhibitor loaded CNT electrode after interaction with 50  $ng.ml^{-1}$  of MMP-14 in PBS (pH 7.40) containing 10  $mmol.ml^{-1}$  of  $K_4[Fe(CN)_6]^-$ , 10  $mmol.ml^{-1}$  of  $K_3[Fe(CN)_6]^-$  and 10  $mmol.ml^{-1}$  of NaCl, applied potential of +0.20V, from 50kHz to 500Hz, amplitude 50 mV. .... 166
- Figure S 4.2** - Linear fit of  $\log R_{ct}$  response for different concentrations of MMP-14. Protein concentration varying from 10  $ng.ml^{-1}$  to 100  $ng.ml^{-1}$ , applied potential of +0.20V, from 50kHz to 500Hz, amplitude 50 mV ..... 166
- Figure S 4.3** - EIS response of inhibitor loaded CNT after interaction with MMP-14, varying concentration from 0 to 250  $ng.ml^{-1}$ , in PBS (pH 7.40) containing 10  $mmol.ml^{-1}$  of  $K_4[Fe(CN)_6]^-$ , 10  $mmol.ml^{-1}$  of  $K_3[Fe(CN)_6]^-$  and 10  $mmol.ml^{-1}$  of NaCl (applied potential of +0.20V, from 50kHz to 500Hz, amplitude 50 mV)..... 167

**Figure S 4.4** - (A) EIS response of acylated CNT after interaction with 50 ng.ml<sup>-1</sup> of MMP-14 and (B) EIS response in absence of protein for acylated and inhibitor loaded CNT in PBS (pH 7.40) containing 10 mmol.ml<sup>-1</sup> of K<sub>4</sub>[Fe (CN)<sub>6</sub>]<sup>-</sup>, 10 mmol.ml<sup>-1</sup> of NaCl, applied potential of +0.20V, from 50kHz to 500Hz, amplitude 50 mV..... 167

## List of Tables

<b>Table 1.1</b> Abnormal zinc levels in tissues, fluids, and secretions of cancer patients .....	33
<b>Table 1.2</b> Abnormal expression of most relevant MMPs in cancer.....	37
<b>Table 1.3</b> - Percentages of samples with mutated p53 by tumour type .....	39
<b>Table 1.4</b> - Nanocarbon-based electrodes for zinc ion sensing .....	52
<b>Table 1.5</b> - Nanometal-based electrodes for zinc ion sensing .....	62
<b>Table 1.6</b> - Recognition elements-based electrodes for zinc ion sensing.....	62
<b>Table 2.1</b> - Some examples of abnormal expression of salivary and urinary zinc for different types of cancer. ....	91
<b>Table 2.2</b> - Chemical composition of commercial artificial urine and saliva.....	94
<b>Table 2.3</b> - Comparison of reported electrochemical quantification of zinc in different body fluids. ....	109
<b>Table 4.1</b> - Abnormal expression of MMP-14 for different types of cancer and body samples	161

## List of Abbreviations

ABS	Acetate buffer
AMPA	$\alpha$ -amino-3-hydroxyl-5-methyl-4-isoxazole-propionate
ANOVA	Analysis of Variance
ASV	Anodic stripping voltammetry
ATP	Adenosine triphosphate
BDD	Boron-doped diamond
BFE	Bismuth film electrode
CH, C2H2, C2HC, C2C2	Cysteine - Histidine motifs
CA	Carbonic Anhydrase
Cys	Cysteine
CNS	Central nervous system
CNT	Carbon nanotube
COMU	1-Cyano-2-ethoxy-2-oxoethylidenaminoxy)dimethylamino-
COOH	Carboxyl group
CSV	Cathodic stripping voltammetry
CV	Cyclic voltammetry
DCT-1	Divalent cation transporter 1
DMF	Dimethylformamide
DNA	Deoxyribonucleic acid
DPV	Differential pulse voltammetry
ECM	Extra cellular matrix
EDS	Energy-dispersive X-ray spectroscopy
EDTA	Ethylenediaminetetraacetic acid
EG	Exfoliated graphite
EGFR	Epidermal growth factor receptor
EIS	Electrochemical impedance spectroscopy
ELISA	Enzyme-linked immunosorbent assay
ERGO	Reduced graphene oxide
FAAS	Flame atomic absorption spectrometry
FISH	Fluorescent in situ hybridization
FRQ	Fonds de recherche du Québec
FTIR	Fourier-transform infrared spectroscopy
GCE	Glassy carbon electrode
GFAAS	Graphite furnace atomic absorption spectrometry
GO	Graphene oxide
GOx	Glucose oxidase enzyme
GPR39	G Protein-Coupled Receptor 39
H	Hydrogen
H <sub>2</sub> O	Water
H <sub>2</sub> O <sub>2</sub>	Hydrogen peroxide
H <sub>2</sub> SO <sub>4</sub>	Sulfuric acid
HCl	Hydrochloric acid

HCO <sub>3</sub>	Bicarbonate
HEPES	N-2-hydroxyethylpiperazine-N'-2-ethanesulfonic acid
His	Histidine
HNO <sub>3</sub>	Nitric acid
HNSCC	Head and neck squamous cell carcinomas
HPLC	Liquid chromatography
HRP	Horseradish peroxidase
ICP-AES	Inductively coupled plasma atomic emission spectrometry
ICP-MS	Inductively coupled plasma mass spectrometry
IGFBP	Insulin Like Growth Factor Binding Protein 3
IIP	Ion-imprinted polymers
JCPDS	Joint Committee on Powder Diffraction Standards
KCL	Potassium chloride
KNO <sub>3</sub>	Potassium Nitrate
KPS	Potassium persulfate
LOD	Limit of detection
LSV	Linear sweep voltammetry
MMP	Matrix metalloproteinases
MS	Mass spectrometry
MT	Metallothioneins
MTF	Metal-responsive transcription factor 1
MWCNT	Multi-walled carbon nanotubes
NBC	Sodium bicarbonate cotransporter
NHE1	Sodium-hydrogen antiporter 1
NMDA	N-methyl-D-aspartate receptor
NSERC	Natural Sciences and Engineering Research Council of Canada
NTC	Nanotubes de carbone
PANI	Polyaniline
PBS	Phosphate-buffered saline
PCR	Polymerase chain reaction
PDA	Polydopamine
PEI	Polyethyleneimine
PEX	Hemopexin domain
POC	Point-of-care
PSE	Pyrene-pyridinyl disulphide
PVP	Polyvinylpyrrolidone
R <sub>CT</sub>	Resistance to charge
RNA	Ribonucleic acid
SCE	Saturated calomel electrode
SD	Standard error
SELEX	Systematic evolution of ligands by exponential enrichment
SEM	Scanning Electron Microscopy
SPAuE	Screen printed gold electrodes
SPE	Screen printed electrodes
SWCNT	Single-walled carbon nanotubes

SWV	Square Wave Voltammetry
TBS	Tris-buffered saline
TCEP	Tris(2-carboxyethyl)phosphine
TEM	Transmission electron microscopy
TFME	Thin-film mercury electrodes
TIMP	Tissue inhibitors of metalloproteinases
UV-vis	Ultraviolet-visible spectroscopy
VEGF	Vascular endothelial growth factor
XRD	X-Ray diffraction analysis
ZEB1	Zinc Finger E-Box Binding Homeobox 1
ZIP	Zrt-/Irt-like protein
ZNF	Zinc finger protein

## Introduction

In 2020, cancer affected ~230,000 people in Canada <sup>[1]</sup>, and ~20 million people in the world <sup>[2]</sup>. The biggest challenge in cancer remains its early detection, allowing a better management of the treatment and avoiding the spread of the cancerous cells to the surround tissues and organs <sup>[3-5]</sup>. For many years biopsy has been the gold standard diagnostic tool; however, despite innovations in the quality of the microscopic imagery, it is still limited in the ability to detect cancer at the earliest stage of development; and unfortunately, sometimes too late for successful intervention <sup>[4]</sup>. For most types of cancer, the earlier the detection, the greater the chances of survival <sup>[6]</sup>.

In this scenario, biomarkers, molecular alterations in normal and abnormal biological process, can be recognized and monitored <sup>[6-8]</sup>. Biomarkers can play essential roles in different steps of cancer development, including risk assessment, screening, diagnosis, therapy guidance and detection of recurrence <sup>[7,8]</sup>. Biomarkers are measurable in different biological samples, including tissues, cells, or fluids; however, serum, saliva, and urine represent the most advantageous fluids because they allow a minimally invasive and a low-cost screening <sup>[3,7,8]</sup>. Although several sophisticated technologies are in place for the identification and quantification of biomarkers, accessible and user-friendly methods of detection in a daily clinical scenario are still a challenge <sup>[6,8]</sup>.

The current investigations have emphasized the relevance of metals and metal-containing proteins as key agents in different biological process <sup>[9,10]</sup>, revealing their importance as markers for cancer monitoring. Zinc, the most expressive metal in the body, participates in many of these biological processes <sup>[10-12]</sup>. It contributes to the cells proliferation, reproduction, immune function, and defense against free radicals <sup>[12]</sup>. Abnormal levels of zinc and zinc-related biomarkers have been noticed in different types of cancer, including prostate <sup>[13-15]</sup>, liver <sup>[16-18]</sup>, breast<sup>[19-22]</sup> and head and

neck [23–25]. Zinc can be found as “free” ions or, most common, attached to transporters and/or as catalytic center of proteins [12,26].

Most of the existing detection methods applied for metal-related biomarkers require expensive machinery, high qualified personal and long process [27–29]. Among these methods, enzyme-linked immunosorbent assay (ELISA) is the most clinically applied; and recently, liquid chromatography–mass spectrometry (LC-MS) is gaining a lot of interest [30–32]. However, besides their high specificity, the mentioned limitations restrict their use as clinical diagnostic practice. Therefore, novel technologies are needed to facilitate and make metal-related biomarkers as applicable sources in cancer management.

Electrochemical methods can present as valuable candidates to invest on [30]. By measuring the electrical response in function of the target species concentrations, electrochemical detection is a fast, low-cost and a very user-friendly method [19,33]. In addition, it can be easier miniaturized, allowing a convenient tool to access the most challenging and poor areas [5,33]. Given the crucial role that zinc-related biomarkers play in cancer development, we proposed in this work a comprehensive study on the innovative strategies to successful design electrochemical systems towards the sensing of zinc-related biomarkers, facilitating the earlier detection of cancer and improving treatment guidance.

As well discussed in the chapter 1, there are many current strategies to enhance the sensitivity and specificity of electrochemical sensors. Note that sensitivity refers to the sensor response in function of the analyte concentration and it is related to the limit of detection (LOD), the lowest concentration of the target specie that can be quantified. While specificity, or selectivity, is the binding affinity between the sensor and the target specie, excluding any interfering molecules [34].

By improving both, a more qualified sensor will be available and may be applicable in the real clinical scenario.

The use of nanomaterials on the design of electrochemical sensors is the most exciting strategy recently discussed [34,35]. Nanomaterials allow a higher surface, increasing the active area of the sensors [34,36,37]. In addition, a lot of nanomaterials are easy to functionalize, biocompatible and present a very good interaction with biological components [38]. Functionalized nanostructures have been gaining great attention on biosensing. The combined design of nanostructures with bio recognition elements, as such as enzymes, peptides, aptamers, etc., allowed a great advance in the specificity and sensitivity of sensors [35,37]. However, the downside of bioelements, including high-cost, complex synthesis, instability, and short shelf-life, limit their broadly use [39,40].

In this work, the main objective covered the overcoming of bio recognition elements limitations by applying non biological components (e.g., organic, and inorganic molecules) as the recognition elements, assuring their unique interaction with the target species. We hypothesized that the non biological elements may provide accessibility, stability, longer shelf-life, storage ability, simple synthesis, and low-cost when compared to the traditional bioelements.

The objectives of this work are:

- 1) To discuss and understand the importance of zinc-related biomarkers in the development of cancers and the current strategies applied on their electrochemical detection (Chapter 1).
- 2) To design a simple and specific electrochemical system towards the “free” zinc ions detection in biofluids using a non biological recognition element (Chapter 2).

Although the literature describes a variety of electrochemical sensors with a very low limit of detection, most of the systems lack in specificity for the mobile zinc in biofluids. Because biofluids present many interferences, including other metals, the electrical current response is extremely affected. The lack of the specificity significant limits the use of electrochemical sensors in the clinical setting.

- 3) To design new strategies to increase the specificity and sensitivity of electrochemical sensors towards the detection of zinc-containing proteins using non biological recognition elements (Chapter 3 and 4).

The biggest challenge in the electrochemical detection of metalloproteins to overcome is to reach the redox center in the catalytic domain buried in the insulating protein shell. Here, two strategies were applied: i) the creation of longer and conductive nanostructures to reach the catalytic center, allowing the electron transfer between the redox center and the sensor surface (Chapter 3); and ii) the identification and detection of different domains of the proteins (Chapter 4).

## References

- [1] S. Lee, “Cancer statistics at a glance,” can be found under <https://cancer.ca/en/research/cancer-statistics/cancer-statistics-at-a-glance>, **n.d.**
- [2] “Cancer Facts & Figures 2022| American Cancer Society,” can be found under <https://www.cancer.org/research/cancer-facts-statistics/all-cancer-facts-figures/cancer-facts-figures-2022.html>, **n.d.**
- [3] X. Wang, K. E. Kaczor-Urbanowicz, D. T. Wong, *Medical Oncology* **2017**, *34*, 1.
- [4] R. S. Negm, M. Verma, S. Srivastava, *Trends in molecular medicine* **2002**, *8*, 288.
- [5] S. Campuzano, M. Pedrero, P. Yanez-Sedeno, J. M. Pingarron, *Sensors and Actuators B: Chemical* **2021**, *345*, 130349.
- [6] P. D. Wagner, M. Verma, S. Srivastava, *Annals of the New York academy of sciences* **2004**, *1022*, 9.
- [7] J. A. Ludwig, J. N. Weinstein, *Nature Reviews Cancer* **2005**, *5*, 845.
- [8] S. Kumar, A. Mohan, R. Guleria, *Biomarkers* **2006**, *11*, 385.
- [9] S. M. Yannone, S. Hartung, A. L. Menon, M. W. Adams, J. A. Tainer, *Current opinion in biotechnology* **2012**, *23*, 89.
- [10] W. Shi, M. R. Chance, *Current opinion in chemical biology* **2011**, *15*, 144.
- [11] A. S. Prasad, O. Kucuk, *Cancer and metastasis Reviews* **2002**, *21*, 291.
- [12] C. T. Chasapis, P.-S. A. Ntoupa, C. A. Spiliopoulou, M. E. Stefanidou, *Archives of toxicology* **2020**, *94*.
- [13] S. K. Ghosh, P. Kim, X. Zhang, S.-H. Yun, A. Moore, S. J. Lippard, Z. Medarova, *Cancer research* **2010**, *70*, 6119.
- [14] S.-T. Lo, A. F. Martins, V. C. Jordan, A. D. Sherry, *Israel journal of chemistry* **2017**, *57*, 854.
- [15] Y. Song, E. Ho, *Current opinion in clinical nutrition and metabolic care* **2009**, *12*, 640.
- [16] L. Sun, Y. Lin, G. Wang, L. Zhang, L. Hu, Z. Lu, *Bioscience Reports* **2021**, *41*.
- [17] M. Stepien, D. J. Hughes, S. Hybsier, C. Bamia, A. Tjønneland, K. Overvad, A. Affret, M. His, M.-C. Boutron-Ruault, V. Katzke, *British journal of cancer* **2017**, *116*, 688.
- [18] Y. Tamai, M. Iwasa, A. Eguchi, R. Shigefuku, K. Sugimoto, H. Hasegawa, Y. Takei, *PLoS One* **2020**, *15*, e0237370.

- [19] F. Cui, Z. Zhou, H. S. Zhou, *Journal of The Electrochemical Society* **2019**, *167*, 037525.
- [20] F. Lerner, S. Shousha, R. C. Coombes, *Biomarkers in Medicine* **2015**, *9*, 379.
- [21] D. Riesop, A. V. Hirner, P. Rusch, A. Bankfalvi, *Journal of cancer research and clinical oncology* **2015**, *141*, 1321.
- [22] G. An, L. Feng, L. Hou, X. Li, J. Bai, L. He, S. Gu, X. Zhao, *Gene* **2022**, *828*, 146471.
- [23] Y.-J. Jou, C.-D. Lin, C.-H. Lai, C.-H. Tang, S.-H. Huang, M.-H. Tsai, S.-Y. Chen, J.-Y. Kao, C.-W. Lin, *Clinica Chimica Acta* **2011**, *412*, 1357.
- [24] D. A. Gaykalova, R. Vatapalli, Y. Wei, H.-L. Tsai, H. Wang, C. Zhang, P. T. Hennessey, T. Guo, M. Tan, R. Li, *PloS one* **2015**, *10*, e0142148.
- [25] A. Ressnerova, M. Raudenska, M. Holubova, M. Svobodova, H. Polanska, P. Babula, M. Masarik, J. Gumulec, *Current medicinal chemistry* **2016**, *23*, 1304.
- [26] M. Murakami, T. Hirano, *Cancer science* **2008**, *99*, 1515.
- [27] B. J. Bolann, R. Rahil-Khazen, H. Henriksen, R. Isrenn, R. J. Ulvik, *Scandinavian journal of clinical and laboratory investigation* **2007**, *67*, 353.
- [28] A. C. Davis, P. Wu, X. Zhang, X. Hou, B. T. Jones, *Applied Spectroscopy Reviews* **2006**, *41*, 35.
- [29] V. A. Lemos, A. L. de Carvalho, *Environmental monitoring and assessment* **2010**, *171*, 255.
- [30] B. V. Chikkaveeraiah, A. A. Bhirde, N. Y. Morgan, H. S. Eden, X. Chen, *ACS nano* **2012**, *6*, 6546.
- [31] J. D. Wulfkuhle, L. A. Liotta, E. F. Petricoin, *Nature reviews cancer* **2003**, *3*, 267.
- [32] S. N. Topkaya, M. Azimzadeh, M. Ozsoz, *Electroanalysis* **2016**, *28*, 1402.
- [33] M. R. Hasan, M. S. Ahommed, M. Daizy, M. S. Bacchu, M. R. Ali, M. R. Al-Mamun, M. A. S. Aly, M. Z. H. Khan, S. I. Hossain, *Biosensors and Bioelectronics: X* **2021**, *8*, 100075.
- [34] K. Beaver, A. Dantanarayana, S. D. Minter, *The Journal of Physical Chemistry B* **2021**, *125*, 11820.
- [35] C. Zhu, G. Yang, H. Li, D. Du, Y. Lin, *Analytical chemistry* **2015**, *87*, 230.
- [36] N. Wongkaew, M. Simsek, C. Griesche, A. J. Baeumner, *Chemical reviews* **2018**, *119*, 120.
- [37] H. Karimi-Maleh, F. Karimi, M. Alizadeh, A. L. Sanati, *The Chemical Record* **2020**, *20*, 682.
- [38] A. de la Escosura-Muñiz, A. Merkoçi, *Expert Opinion on Medical Diagnostics* **2010**, *4*, 21.

- [39] S. Mondal, C. Subramaniam, *ACS Sustainable Chemistry & Engineering* **2019**, 7, 14569.
- [40] K. Y. Goud, S. K. Kailasa, V. Kumar, Y. F. Tsang, K. V. Gobi, K.-H. Kim, *Biosensors and Bioelectronics* **2018**, 121, 205.

**Chapter 1. A review on the electrochemical detection of Zinc-related biomarkers observed in cancer.**

This chapter includes the literature review. The bibliographic details of the coauthored paper, including all authors, are:

*Daniela Vieira*, Edward Harvey, and Geraldine Merle

My contributions to the paper involved: Design and implementation; Data collection and analysis; Preparation of the manuscript.

## A review on the electrochemical detection of Zinc-related biomarkers observed in cancer

*D. Vieira<sup>1</sup>, E. Harvey<sup>1,2</sup>, G. Merle<sup>\*1,3</sup>*

<sup>1</sup> McGill University, Faculty of Medicine, Department of Experimental Surgery

<sup>2</sup> Department of Surgery, McGill University, Montreal, Canada

<sup>3</sup> Polytechnique Montreal, Department of Chemical Engineering

*\*Corresponding author*

### **Abstract**

Zinc and zinc-containing proteins have been emphasized as relevant biomarkers because of their contribution in different physiological functions. Abnormal levels of these biomarkers lead to, or are associated with, a broad range of diseases, including cancer. Biomarkers detection offers a reliable and cost-effective strategy of monitoring risk or early detection of the development of cancer. In this scenario, electrochemical sensing methods offer great advantages because their rapid, simple, and low-cost detection when compared to the standard methods. Recent developments in electrochemical sensors have significantly improved the sensitivity in detection of low concentrations of zinc-related biomarkers present in the early stages of cancer. Moreover, the combined effect of adding nanomaterials, such as carbon, gold, and bismuth nanostructures, to sensor recognition elements offers multiple capabilities for a fast, precise, and specific quantification of these biomarkers. This review will discuss relevant zinc-related biomarkers and their role in cancer development and progression. It will also present a comprehensive analysis on the recent strategies to increase the sensitivity and specificity of zinc-related electrochemical sensors.

**Keywords:** zinc, zinc-containing proteins, electrochemical detection, nanostructures, biosensors, cancer

## 1. Introduction

Zinc (Zn) is the most abundant trace element in the body. The human body contains ~3g of Zn, where muscles, bones, and liver/skin store 60, 30, and 5% of its total, respectively <sup>[1]</sup>. It is involved in a variety of cellular process, including cell proliferation, reproduction, immune function, and defense against free radicals. Zinc acts as a structural, catalytic, and co-catalytic component of various proteins, including enzymes and transcription factors. Over 300 enzymes require zinc for functionality and over 2000 transcription factors, involved in gene expression, need zinc for integrity and binding to DNA <sup>[2-6]</sup>. Zinc is found in two forms: as zinc ion or/and associated to a protein. Free intracellular/extracellular zinc is usually regulated by Zn-transporters (ZnT, ZIP-transporters, DCT-1), Zn-bindings (metallothioneins – MTs, p53), or Zn-sensing agents (MTF-1, ZnR/GPR39, AMPA, NMDA). It is important to mention that “free” zinc ion is most of the time weakly bound to the His-rich portion of these ligands (Zn<sup>2+</sup>/H<sup>+</sup> exchanger), and rarely zinc is totally free in solution in the healthy systems. While in the protein-bound form, zinc presents structural (e.g. protein kinase C) or catalytic/co-catalytic functionality (e.g. Carbonic anhydrase, carboxypeptidase A, superoxide dismutase), held by stronger binding forces coordinated by amino acids, with His being the most frequent, followed by Glu, Asp and Cys <sup>[5,7-10]</sup>.

Given its essential role in many biological processes, including the immune system, wound repair, insulin synthesis and secretion, and even blood pressure regulation, Zn is present in organs, fluids, and secretions of the body. Further, it regulates gene expression, homeostasis, and the expression of metallothioneins. Because of its involvement in so many different functions in the body, abnormal levels of zinc and/or zinc-containing proteins lead to or are associated with a broad range of diseases, including atherosclerosis, vascular diseases, neurodegeneration, immunologic disorders, the aging process, mutagenesis, and cancer <sup>[2,6,11,12]</sup>. Zinc and zinc-containing protein

are involved in cancer initiation and progression, making them potential biomarkers for different types of cancer <sup>[11,13]</sup>. Studies report not only abnormal level of “free” zinc but also an alteration in content of zinc-containing proteins in head and neck <sup>[14,15]</sup>, breast <sup>[5,16–19]</sup>, prostate <sup>[19–25]</sup>, lung, pancreas <sup>[8,10,20,26]</sup>, and others cancer. These advances have resulted in the recognition of zinc and zinc-proteins as biomolecular targets for disease mediation <sup>[1,13]</sup>. In this review, we summarize the abnormal level of zinc and zinc-containing proteins in cancer and outline the strategies on the electrochemical sensors for zinc-related biomarkers detection thus leading to a potential parallel toolkit for cancer prevention, diagnosis, and monitoring.

## **2. Zinc expression in cancer**

Free zinc in cancer has received an escalated attention, but its role is not yet fully established. Zinc homeostasis is critical for a healthy condition and human body is not able to store it, thus homeostasis is achieved through the action of Zn-transporters/binding ligands that allow zinc uptake, distribution, and excretion <sup>[8,27]</sup>. In tumors, zinc homeostasis is unstable because of the abnormal transporter/binding ligands expression. This is directly correlated to tumor malignancy, contributing to the initiation and progression of cancer. <sup>[4,5,7,8]</sup> The inefficient maintenance of the zinc flow results in an altered level of the intracellular/extracellular zinc <sup>[5]</sup>.

Abnormal levels of zinc have been reported in tissues, fluids, and other secretions of cancer patients. For example, in healthy individuals, the zinc concentration in prostatic fluid is up to 10-fold greater than in any other soft tissue. However, the concentration of zinc in cancerous prostate tissue is ~75% lower than normal prostate. Additionally, significant changes in serum, urine, and saliva zinc levels have been observed in prostate cancer patients <sup>[4,8,20–23]</sup>. Opposite observation has been found for breast cancer patients, where there is an increase of ~70% of zinc level in

cancerous tissue when compared to healthy tissues, followed by abnormally low levels of serum, salivary and urinary zinc [5,7,8]. **Table 1.1** summarizes the zinc expression in different types of cancer.

**Table 1.1** Abnormal zinc levels in tissues, fluids, and secretions of cancer patients

Type of cancer	Zinc expression	Zn-transporter/cause associated	Ref.
<b>Prostate</b>	Reduction of the zinc level in tissue and serum. Increase of excretory zinc in urine and saliva	Lower expression of ZIP1	[19-25]
<b>Breast</b>	Increase of the zinc level in tissue. Reduction of zinc level in serum (migration of zinc into the cytosol from the serum)	Overexpression of ZIP6 (LIV-1), ZIP7 and ZIP10.	[5,16-19]
<b>Oral</b>	Increase of the zinc level in serum and in saliva.	Associated to the inflammatory process of lesions where zinc participates actively in transcription and in the enzymatic antioxidant processes.	[14,15,28]
<b>Lung</b>	Lower level of zinc in serum when compared to health group	Decreased zinc may be because of deformed protein structures (thymidylate synthetase, dihydrofolate reductase, p53, p16, K-ras)	[29,30]
<b>Pancreas</b>	Increase of zinc levels in the tissue	Overexpression of ZIP4 and ZIP3	[8,10,20,26]

It has been established that zinc holds a role in cancer growth and development, but the quantification of zinc levels in cancer remains contradictory. First, zinc levels could be affected by the microenvironment surrounding the cancerous tissue, the intake of zinc in foods and drinks, and the biological time of each individual [7,8]. Furthermore, the standard analytical techniques available to measure the total amount of extracellular zinc (i.e. atomic absorption spectrometry or inductively coupled plasma mass spectrometry) generate inaccurate and/or inconclusive responses because of the low concentration of “free” zinc in body fluids (e.g. blood plasma contains only

approximately 1  $\mu\text{g}\cdot\text{ml}^{-1}$ ) [11,12]. Therefore, additional well-designed studies using standardized samples and methodology to clarify zinc status might better define the role of zinc in cancer.

### 3. Zinc-metalloprotein expression in cancer

The following sections will summarize relevant zinc-containing proteins and their association in different cancers.

#### 3.1 Carbonic anhydrase (CA)

Cancer cells get energy through aerobic respiration of glucose or anaerobic glycolysis. Both bioprocesses generate metabolic acids ( $\text{CO}_2$ , lactate<sup>-</sup>, and  $\text{H}^+$ ). To maintain the intracellular pH, these molecules are extruded to the extra cellular environment.  $\text{CO}_2$  is removed by passive diffusion through the plasma membrane and lactate, as a charged ion, is removed via monocarboxylate transporters [31-34]. However, the removal of metabolic acids is not sufficient for efficient intracellular pH maintenance; and additional pH regulatory proteins are required, such as NHE1, ATPases, NBCs and carbonic anhydrase [33,34].

Carbonic anhydrase (CA) is an extracellular transmembrane zinc metalloenzyme acting as an efficient catalyst of reversible hydration of carbon dioxide to bicarbonate ions and protons ( $\text{CO}_2 + \text{H}_2\text{O} \leftrightarrow \text{HCO}_3 + \text{H}^+$ ) [31,32]. Curiously, CA was the first metalloenzyme identified in 1941 by Keilin and Mann [35]. Low expression of CA is found in normal tissues, but abnormal behavior is observed in hypoxic tumors, including brain, head & neck, breast, lung, bladder, cervix uteri, colon, rectum and kidney [31]. There are 12 isoforms of CA in humans where CAI and CAII (cytoplasmic) and, CAIX and CAXII (membrane-associated) are associated with cancer progression [33,34]. CAIX is the most studied because of its presence in 85% of all hypoxic tumors [31-34], but CA I and II have

demonstrated potential utility as biomarkers for colorectal, rectal, lung, and haematological cancer [36]. Through CA regulation of the intracellular environment, excessive acidification of the extracellular milieu occurs because of the presence of carbon dioxide and protons [32,34,36]. It has been established that low pH in the tumor microenvironment facilitates the growth of cancer cells and impacts negatively the normal and immune cells [32,33]. Therefore, CA helps to produce and maintain an alkaline intracellular pH favorable for tumor growth, and, contributes to the generation of an acidic extracellular environment, facilitating tumor cell invasiveness [32,33].

### *3.2 Matrix metalloproteinases (MMPs)*

Matrix metalloproteinases (MMPs) are the second most investigated metalloproteins for biomedical applications because of their role in several diseases [35]. MMPs are extracellular zinc dependent endopeptidases responsible for the degradation of extra cellular matrix (ECM) proteins, such as collagen, laminin, elastin, fibronectin, and others. [37–39]. There are 24 human MMPs and they are divided into subgroups based on their specificity (for ECM component) and structure (secreted or membrane anchored), including collagenases, gelatinases, stromelysins and matrilysins, membrane type and others [38,40]. MMPs consist of at least three domains (a) amino-terminal signal peptide, (b) pro-peptide, (c) catalytic, (d) fibronectin and (e) hemopexin domain, where pro-peptide, catalytic and hemopexin are the most common [39]. The pro-peptide domain is responsible for activation of the enzyme; the catalytic domain, which contains 2 zinc ions, is responsible for the proteolytic activity of the enzyme. The hemopexin domain interacts with substrate such as gelatin and collagen. Except for MMP-7, MMP-26 and MMP-23, all MMPs containing the hemopexin domain [37].

MMPs play essential role in cell behavior, including proliferation, adhesion, migration, differentiation, and apoptosis [39-41]. However, their functions are not limited to the cell mechanism but also MMPs act in the embryogenesis and embryo development, tissue remodeling, wound healing, inflammation, and angiogenesis [39-41]. MMPs are tightly regulated and expressed at low level in healthy conditions; however, dysregulation and overexpression of these enzymes are related to a variety of diseases including neurodegenerative, cardiovascular, arthritis, central nervous system (CNS) disorders, and cancer [37,38,40]. More specifically, MMPs overexpression has been identified and correlated with cancer development, progression, aggressivity and metastasis [42]. MMPs regulate the tumour microenvironment, and their expression and activation are significant especially in cancerous tissues versus control tissues [37,38,40,41]. The expression of MMPs is heterogenous across cancers [41]. Among MMPs, -2, -7, -9, -11 and -14 characterize the higher expression in most cancer types [41,43] (**Table 1.2**). MMPs act in different mechanism to aid development and growth of cancer by affecting growth signals, altering the availability or functionality of TGF-Beta, EGFR (MMP-2, 9 and 14), regulating the apoptosis -cleaving ligands (Fas) or receptors that transduce proapoptotic signals (MMP 7), and by improving the tumor vascularization through the angiogenic or lymphangiogenic processes and altering VEGF (MMP-2, 9 and 14) [39]. Extensive reviews of MMPs function in different types of cancer can be found in literature [39-41]. As observed in **Table 1.2**, MMPs have great potential as cancerous biomarkers in tissues and serum. The tissue MMPs quantification is usually performed through invasive and complexes techniques. Therefore, there is a need to develop minimally or non-invasive approaches to evaluate MMPs as prognostic and treatment guidance biomarkers. The detection of MMPs through biofluids, such as serum, urine and saliva would represent a great advance in this direction.

**Table 1.2** Abnormal expression of most relevant MMPs in cancer

MMPs	Mechanism	Cancer	Serum expression (ng.ml <sup>-1</sup> )		Tissue expression (ng.mg <sup>-1</sup> )		Ref.
			Healthy	Unhealthy	Healthy	Unhealthy	
<b>MMP-2</b>	Proteolytic degradation of extracellular proteins in tumor invasion, collagenolytic pathway driver for lymphatic vessel formation, tumor angiogenesis [41,43]	Breast	~594	~695	~6.7	~30.5	[44–46]
		Ovarian	~227	~280	~470	~1200	[47,48]
		Prostate	~471	~893	~2	~8.8	[49–51]
		Head & Neck	ns	ns	~3.8	~10.2	[40,52,53]
		Lung	~700	~900	~8	~12	[54,55]
<b>MMP-7</b>	Contributes to invasive potential, proliferation, anti-apoptotic, immune surveillance [41,43]	Ovarian	~3	~11	~1	~4	[47,56]
		Colon	~4	~13.5	~0	~2.5	[40,57,58]
		Brain	~1.5	~2.5	-	-	[59]
		Renal	~2.9	~6.6	*	*	[60,61]
		Head & Neck	ns	ns	-	-	[62]
<b>MMP-9</b>	Proteolytic degradation of extracellular proteins during tumor invasion [41,43]	Lung	~2	~4	*	*	[63,64]
		Breast	~270	~371	~2	~12	[45,65]
		Bladder	~417	~786	*	*	[66–68]
		Prostate	~169	~486	*	*	[50,69]
		Head & Neck	~291	~1590	~4	~11	[40,52,70]
<b>MMP-11</b>	Produced by peritumoral stromal fibroblasts; regulates early tumor invasion, implantation, and expansion; prevents apoptosis of early cancer cells [41,43]	Lung	~436	~1390	~31	~63	[55,71]
		Breast	~8	~54	~0.2	~0.6	[72,73]
		Colon	~6	~39	*	*	[74,75]
		Gastric	~6.5	~42	*	*	[76,77]
		Head & Neck	~5	~17	*	*	[78,79]
<b>MMP-14 (MT1-MMP)</b>	Cleaves other MMPs (mainly MMP2) to activate them, role in invasive blood vessel growth, and promoting metastasis. In vitro has been shown to promote invasion [41,43]	Lung	~2.5	~8	~0.01	~0.05	[80,81]
		Breast	~8.5	~17	*	*	[82,83]
		Ovarian	~6	~12	*	*	[84,85]
		Gastric	~8	~39	~1.3	~3.6	[86,87]
		Head & Neck	-	-	*	*	[88]
		Lung	-	-	*	*	[89]

“ns” – no significant difference; “\*” – MMP is overexpressed in cancerous tissue, but quantification (ng/ml) was not obtained; “-” – data not available.

Note: Some values were converted to ng/ml from relative expression.

### 3.3 Tumor suppressor p53

Although the previous proteins reviewed were found in either intra and/or extracellular environment, p53 is an intracellular nuclear transcription protein which lead to >50% of all human cancers when carry loss of function mutations in the p53 gene <sup>[90-92]</sup>. It is composed by three domains, including transactivation and proline, central DNA-binding, and oligomerization. The majority of mutations occur in the central DNA domain, inactivating the transcription factor function <sup>[93,94]</sup>. The p53 protein uses a tetrahedrally-coordinated zinc ion to stabilize its DNA recognition motifs. It binds zinc extremely tightly when folded but is unstable in the absence of zinc at body temperature <sup>[91]</sup>. The p53 protein is a critical component for the DNA repair and the inhibition of angiogenesis, however, the main role of p53 is the ability to inhibit growth of abnormal or stressed cells <sup>[90,95]</sup>. In other words, they prevent cancer formation. Because p53 is responsible for such a critical mission, it is expected that the loss of p53 function would lead to uncontrolled cell growth <sup>[91]</sup>.

Known as the most mutated gene in human cancer to date, over 3000 mutations have been identified <sup>[90-92]</sup>. Mutant p53 can appear at both the initial or late-stage and strongly accelerate the progression of cancers <sup>[91,93,96]</sup>. Mutant forms of p53 act in the transactivation of oncogenic potential genes (including the multiple drug resistance gene 1, c-myc, proliferating cell nuclear antigen, interleukin-6 (IL-6), insulin-like growth factor 1, fibroblast growth factor and epidermal growth factor receptor (EGFR)) possibly directly leading to aggressive cancers <sup>[92]</sup>. Although mutations in p53 have been identified in all types of cancers, their expression are distinct depending on the type of cancer <sup>[94,97]</sup>. Overall, solid tumors trend to present more commonly than haematological malignancies <sup>[97]</sup>. Mutant p53 gene was found in ~95% of ovarian carcinoma, while in renal carcinoma, only ~2% (**Table 1.3**) <sup>[96]</sup>. Mutated p53 gene has been observed most frequently in the

most difficult-to treat cancers such as lung, breast, ovarian and head & neck cancer [97]. Because most of mutant p53 are overexpressed in cancer cells, the detection of these proteins may aid in understanding the aggressivity and progression of cancers, and also act as a guide for the appropriate prognosis and treatment. The design of efficient strategies to target specific mutant p53 is challenging and requires a deeper understanding of its behavior, structure, and degradation pathway.

**Table 1.3** - Percentages of samples with mutated p53 by tumour type

Type of cancer	Ovarian	Lung squamous cell carcinoma	Head & Neck	Colon and Rectal	Lung adenocarcinoma	Bladder	Breast	Glioblastoma	Uterine	Leukaemia	Renal
(%)	94.6	79.3	69.8	58.6	51.8	50	32.9	28.3	27.8	7.5	2.2

Adapted from [96].

### 3.4 Zinc finger proteins (ZNFs)

Zinc finger proteins (ZNFs) is a class of protein characterized by the presence of cysteine (Cys) and histidine (His) with a structure stabilized by a zinc ion [98,101]. Approximately 3% of human genes code for C2H2 proteins, making them one of the most common protein motifs, and an important class of genomic regulator [104]. Despite the high frequency of ZNFs, their specific function is not fully understood. They have been involved in a variety of critical biological process including apoptosis, cell differentiation, cell proliferation, and chromosomal organization [1,98,99]. It is known that ZNFs are key elements in the differentiation and the development of different tissues [98,101]. Abnormal expression of ZNFs contributes to cancer development in different

aspects. ZNFs participate in all the mechanisms of cancer progression, from carcinogenesis to metastasis. ZNFs are involved in cancer because of their transcription factor function. In addition, emerging evidence indicates the importance of zinc finger proteins as structural proteins that regulate cancer cell migration and invasion <sup>[98,99]</sup>. The understanding and detection of ZNFs on the cancer environment may provide insights into one of the largest superfamilies of proteins in the human genome.

Different conformation within these elements directs delivery to several types of ZNFs containing CysCys (CC) or Cys-His (CH) motifs, such as C2H2, C2HC, C2C2, and others. <sup>[1,98–100]</sup>. Among ZNF group, the C2H2 is known as the classical and largest group with ~6000 members <sup>[101–103]</sup>. Among ZNF C2H2 type, ZEB1, ZNF750, ZNF281 and ZNF148 are a few of the examples of members involved in cancer progression <sup>[98]</sup>. ZEB1 possesses intrinsic oncogenic functions, facilitating tumour invasion and metastasis by mediating cells plasticity. Abnormal expression of ZEB1 was observed in pancreatic, lung, liver, osteosarcoma, breast, and colon cancer <sup>[98,105]</sup>; ZNF281 is a novel oncoprotein involved in the DNA damage and the epithelial-mesenchymal transition <sup>[98,106]</sup>. Its abnormal expression has been found in colorectal cancer. Abnormal expression of ZNF750 was reported in oesophagus, lung, and cervix tumors <sup>[98]</sup>. ZNF148 inhibits cell proliferation and promotes growth through stabilization of the p53 protein. It is involved in cancer growth and apoptosis, and several tumors present higher expression when compared to normal tissues, including breast, melanoma, and gastric cancer <sup>[98,107]</sup>.

### *3.5 Metallothioneins (MTs)*

Metallothioneins (MTs) are cysteine-rich proteins able to bind with metals <sup>[27,108,109]</sup>. Some authors consider MTs as a class of zinc finger proteins <sup>[101,102]</sup>. Zinc ions are the primary binding partner

of MTs, but other metals, such as lead, copper, cadmium, mercury, platinum, chromate, bismuth, and silver also possess higher affinity to the MT-binding sites <sup>[110]</sup>. There are four major isoforms of MT (MT1, 2, 3 and 4), where MT1 and MT2 are the most widely distributed in the human system <sup>[27,109,110]</sup>. MTs have different functions, principally in metal-regulatory processes, including control of zinc absorption from intestine and zinc serum levels, storage and sequestration of metal ions, metal donation to different enzymes, interaction with zinc based transcriptional factors, zinc and copper homeostasis, protection against metal toxicity, and oxidative damage <sup>[27,110]</sup>. Because MTs show broad tasks, they also play an important role in various pathological process, including neurodegeneration, cardiovascular and metabolic disorders, and cancer <sup>[110]</sup>.

MTs act in cancer development, treatment resistance, and prognosis <sup>[108,109]</sup>. Tumor cells use MTs as transporters, apoptosis inhibitors, proliferation stimulators and as immunomodulator and enzyme activators <sup>[27]</sup>. Krizkova et al. have provided a comprehensive summary of the expression and regulation of individual MTs isoforms in various types of cancer. MTs can serve as prognostic markers in tumors as they present atypical expression in serum samples. The abnormal expression of MTs has been observed in an inconsistent pattern, where MTs are upregulated in some cancers and downregulated in others <sup>[109]</sup>. In prostatic tumors, for example, healthy tissues showed significant MT staining and remained immunoreactive to MTs, while a considerable reduction of ~73% was observed for the immunostaining intensity in the malignant tissues <sup>[111]</sup>. In head and neck cancer, the opposite behavior was observed, where ~84% of cancerous tissue showed significant higher MTs expression when compared to healthy tissues <sup>[112,113]</sup>. Most of the studies have demonstrated the MTs expression in tumor tissues by immunohistochemical assay <sup>[27]</sup>. However, MTs abnormal expression has also been shown in serum samples. In testicular cancer, healthy patients presented ~0.4 mg.ml<sup>-1</sup> of MTs compared to ~0.6 mg.ml<sup>-1</sup> for unhealthy <sup>[114]</sup>. In

liver cancer, MTs expression was significant lower ( $\sim 0.5 \mu\text{M}$ ) when compared to healthy individuals ( $\sim 1 \mu\text{M}$ )<sup>[115]</sup>.

#### **4. Detection of metals and metal-containing proteins in cancerous samples**

The early detection of cancer is crucial for controlling and preventing disease progression. Although advances in standard diagnostic methodologies (e.g. ultrasound, magnetic resonance imaging, and biopsy) have been improved, they are still inefficient to reach the sensitivity and specificity needed for an early-stage diagnostic<sup>[116,117]</sup>. Most of the cases when a cancer is diagnosed, cancerous cells have already reached the majority of the tissue and metastasized throughout neighbors' tissues<sup>[118]</sup>. The earlier and accurate detection is crucial for the success of treatment, control of the toxicity and decrease of mortality<sup>[117–119]</sup>. The detection and quantification of biomarkers may offer an alternative approach to overcome the limitations of standard methods<sup>[117]</sup>. Biomarker detection offers a reliable and cost-effective strategy of monitoring risk, early detection, and development of cancer. As a consequence, the most appropriate therapy accommodating the projected disease progression, regression, and recurrence could be easily provided<sup>[119]</sup>. Given the crucial role that zinc, and zinc-containing proteins play in cancer, as mentioned before, they are of particular interest in the field of oncology as key biomarkers.

Analysis of trace elements, i.e., zinc, iron, cobalt, etc., in biological fluids and tissues are usually accomplished via atomic absorption and mass spectrometry techniques. Techniques include flame atomic absorption spectrometry (FAAS)<sup>[120,121]</sup>, graphite furnace atomic absorption spectrometry (GFAAS)<sup>[120,121]</sup>, inductively coupled plasma atomic emission spectrometry (ICP-AES)<sup>[120,121]</sup>, and inductively coupled plasma mass spectrometry (ICP-MS)<sup>[120,121]</sup>. In atomic spectrometry techniques, samples are introduced into an atomizer and converted into free atoms and/or ions. For

ICP-MS, the ion source is combined to a mass spectrometer. Mass spectrometer techniques separate and detect the ions produced by the ICP, according to their mass-to-charge ratio, and measures the analyte concentration by mass fractionation <sup>[120]</sup>. Generally, these techniques are attractive because of their sensitivity and accuracy; however, complexity, high cost, and difficult sample collection and processing limit their broad usage especially in clinical environments <sup>[120–122]</sup>. Among them, FAAS is the most frequently applied due to its relatively low cost but insufficient sensitivity restricts its use for many biological samples <sup>[122]</sup>.

The protein detection and quantification occur typically via the specific recognition of proteins in extra and/or intracellular environment, including polymerase chain reaction (PCR), immunoassays techniques, southern blotting, DNA sequencing, and fluorescent in situ hybridization (FISH) <sup>[119,123]</sup>. Current, the enzyme-linked immunosorbent assay (ELISA) represents the most reliable, sensitive and widely available protein-based testing platform for the detection and monitoring of cancer <sup>[118,119,123]</sup>. In conventional ELISA, colorimetric or fluorescent signals are applied to visualize the binding of a target protein to a specific recognition element <sup>[119]</sup>. Despite progress in the development of ELISA-based assays for protein detection, ELISA technique reveals many challenges, such as being time consuming, having a high cost, needing qualified personal and sophisticated instrumentation – all of which limit its application in point-of-care diagnostics. Further, ELISA may not be adequately sensitive for the detection of low protein concentration in the early stages of the cancer, leading to false negatives <sup>[117,119]</sup>. Recently, liquid chromatography-mass spectrometry (LC-MS) has become the major analytical technique in the field of cancerous biomarkers <sup>[116,118,124]</sup>. The combined physical separation of liquid chromatography (HPLC) with the mass analysis of mass spectrometry (MS) allows higher sensitivity and resolution, low limit and wide range of detection, reproducibility, and ability to analyze biofluids with extreme

molecular complexity <sup>[116,118,125]</sup>. Despite its advantages, LC-MS presents very high-cost, sized machinery, qualified staff, and complex sample preparation for routinary clinical applications <sup>[123,124]</sup>. Consequently, the design of alternative and innovative techniques that will allow a more feasible identification and quantification of cancerous biomarkers, including zinc and zinc-containing proteins, is a huge interest to the clinical use. Detection systems must present sensitivity and specificity, ability to convert target-receptor events into measurable signals and low interference of nonspecific biomolecules coexisting in the cancerous environment. In addition, for an accessible point-of-care use (PoC), real-time measurement, portability, user-friendly interface, and low cost are all desirable <sup>[117,119,126]</sup>. Electrochemical techniques have been addressed in a variety of diseases, including cancer, as an alternative method for the detection of biomarkers. The high sensitivity, excellent specificity, low limit of detection, simplicity, and easy miniaturization offered by electrochemical sensors, make them suitable for clinical applications and PoC platforms <sup>[127,128]</sup>.

## **5. Electrochemical detection**

Since its first development, in 1950s, electrochemical sensors have been widely applied in environmental monitoring, instrumentation, and industries, such as automobility, aircraft and telecommunication <sup>[129–131]</sup>. Most recently, it has gained attention for the measurements of biomarkers in the clinical field, including diabetes <sup>[132]</sup>, cardiac diseases <sup>[133]</sup>, bacterial infection <sup>[134]</sup>, neural disorders <sup>[135]</sup> and cancer <sup>[127,128]</sup>. The signal from an electrochemical sensor is usually the electrical response derived from oxidation-reduction reactions (redox) with the electrode surface. This response reflects the correlation between the magnitude of the signal measured and the concentration of the particular species <sup>[136]</sup>. In general, electrochemical responses are based on potential, resistance, and electrical current. Great progress on the development of electrochemical

sensors has been achieved since nanotechnology was incorporated <sup>[131]</sup>. To enhance selectivity, sensitivity, and low limit of detection; new materials, applications, methodologies, and strategies are currently applied in the electrochemical sensing of biomarkers. The monitoring of these biomarkers provides key information and is valuable for multiple purposes, including research, treatment directions, therapeutic effectiveness and as an additional diagnostic tool <sup>[137]</sup>. Below, we will briefly summarize some of the main electrochemical methods available for biosensing, including amperometry, voltammetry and impedance spectroscopy. The electrochemical design strategies and the most recent progress in the detection of zinc and zinc-containing proteins are also reviewed.

### *5.1 Amperometry and voltammetry*

The current-time response of redox reaction of an electroactive species, at a predetermined potential, is monitored in amperometry <sup>[123,131,134]</sup>. The current generated is proportional to the concentration of the electroactive species and is driven by mass transfer (transfer of species from the solution to the electrode interface) and charge transfer (electron transfer on the working electrode surface) <sup>[131,138]</sup>. Chronoamperometry (**Figure 1.1A**) is a popular type of amperometry which applies a potential step and measures the resulting current on the working electrode as a function of time <sup>[138–140]</sup>. Voltammetry, a subclass of amperometry, is a widely used technique which reveals the current response of a redox reaction of a specie in a range of potential <sup>[131,134,140]</sup>. Under different methods, such as linear sweep voltammetry (LSV), cyclic voltammetry (CV), square wave voltammetry (SWV), stripping voltammetry (ASV and CSV) and differential pulse voltammetry (DPV), the current responses in function of the species concentrations are usually observed as a peak <sup>[131,138]</sup>. In cyclic voltammetry (CV) (**Figure 1.1B**), the potential is swept in both forward and reverse directions and the current is monitored <sup>[139]</sup>. CV is the most common,

simple, and fast technique for acquiring qualitative and quantitative information on redox reactions [131]. Stripping techniques, such as anodic (ASV) and cathodic (CSV), are the most sensitive, presenting the lowest detection limit of any of the commonly used electrochemical techniques [138]. Both, ASV and CSV, possess two common steps: the concentration of the target analyte onto the working electrode, and the stripping of the species from the electrode surface by applying a determined potential [138,139] (**Figure 1.1B**). ASV is frequently applied for quantitative analysis of electroactive species such as metals ions. Very low detection limit (up to picomolar range) has been achieved with ASV technique [139].

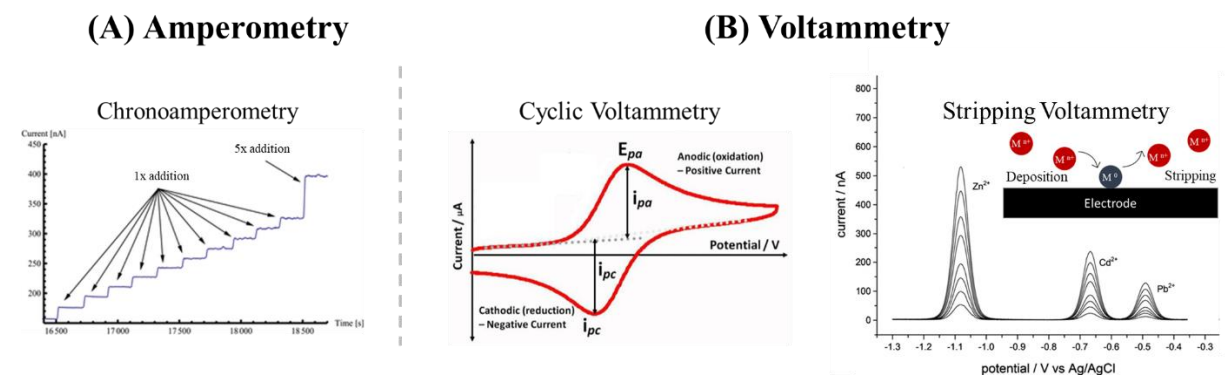


**Figure 1.1** Expected outcomes from (A) amperometry and (B) voltammetry techniques.

Amperometry and voltammetry techniques show many advantages, including a wide concentration range of detection, simplicity and low-cost, which made these techniques broadly applicable in sensor development [131]. However, in both techniques, strategies must be designed to overcome the lack of selectivity because of the signal interference from biological samples [123].

## 5.2 Electrochemical impedance spectroscopy (EIS)

Among the most important electrochemical techniques for biomolecule sensing, electrochemical impedance spectroscopy (EIS) measures the changes in charge transfer resistance ( $R_{ct}$ ) or

interfacial capacitance that occurs on the electrode surface [123,136]. The impedance spectrum is obtained through the response of an alternating current or voltage in function of the change of the frequency over a wide range [138,139]. The concentration of the target species is measured indirectly through a redox agent, such as iron ferrocyanide, which undergoes oxidation and reduction at a fixed potential applied on the surface of the electrode (**Figure 1.2**). As the target species binds to the electrode interface, the available active surface is limited, increasing the resistance to the flow of current in the electrical circuit [136,141]. EIS allows direct determination of the target specie.

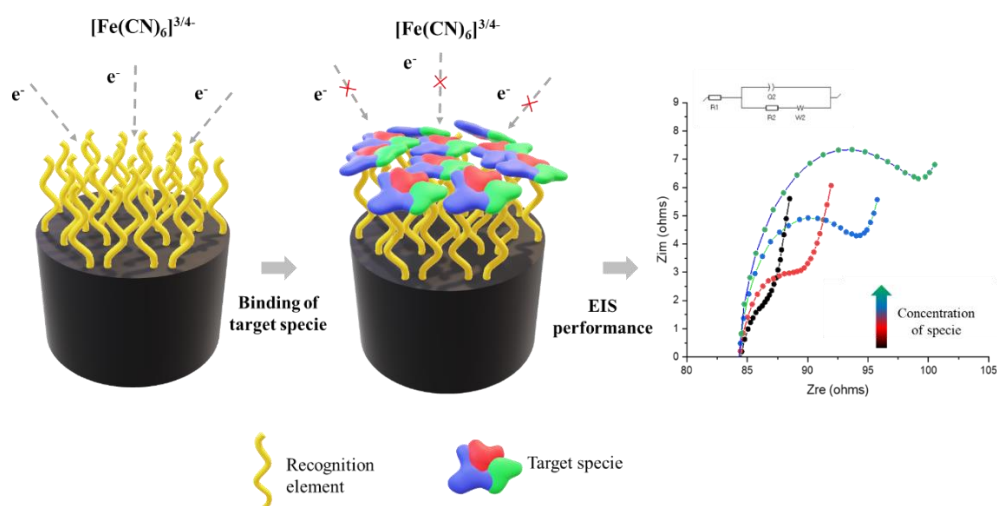


**Figure 1.2** - Schematic of EIS detection where the target specie interact with the electrode surface and an increase in the resistance flow is noted as an outcome.

Unlike amperometry and voltammetry, EIS is less destructive to the measured biological interactions because it is performed in a very limited range of small potentials [123,136]. EIS allows facile manipulation, rapid response, easy miniaturization, low-cost, high sensitivity, and ability to detect very low concentrations [136,141]. The selectivity of EIS is usually facilitated by a recognition bioelement, i.e., enzymes, DNA, peptides, and aptamers, that allows the interaction between target

specie and the electrode interface. However, the selectivity in body fluids (i.e., blood, saliva, serum) is still a challenge and it would produce false-positive “specific” binding [123,141].

### *5.3 Strategies to increase the specificity and sensitivity of electrochemical sensors.*

Given their properties, simplicity and convenience, the electrochemical sensors have been widely applied in biomedical sensing, particularly for the detection of glucose [142,143]. The current challenges of the electrochemical detection include the real-time and *in situ* measurement of biomarkers (wearable sensors, PoC) aiming to an early detection of the diseases [142]. A non-invasive approach is also emphasized in the recent development of electrochemical sensors, where biomarkers can be monitored in sweat, saliva, and urine. In this context, specificity and sensitivity emerge as key features of a sensing system [142]. Sensitivity is the efficacy of a sensor response in function of the variation in the target analyte concentration and is directly related to the limit of detection (LOD), meaning the lowest concentration of the target species that could be measured [142,143]. In the other hand, specificity (or selectivity) is achieved by the unique binding affinity of the designed electrode with a particular species in the analyte [142]. The main reason for a low sensitivity and specificity is related to the interference of substances that are absorbed on the electrode surface, impacting the signal measurement [143,144].

Few strategies have been put in place to modify the electrode surface to reduce interference with undesired species (**Figure 1.3**). Among the most common electrode modifications, the use of nanostructures and the mobilization of recognition elements on the electrode surface have gaining attention as an efficient way to achieve sensitivity and specificity [142–144]. Nanomaterials, including carbon-based and metals, are one of the most common strategies applied to modify the electrode surface. Because of their higher surface area and electrical conductivity, the active surface area is

increased and therefore, the sensitivity enhances considerably [143–145]. Furthermore, the presence of nanostructures on the electrode surface provides a biocompatible environment for biomolecules, significantly increasing the immobilised number of biomolecules on the electrode area [146]. While nanomaterials assure the sensitivity, the use of recognize elements, that present affinity to the target specie, tend to improve the selectivity. Selective molecules, including bio-elements such as enzymes and antibodies, helps to improve the specific interactions, reducing false-positive results [144,145].

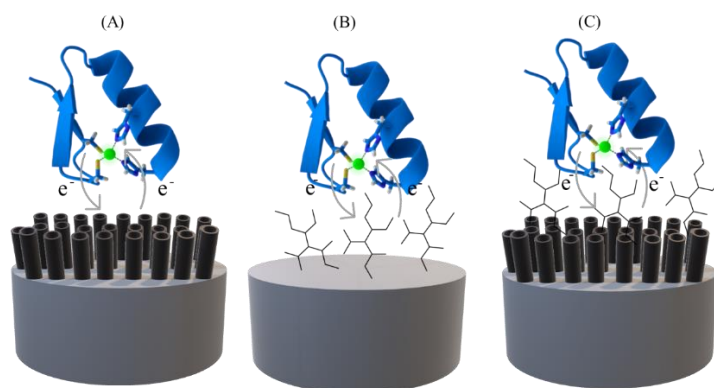


**Figure 1.3** - Strategies to improve sensitivity and specificity of electrochemical sensors in biosensing, including (A) the use of nanostructures, (B) the use of recognition elements and (C) the combined nanostructure and recognition elements strategies.

By modifying the electrodes surfaces, the catalytic activity is improved, accelerating the electron transfer while lowering the activation barrier of the electrochemical reaction, leading to an intensification of the signal and the sensitivity of the sensor [142,143]. In this review, we explore the use of nanocarbon, metal nanostructures, and recognition elements as crucial mechanisms to maximize the analytical performance of electrochemical sensors on the detection of zinc and zinc-containing proteins.

### *5.3.1 Nanocarbon-based strategies*

Carbon materials are widely applied in electrochemical sensors because of their chemical inertness, wide potential window, low background current, low cost, and versatility for different analysis [143,147,148]. Carbon nanomaterials not only possess exceptional electrochemical properties but also a large surface-to-volume ratio, high conductivity, and biocompatibility. In addition, carbon nanomaterials have enhanced interfacial adsorption properties, better electrocatalytic activity, and fast electron transfer kinetics compared to many traditional electrochemical sensor materials [147,148].

Among the carbon-based nanomaterials, graphene, carbon nanotubes (CNT), and carbon nanoparticles are the most applied in biosensing [147]. Graphene, the 2D-carbon structure, is an abundant and low-cost source material [148]. The sp<sup>3</sup> hybridized carbons on the edge plane and the defects on the basal plane can be oxidized to provide functional groups and further enhance the electron transfer with biological molecules [143,148,149]. CNTs are rolled sheets of graphene in a cylindrical structure [148]. There are two varieties of CNTs, including single-walled (SWCNT) and multi-walled (MWCNT) carbon nanotubes [150,151]. CNTs are usually acidic treated to remove the end caps, which also creates defect sites and oxygen functional groups that are thought to aid in adsorption and electron transfer [143,148]. Besides oxidized carbon nanomaterials result in lower electrical conductivity, the defects are very beneficial when applying these materials in electrochemical sensors [143]. In addition, the oxygen-containing groups can serve as anchoring sites for functionalization with a wide variety of recognition molecules, improving the specificity of the sensors [143].

Carbon-based electrodes have emerged as an alternative to the toxic mercury electrodes on the detection of zinc ions <sup>[149]</sup>. Further, the nanostructure of carbon allowed the miniaturization of sensors, making them more portable for easy analysis. Several researchers explore the use of carbon nanostructures for the detection of zinc in environmental or in biological fluids (**Table 1.4**). Kudr et al. <sup>[149]</sup> electrodeposited graphene oxide (GO) on glassy carbon electrodes (GCE) using a fixed +1V potential *vs* Ag/AgCl/KCl electrode and, subsequently, the GO was subjected to electrochemical reduction to generate reduced graphene oxide (ERGO) using cyclic voltammetry. By stripping voltammetry, the zinc ions were deposited on the electrode surface and afterwards measured by differential pulse voltammetry (DPV). Besides the low LOD of 5 ng.ml<sup>-1</sup>, graphene alone does not offer a great specificity and the system was not tested against relevant samples.

A wearable sensor was developed to detect the zinc concentration in sweat using a disposable and flexible graphite electrode <sup>[152]</sup>. The sensor was fabricated by applying solid-solid deposition of graphite powder on polyester films using a press machine, an oven, and a torque wrench. The environmentally friendly system presented LOD of 4.31 ng.ml<sup>-1</sup> and linear range of detection of 50 to 2000 ng.ml<sup>-1</sup>. Guo et al. <sup>[153]</sup> placed organized CNTs to allow a better exposition of the edges, aiming to increase the performance of the detection of zinc ions. By anodic stripping voltammetry (ASV), the highly aligned multi-wall carbon nanotube (MWCNTs) tower electrodes were tested in an acetate buffer solution containing zinc ions and other heavy metals. The system presented LOD of ~12 ng.ml<sup>-1</sup>, however, the lack of specificity was still present. Aiming to enhance the specificity of carbon-based electrodes, researchers have modified and functionalized carbon material with elements that are able to interact exclusively with zinc ions. A common approach to the detection of zinc ions is the use of auxiliary bismuth to increase the sensitivity and to facilitate the nucleation during zinc ion deposition <sup>[154]</sup>. We will further explore the functionalized-carbon

nanostructures in the sections 5.3.2 *Nanometal-based strategies* and 5.3.3 *Recognition elements-based strategies*.

Another strategy applied to enhance specificity of carbon-based electrodes is the use of ion-imprinted polymers (IIP), where binding sites are designed to match the charge, size, and coordination number of the target ion <sup>[155]</sup>. IIP was synthesized using 8-hydroxyquinoline and styrene and casted on a glassy carbon electrode (GCE) utilizing Nafion <sup>[155]</sup>. By ASV, the system showed LOD of 0.06 ng.ml<sup>-1</sup> and a range of detection of 0.06 to 0.12 ng.ml<sup>-1</sup> in HCl solution. Besides very low LOD, the system did not present a wide range of detection, limiting its application in different cancerous fluids.

**Table 1.4** - Nanocarbon-based electrodes for zinc ion sensing

Electrode	Solution	LOD (ng.ml <sup>-1</sup> )	Linear Range (ng.ml <sup>-1</sup> )	Method	Limitations	Ref.
Reduced graphene oxide (ERGO) on GCE	Acetate buffer (pH 5)	5	50 – 3125	DPV	Low specificity	[149]
Graphite on polyester films	Sweat	4.31	50 to 2000	ASV	Low specificity	[152]
Highly aligned MWCNTs tower	Acetate buffer (pH 4.4)	12	Not informed	ASV	Low specificity	[153]
GCE-IIP	1 mM HCl (pH 3)	0.06	0.06 to 0.12	ASV	Low range of detection	[155]

Nanocarbon-based electrodes have also been widely employed for the detection of metal-containing proteins. Nanocarbon structures, such as CNTs and graphene, have been suitable platforms for transducing biorecognition events into valuable electroanalytical signals <sup>[156]</sup>. One of the greatest challenges for the detection of metal-containing proteins is the establishment of satisfactory electrical interaction between the active site of the protein and the electrode surface.

The redox center of most metal-containing proteins is electrically insulated by the protein shell, hampering the oxidation or reduction reactions of an electrode at any potential <sup>[156–158]</sup>. The direct electron-transfer between proteins and electrode surfaces could be advanced by auxiliary mediators (e.g. recognition elements) that allow efficient transduction of the biorecognition event and nanostructures that decrease the electrode and the redox center distance <sup>[157]</sup>. Nanocarbon-based electrodes have been highly valued as suitable substrates for anchoring proteins without the loss of the bioactivity and also for allowing a more direct electron transfer with the protein electroactive center <sup>[156,158,159]</sup>.

Gupta et al.<sup>[158]</sup> analyzed the electron transfer ability of a variety of nanostructured graphene, including monolayer graphene, graphene oxide (GO) and reduced GO, towards iron-containing proteins. The study demonstrated the efficient direct electron transfer between the graphene nanostructures and all redox centers of the proteins applied, without the requirement of any mediators. Note that proteins retained their structural integrity and biological activity after interaction with graphene nanostructures. Additionally, the presence of edge defects, functional and residual oxygen functional groups supported the interaction of proteins with all nanostructures studied.

Besides the lack of specificity, it is interesting how carbon nanostructures demonstrate the ability to transfer electrons with the buried redox center of proteins. As an efficient substrate to be functionalized with recognition elements, carbon nanostructures demonstrate their promising application for the development of point-of-care sensors towards the detection of metal-containing proteins. We will explore the functionalized nanocarbon structures towards the detection of zinc-containing proteins in the section *5.3.3 Recognition elements-based strategies*.

### 5.3.2 Nanometal-based strategies

The advantages of metallic nanoparticles caused them to be a desired strategy for the detection of metals and metal-containing proteins. Not only by increasing the surface area but also increasing the mass-transport rate and allowing a faster electron transfer; nanometals have been widely explored to assure sensitivity <sup>[160,161]</sup>. Among the metals, silver (Ag) and gold (Au) are the most explored for the detection of different heavy metals <sup>[160,161]</sup>, including cadmium (Cd), chromium (Cr), copper (Cu), lead (Pb), zinc (Zn), etc.

In addition, gold nanoparticles (AuNPs) are the most popular nanometal applied as substrates for metal-containing protein detection <sup>[162,163]</sup>. Similar to carbon nanostructures, AuNPs provide stable immobilization of biomolecules while retaining their bioactivity and allowing direct electron transfer with the redox center of proteins with no need for mediators <sup>[164,165]</sup>. AuNPs are one of the most appropriate metallic nanomaterials to be functionalized and applied as biosensor substrates. We will explore the functionalized-AuNPs toward the detection of zinc-containing proteins in the section *5.3.3 Recognition elements-based strategies*.

Particularly, for zinc ion detection the use of mercury (Hg) and bismuth (Bi) metal electrodes have been extensively investigated in environmental and biological samples. Because of its low toxicity and similar electrochemical performance when compared to mercury, bismuth is positioned as the major metallic material applied on the electrochemical detection of zinc <sup>[161,166]</sup>. Recently, metal oxides have also gained attention for the detection of zinc because of their low cost, decreased toxicity and, occasionally, needed biodegradability <sup>[167–169]</sup>. However, metal oxides are usually not the main metal in the electron transfer mechanism and require to be combined to a second material to achieve enhanced electrochemical performance <sup>[170]</sup>. In this section we will briefly present a few

strategies used to detect zinc ions by applying Au and Hg electrodes. We will explore the Bi approach because of its importance on the detection of zinc (**Table 1.5**).

Gold nanostructures have been shown to improve the sensitivity of the electrochemical electrodes, improving the limit of detection <sup>[161]</sup>. Several works describe the successful use of gold nanoparticles-modified electrodes on the detection of zinc. Shao et al developed a polyaniline-multi-walled carbon nanotubes (PANI-MWCNTs) screen printed electrode coated with electrodeposited gold nanoparticles (AuNPs) <sup>[171]</sup>. The deposited layer of AuNPs improved the conductivity and active surface area when compared to PANI-MWCNTs alone. By anodic stripping voltammetry (ASV), the system showed linear range of detection of 1-180 ng.ml<sup>-1</sup> and LOD of 39 pg.ml<sup>-1</sup> in ABS (pH 5). The system was tested in real water samples, showing consistent results when compared to the standard ICP-MS technique.

A flexible electrochemical system was developed on Au-electrode modified with titanium carbide and multiwalled carbon nanotubes for the detection of zinc in urine and sweat <sup>[172]</sup>. Applying antimony (Sb) as an auxiliary co-deposition element, the system showed range of detection of 350 – 830 ng.ml<sup>-1</sup> and LOD of 1.5 ng.ml<sup>-1</sup> in acetate buffer solution (pH 4.6). When applied in biofluids, urine and sweat, the system showed current response with zinc concentration varying from 200-600 ng.ml<sup>-1</sup> and 50-1500 ng.ml<sup>-1</sup>, respectively. Although gold-based electrodes offer higher conductivity and active surface area, the elevated cost and lower specificity limit their application as a specific tool in the clinical applications.

Despite higher toxicity of mercury (Hg), some studies are still applying Hg as a component to detect zinc. The interest for Hg-based sensors is due to their unique physico-chemical properties and the wide cathodic potential window <sup>[149]</sup> that are extremely relevant for the detection of zinc

as it occurs in a more negative deposition potential <sup>[166]</sup>. To overcome the high toxicity, *in situ* and *ex-situ* thin-film mercury electrodes (TFME) have been explored, aiming to decrease the Hg concentration and enabling a better electrode manipulation <sup>[149,173]</sup>. *In situ* method consists in the simultaneously deposition of Hg and the target metal, like the bismuth strategy cited earlier. This method facilitates the specificity of the electrode; however, co-deposition techniques are not widely applicable in clinical scenarios, and the toxicity of Hg eliminates this method. Ensafi et al <sup>[174]</sup> developed an *in situ* TFME on carbon paste electrode in order to detect zinc in different real water samples (lake, tap and spring waters). Using ASV, the system showed range of detection of 8-220 ng.ml<sup>-1</sup> and LOD of 5.5 ng.ml<sup>-1</sup> in 0.10 M KNO<sub>3</sub>/50 M HCl solution. The carbon-TFME system showed good agreement between the known quantities of zinc presented in and added to the samples and the quantities measured, confirming the accuracy of the method.

*Ex-situ* TFME is mainly represented by the Hg nano/microdroplets on the electrode surface <sup>[173,175]</sup>. Typically, the nano/microfilm is formed by the electrochemical reduction of the absorbed Hg<sup>+2</sup> on the working electrode surface before electrode immersion in the analyte containing zinc <sup>[175]</sup>. Oliveira et al <sup>[173]</sup> designed a biochar Hg nanodroplet electrode. Biochar is a highly functionalized alternative carbon material originally from biomass and charcoal that allows a facile adsorption of ionic species such as Hg<sup>+2</sup>. After preparing the biochar carbon paste, the Hg<sup>+2</sup> was electrodeposited for 2 minutes in acetate buffer solution (pH 6) containing 1.0 × 10<sup>-4</sup> M of Hg<sup>+2</sup>. By applying ASV in acetate buffer containing different amounts of zinc, the system showed range of detection of 20-3260 ng.ml<sup>-1</sup> and LOD of 11 ng.ml<sup>-1</sup>. The biochar-Hg electrode was evaluated using collyrium and ointment samples showing similar results when compared to ICP method.

As mentioned, Hg electrodes shows remarkable sensitivity for the detection of metals (including zinc) by stripping techniques; however, the Hg high toxicity unable further applications specially in

environmental and clinical samples [166]. Currently, the only alternative to Hg for stripping technique is the Bismuth-modified electrode [176]. Bismuth (Bi) offers several advantages, including reproducible voltametric response, distinct stripping peak, more negative potential window, and high signal-to-background ratio [177]. Bi is mainly applied as films on electrodes materials, but nanostructured Bi can also be implemented. Bismuth-based electrodes are environmentally friendly, present comparable electrochemical behavior to TFMEs and have been shown better specificity between intermetallic compounds [161,166]. Bismuth-based electrodes can be prepared by *in situ* and *ex situ* techniques. Jothimuthu et al [166] designed a miniaturized lab-on-a-chip sensor for measurement of zinc in serum samples. The sensor was fabricated using a combination of *ex situ* deposited bismuth film (BFE) on gold substrate by electroreduction of  $\text{Bi}^{3+}$  from an acetate buffer solution containing  $500 \text{ mg.L}^{-1}$  of bismuth at  $-800 \text{ mV}$  for 240 s. By ASV, the system showed range of detection of  $0.9\text{-}9 \text{ }\mu\text{g.ml}^{-1}$  in acetate buffer (pH 6) and LOD of  $1.1 \text{ }\mu\text{g.ml}^{-1}$ . Although the sensor demonstrated measurement of zinc in serum (typical concentration of  $1.8\text{-}9 \text{ }\mu\text{g. ml}^{-1}$ ), the sensitivity of detection demonstrated was lower for a clinical application.

The same research group optimized the fabrication steps of the lab-on-a-chip gold-BFE by applying a pre plasma treatment and a direct placement of evaporated Bi on gold substrate [178]. Besides its complex synthesis, the system performance was improved with a range of detection of  $180\text{-}4500 \text{ ng.ml}^{-1}$  and LOD of  $11 \text{ ng.ml}^{-1}$ . Li et al prepared an *ex situ* Bi-gold electrode by plating bismuth on screen printed gold electrodes (SPAuE) at  $0.08\text{V}$  for 120s [179]. The efficacy of the designed Bi-SPAuE was compared to the *in situ* simultaneous co-deposition of Bi and Zn ion on the SPAuE. By ASV, both electrodes were evaluated in acetate buffer (pH 5.5) containing  $50 \text{ ng.ml}^{-1}$  of zinc. Insignificant current response was observed for zinc with the *in-situ* Bi-SPAuE. However, the *ex-situ* Bi-SPAuE showed significantly higher current response with well-defined voltametric

peak. The *ex-situ* Bi-SPAuE showed range of detection of 1-120 ng.ml<sup>-1</sup> and LOD of 0.05 ng.ml<sup>-1</sup>. The author attributed the great sensitivity of Bi-SPAuE to the compact growth of smaller bismuth particles and its uniform and flat surface. The system was evaluated in real water samples and demonstrated coherent results.

*Ex situ* and *in situ* Bi were also placed on carbon substrates. By taking advantage of the bismuth's ability to form low-temperature alloys with heavy metals, Thanh et al simultaneously deposited *in-situ* bismuth and the targeted heavy metals, including zinc, directly on glassy carbon (GCE) substrate [180]. The detection was measured by stripping voltammetry in 0.1M acetate buffer (pH 4.5). After 120s of deposition at -1.4V the zinc metal was stripped from the electrode and its concentration was determined in function of the current response. The system showed a range of detection of 5 to 110 ng.ml<sup>-1</sup> and LOD of 1.02 when only zinc is present and LOD of 2.95 ng.ml<sup>-1</sup> when different metals are present in the solution. The system was also tested in river water samples and showed similar response.

Graphene–polyaniline (G-PANI) nanocomposite electrode was prepared by reverse-phase polymerization in the presence of polyvinylpyrrolidone (PVP) [154]. Polyaniline (PANI) shows excellent electrochemical properties, is easily synthesized and functionalized, has good environmental stability, and is relatively nontoxic. The G-PANI composite was placed on paper-based and plastic-based devices and tested in acetate buffer solution and in human serum samples. By ASV, adding bismuth as the co-deposited element (*in-situ* film), the system showed LOD of 1 ng.ml<sup>-1</sup> and range of detection of 10 to 300 ng.ml<sup>-1</sup> in buffer. In serum samples the system demonstrated good efficiency in the range of 10 to 50 ng.ml<sup>-1</sup>.

Using *in-situ* bismuth film, magnetic nanoparticle/graphene nanocomposite has also been studied because of its stability, large surface area, and catalytic activity. Lee et al. <sup>[181]</sup> using thermal decomposition designed an iron oxide/graphene nanocomposite by to be dropped on GCE. Zinc ions were detected by ASV in acetate buffer solution containing bismuth, showing a LOD of 0.11 ng.ml<sup>-1</sup> and range of detection of 1 to 100 ng.ml<sup>-1</sup>. To achieve a low-cost sensor, S. Cinti *et al* <sup>[182]</sup> developed a carbon-ink screen printed electrode on an office paper to detect zinc in acetate buffer and biofluids. ASV was applied to detect zinc ions by co-deposition of bismuth film, presenting LOD of 25 ng.ml<sup>-1</sup> and range of detection of 80 to 2000 ng.ml<sup>-1</sup> in sweat and serum. Besides the innovative and accessible approach, the use of *in-situ* bismuth might be limited in its clinical applications.

The physiological level of Zn in human sweat is very low and ranges between 0.39 and 1.56 µg.ml<sup>-1</sup> <sup>[183]</sup>. A wearable temporary sensor was designed to monitor zinc concentration in human sweat during exercise <sup>[184]</sup>. By placing *ex situ* Bi film on carbon ink with an auxiliary layer of Nafion, the wearable sensor monitored zinc concentration in sweat by ASV <sup>[184]</sup>. The sensor was first evaluated in acetate buffer (pH 4.6) showing range of detection of 100-2000 ng.ml<sup>-1</sup> and LOD of 50 ng.ml<sup>-1</sup>. The system was tested in athletes after 15-20 minutes of exercising and showed well-defined Zn stripping peaks, indicating a zinc sweat concentration of 0.34 µg.ml<sup>-1</sup>, which is consistent with the literature. Further studies are necessary to focus on miniaturization and integration of electronics for data acquisition.

Xuan et al designed an *ex-situ* electrodeposition method of structured bismuth on the surface of a flexible graphene-based electrode <sup>[185]</sup>. The bismuth nature-inspired branched structures were applied for zinc ion detection in human sweat, aiming for a strategic bonding of the zinc on the electrode surface. By applying ASV in acetate buffer (pH 4.6 ), the system showed range of zinc

detection of 100-1600 ng.ml<sup>-1</sup> and LOD of 40 ng.ml<sup>-1</sup>. The system demonstrated ability to detect zinc in human sweat; however better outcomes are expected after design improvements, such as stability and reduction of the bismuth nature-inspired structure and the development of miniaturized flexible circuitry to realize wireless real-time Zn detection.

Bismuth can also be combined with different substrates to improve sensitivity. Zhu et al designed a MXene (Ti<sub>3</sub>C<sub>2</sub>) nanosheets as matrix for bismuth nanorods<sup>[186]</sup>. MXenes are 2D layered materials and present rich surface chemistry (various termination groups and exposed sites) and conductivity; however, their high LOD and specificity limit their use alone. The Bi-Ti<sub>3</sub>C<sub>2</sub> layer offers ample active sites to form alloys with the target zinc metal during the cathodic reduction. After integration to a microelectrode assembly, the system was evaluated by ASV in acetate buffer (pH 4.5) demonstrating range of detection of 1-20 ng.ml<sup>-1</sup> and LOD of 0.5 ng.ml<sup>-1</sup>. Besides its high cost and limited range of detection, the system was tested in water samples and demonstrated an ability to be applicable in biofluids.

Boron-doped diamond (BDD), a unique material for electrochemical sensing applications, was applied as a substrate for *in situ* Bi deposition with zinc<sup>[187]</sup>. By taking advantage of the optimized surface morphology and the active sites formed by incorporated boron, the system showed great LOD of 0.4 ng.ml<sup>-1</sup> in acetate buffer (pH 5). The Boron-doped diamond-Bi electrode is very innovative and could be applied in different types of samples; however, high cost and *in-situ* approach could limit its applications.

Bismuth and copper (Cu) alloy nanoparticles (ANPs) were encapsulated in a flexible carbon film electrode for a real-time on-site detection of zinc in the different human biofluids and water environment<sup>[188]</sup>. The BiCu-ANPs improved the electrocatalytic activity and the acid resistance,

while the carbon film assured the high electrical conductivity and fast electrochemical kinetics and effectively increased the active surface area of the electrode. By ASV, the designed system showed range of detection of 150 to 600 ng.ml<sup>-1</sup> and LOD of 35 ng.ml<sup>-1</sup> in acetate buffer (pH 4.5). The system showed efficacy of performance in urine and blood samples when compared to atomic absorption spectrometry.

**Table 1.5** - Nanometal-based electrodes for zinc ion sensing

Electrode	Solution	LOD (ng.ml <sup>-1</sup> )	Linear Range (ng.ml <sup>-1</sup> )	Method	Limitations	Ref.
Au/PANI-CNTs	Acetate Buffer (pH 5)	0.039	1-180	ASV	High cost and lower specificity	[171]
Au/Ti-CNTs	Acetate buffer (pH 4.6)	1.5	350-830	ASV	Complex synthesis, co-deposition of Sb to increase sensitivity	[172]
Carbon-TFME	KNO <sub>3</sub> / HCl	5.5	8-220	ASV	High toxicity of mercury	[174]
Biochar-TFME	Acetate buffer (pH 5)	11	20-3260	ASV	High toxicity of mercury	[173]
Gold-BFE	Acetate buffer (pH 6)	1100	900-9000	ASV	Low sensitivity	[166]
Gold-BFE	Acetate buffer (pH 6)	11	180-4500	ASV	Complex synthesis	[178]
Bi-SPAuE	Acetate buffer (5.5)	0.05	1-120	ASV	Limited range of detection	[179]
GCE-BFE	Acetate buffer (pH 4.5)	1.02	5-110	ASV	<i>In situ</i> approach limits clinical application	[180]
Graphene-PANI	Acetate buffer (pH 4.5)	1	10-300	ASV	Addition of in situ bismuth	[154]
Fe <sub>2</sub> O <sub>3</sub> /Graphene	Acetate buffer (pH 4.5)	0.11	1 to 100	ASV	Addition of in situ bismuth	[181]
C-ink on paper	Sweat and Serum	25	80 to 2000	ASV	Addition of in situ bismuth	[182]
C-Nafion-BFE	Acetate buffer (pH 4.6)	50	100-2000	ASV	Needs further studies to be used as portable sensor	[184]
Bi-Graphene	Acetate buffer (pH 4.6)	40	100-1600	ASV	Instability and large Bi structure	[185]
Bi-Ti <sub>3</sub> C <sub>2</sub>	Acetate buffer (pH 4.5)	0.5	1-20	ASV	High cost, limited range of detection	[186]
BDD-Bi	Acetate buffer (pH 5)	0.4	Not informed	ASV	High cost and <i>in situ</i> approach	[187]
BiCu-C	Acetate buffer (pH 4.5)	35	150-600	ASV	Complex synthesis	[188]

### 5.3.3 Recognition elements strategies

The use of recognition elements is an important strategy to improve the specificity of electrochemical sensors. Recognition elements are bio or non-bio molecules that selectively interact with the target species and generate an electrical signal that is related to the concentration of the desired analyte <sup>[189,190]</sup>. Among the recognition elements, enzymes <sup>[191–193]</sup>, amino acids <sup>[194–196]</sup>, peptides <sup>[195–197]</sup> and nucleic acids <sup>[198]</sup> are most often applied to detect heavy metals <sup>[190]</sup>, but other elements have also been explored as such as engineered bacteria <sup>[195,199,200]</sup>, hormones <sup>[201,202]</sup> and small chemical molecules <sup>[195,203–206]</sup>. For metal-containing proteins, usually the recognition layer is designed using enzymes, antibodies, cells, nucleic acids, peptide, and other aptamers <sup>[207]</sup>. Although bio recognition elements have often improved the specificity and sensitivity of electrochemical sensors, their shelf life, reliability, reproducibility, homogeneous immobilization, and high costs are still a challenge and may indicate incorrect target species quantification <sup>[205]</sup>.

The combined action of recognition elements and nanostructures is one of the most successful strategies to overcome these challenges allowing a better sensor performance <sup>[157,190]</sup>. The successful design of functionalized-nanostructured systems is achieved by the immobilization of recognition elements on the surface of the substrate, usually accomplished by entrapment, adsorption, covalent bonding, and/or cross-linking techniques <sup>[208]</sup>. Functionalized-nanostructures provide a synergic effect between catalytic activity, conductivity, and biocompatibility to accelerate the electrical signal and also intensify the biorecognition event, leading to highly sensitive biosensing <sup>[145,208]</sup>.

Two approaches are employed when recognition elements are integrated to electrochemical systems: the label and label-free detection. The label approach employs a molecule, that is

chemically or temporarily attached to the target species, to convert binding response or activity into electrical signals. It requires a labeling process as a preparation step, combining synthesis and purification [209]. The label-free method identifies the electrode and target species interactions or activity directly by electrical signals, with no need of a label element. The advantages of a label-free approach is essentially the immediate and real time detection [209,210]. Several electrochemical sensors employing different recognition elements and strategies have been developed for the detection of metals and metal-containing proteins. In this section, we will highlight a few works where enzymes, antibodies, peptides, nucleic acids, and other aptamers were used as biorecognition elements. Furthermore, we will also explore how the non bio recognition elements have been applied for the electrochemical detection of these species (**Table 1.6**).

Metal ions have a particularly strong affinity for certain enzymes. The enzyme's active center is modified by the interaction with the metal ion, decreasing its activity. The changes generated in the enzyme-substrate interaction, such as the color, conductivity and pH value, can be indirectly measured by monitoring the electrical signal [161,211]. AuNPs and carbon-based electrodes have been used as excellent substrates for loading enzymes [145,165]. Glucose oxidase enzyme (GOx) was immobilised via cross-linking by glutaraldehyde on carbon-poly(neutral red) film electrode [191]. The effect of the zinc on the activity of the GOx was evaluated in phosphate buffer solution at pH 7.0 at a fixed potential of  $-0.35$  V vs. SCE, in the presence of 0.2 mM glucose. The system showed range of detection of 410 to 14500 ng.ml<sup>-1</sup> and LOD of 9 ng.ml<sup>-1</sup>. The system was successful evaluated in water, wine, and milk samples.

By taking advantage of the unique interaction between substrate and enzyme, a biosensor for collagenase (zinc-protein MMP-I) detection was developed to monitor the change in the impedance caused by the proteolytic digestion of gelatin coated gold electrodes [212]. However, the

system was only suitable for measurements at very low collagenase concentrations (<2 mM) because the impedance of the gelatin layer was very similar to the electrolyte solution at higher ionic strength. Enzymatic sensors assure high selectivity, however, their instability and critical microenvironmental factors limit their use. These limitations encouraged the design of non-enzymatic electrochemical sensors with simpler modification procedures and better stability [145].

Antibody-based (immunosensors) electrodes explore the specific antigen (Ag) – antibody (Ab) recognition interaction. Because of the unique interface between Ab-Ag, these electrodes present high specificity and sensitivity [145,207]. There are 2 types of Ab, polyclonal (pAb) and monoclonal (mAb), and they differ from each other by the binding mechanism with the target antigen, where pAb presents multiple binding sites and mAb presents one type of affinity. Monoclonal Ab presents higher sensitivity when compared to polyclonal Ab [207]. Au-based, carbon-based, and combined Au-Carbon electrodes have been employed as a substrate to immobilize antibodies on the electrode surface.

An immunosensor for MMP-9 detection was designed by depositing AuNPs on polydopamine functionalized silica nanospheres (PDA/silica) surfaces followed by the adsorption of MMP-9 antibodies [213]. The high surface area of the electrode allowed an increase in the binding capacity by supplying a larger number of immobilized antibodies. Cyclic voltammetry in  $[\text{Fe}(\text{CN})_6]^{4-/3-}$  solution (pH 7.0) containing 0.1 M KCl allowed the proposed immunosensor to be tested for the determination of MMP-9. There was a range of detection of 0.1 to 150 ng.ml<sup>-1</sup> and LOD of 0.06 ng.ml<sup>-1</sup>. The immunosensor was also successfully used for MMP-9 determination in serum sample and showed comparable results to the conventional ELISA assay.

Nitrogen-doped graphene (NG) nanostructures were functionalized with AuNPs to serve as substrates for the adsorption of horseradish peroxidase MMP-2 antibody (HRP-Ab2) [214]. The AuNPs-NG system increased the surface area to capture large amounts of MMP-2 and to facilitate the electron transfer between the electrode surface and the target species. By DPV, in PBS (pH 7.4) containing H<sub>2</sub>O<sub>2</sub>, the system showed a range of detection of 0.0005 to 50 ng.ml<sup>-1</sup> and LOD of 0.00011 ng.ml<sup>-1</sup>. The Au-NG immunosensor showed similar results compared to ELISA assay in human plasma samples.

AuNPs and graphene oxide have also been used to detect MMP-1. An MMP-1 immunosensor has been designed based on a gold nanoparticle, polyethyleneimine, reduced graphene oxide (AuNP/PEI/rGO) screen-printed electrode (SPE) [215]. Mercaptopropionic acid was utilized to assemble all of the layers by sulfur-gold bonding technique. MMP-1 antibody was immobilized by cross-linking using N-(3-dimethylaminopropyl) and N' ethyl carbodiimide hydrochloride method. The system was tested by DPV, in PBS solution containing [Fe(CN)<sub>6</sub>]<sup>3-/4-</sup> and KCl (pH 7.4), showing range of detection of 1 to 50 ng.ml<sup>-1</sup> and LOD of 0.22 ng.ml<sup>-1</sup>. The immunosensor was successfully applied for MMP-1 detection in urine, saliva, bovine serum, and cell culture media of oral and brain cancers showing results comparable to ELISA assay.

Peptides are one of the most applied recognition elements on the free-label detection of metal-containing proteins, in particular for matrix metalloproteinases (MMPs) [216-218]. Peptides offer a better cost and long shelf-life when compared to antibodies and enzymes [219,220]. The enzymatic cleavage of peptides immobilized on the electrode surface results in the release of peptides fragments, facilitating the electron transfer between the electrode and the target species and increasing the intensity of the current response [219]. However, the electrical response is usually very small, and there is a need to amplify its intensity [220]. As a result, nanostructures have been

extensively applied as signal amplifier on peptide-based electrochemical sensors [219,221]. In addition, the fluctuation of the electrochemical response can be affected by the difficult immobilization of peptides, and peptides-based sensors are also one-time use due to the unique peptide cleavage [220]. The tertiary structures of peptides allow unique conformations where metal ion can be bonded. Peptides can be synthesized and selected for a specific target species and are extremely powerful receptors [161].

The great affinity of peptides to different metal ions is influenced by the higher number of potential donor atoms content in the amino acid chains [222]. Liu et al applied a specific zinc binding peptide (CCPGCGDGE) to detect zinc ions on AuNPs-GCE surface [197]. The AuNPs-GCE was prepared by depositing AuNPs on pre-treated GCE with poly-diallyldimethylammonium chloride. Standard zinc solutions were blended with 1  $\mu\text{M}$  peptide in HEPES and TCEP solution. After, AuNPs-GCEs were incubated with the mixtures for 2h, followed by the treatment of mercaptohexanol for another 0.5h. By electrochemical impedance spectroscopy (EIS) in  $[\text{Fe}(\text{CN})_6]^{3-/4-}$  buffer the system showed a range of detection of 1.4 to 68  $\text{ng}\cdot\text{ml}^{-1}$  and LOD of 0.68  $\text{ng}\cdot\text{ml}^{-1}$ . The system showed satisfactory results when applied to urine samples.

Oxytocin, a peptide hormone, is also a recognition element for detection of zinc ions. Oxytocin binds both copper and zinc with similar affinities, but by two different mechanisms, where zinc binds through the amide carbonyls, and copper uses the terminal amine and deprotonated amides for binding. By taking advantage of the binding mechanism, Mervinetsky et al developed a zinc selective oxytocin-based sensor by coupling oxytocin with COMU reagent on lipoic acid pre-treated gold (Au) surface [201]. The oxytocin terminal amine was directly coupled to the lipoic acid layer, eliminating the anchoring site for the copper ions. After, the modified Au-Oxytocin electrode was exposed to different concentrations of zinc solutions. The system was evaluated by EIS in

$[\text{Fe}(\text{CN})_6]^{3-/4-}$  buffer presenting range of detection of  $0.01 \text{ ng.ml}^{-1}$  to  $20 \text{ } \mu\text{g.ml}^{-1}$ . This innovative work provided a new tuning strategy for the target ion binding by peptides in which the affinity toward other metals could be eliminated by inactivating a specific binding site.

A peptide decorated AuNPs and CNTs electrochemical sensor was designed for the detection of MMP-7 [219]. The system was built by depositing a thin layer of CNTs on gold electrodes before the electrochemical deposition of AuNPs. The peptide (JR2EC) was immobilized on the substrate by using gold-thiol chemistry. The system was evaluated by DPV in PBS solution containing  $\text{K}_4[\text{Fe}(\text{CN})_6]^{4-/3-}$  (pH = 7.4) after 30 minutes of protein immobilization, showing range of detection of  $0.01$  to  $1000 \text{ ng.ml}^{-1}$  and LOD of  $0.006 \text{ ng.ml}^{-1}$ . The system was also performed in the presence of human serum and synthetic urine, demonstrating the potential of the biosensor for clinical applications.

The degradation of peptide-coated hydrogel film by MMP-9 was another strategy employed to detect the metal-containing protein [223]. The biosensor was produced by drop-coating cysteamine on pre-treated interdigitated gold electrodes with oxidized dextran followed by cross-linking with peptide containing specific cleavage sites for MMP-9 (Leu–Gly–Arg–Met–Gly–Leu–Pro–Gly–Lys). The exposure of the functionalized films to MMP-9 resulted in the degradation of the films and it was monitored by EIS, in tris buffer solution containing calcium chloride (pH 7.5). The innovative sensor showed range of detection of  $50$  to  $400 \text{ ng.ml}^{-1}$  and LOD of  $15 \text{ ng.ml}^{-1}$ .

The interaction of nucleic acids with metallic ions have also been explored as a recognition element on the electrochemical detection of zinc. A paper-based sensor designed with reduced graphene oxide (rGO), iron-porphyrinic MOF ((Fe-P)n-MOF) and G-quadruplex-hemin was developed for a point-of-care field, including on-site environmental monitoring, food safety, and disease

diagnosis [198]. To assure better sensitivity and specificity, rGO was applied to provide large surface area, providing better conductivity, and increasing the amount of (Fe-P)n-MOF and enhancing its catalytic properties. Then, the use of G-quadruplex-hemin structure acted as the recognition element to interact with the zinc molecule. By applying DPV in PBS containing H<sub>2</sub>O<sub>2</sub> and o-PD, the system showed a range of detection of 0.02 to 950 ng.ml<sup>-1</sup> and LOD of 4 pg.ml<sup>-1</sup>. This complex but innovative system was successful tested in HepG2 cells extract and water samples.

AuNP-decorated graphene electrodes have been functionalized via gold-thiol interactions with lung cancer DNA sequence for the detection of p53 [224]. Graphene layers were produced by the direct electrical exfoliation in presence of glycine and dropped on gold electrodes, the surface was further decorated with AuNP prepared by citrate reduction method prior to the DNA immobilization. The DNA multilayered graphene –AuNPs surface was incubated with p53 antibody for 1 h prior the electrode evaluation. The system was performed by EIS in PBS in presence of [Fe(CN)<sub>6</sub>]<sup>3-/4-</sup> (pH 7.4). The p53 cancer biomarker could be detected in the concentration range of 0.0001 ng.ml<sup>-1</sup> to 0.1 ng.ml<sup>-1</sup>, presenting LOD of 0.006 pg.ml<sup>-1</sup>.

Aptamer-based sensors are the new era of electrochemical sensors and have been investigated for the detection of proteins as one of the most promising candidates for biosensors [207]. Aptamers are synthetic nucleic acids obtained through an *in-vitro* process named systematic evolution of ligands by exponential enrichment (SELEX) [225,226]. Aptamers are designed to enhance their affinity and stability to the target species, including metal ions, organic molecules, and cells. Aptamers are as selective as traditional antibodies; however, they offer better stability, easier immobilization and simpler refolding ability. [225,226]. Besides its advantages, the rapid degradation, the complex synthesis, and the lack of standardized fabrication protocols of aptamers can limit their wide application as point-of-care devices [227].

An aptamer-based sensor for detection of MMP-9 and MMP-2 was designed based on the thiol–pyridyl disulphide exchange reaction <sup>[228]</sup>. Interdigitated gold electrodes were modified by chemical vapor deposited graphene prior to the MMP-9 and MMP-2 aptamers immobilization. The modified electrode was then immersed in pyrene-pyridinyl disulphide (PSE) solution, and subsequently, aptamer solutions were dropped onto the graphene surface and incubated for 2 h. PSE not only provided a robust surface anchoring, but also allowed facile modification with thiolated bioreceptors. By DPV, in PBS solution containing ferrocenemethanol (pH 7.4), the aptamer-graphene sensor showed LOD of 0.0092 ng.ml<sup>-1</sup> and 0.95 ng.ml<sup>-1</sup> for MMP-9 and MMP-2 respectively.

As mentioned previously, biomolecules combined with nanostructures could assure higher sensitivity and specificity to target zinc-related biomarkers on biofluids, in which a variety of components could affect the sensitivity of a sensor. However, the challenges regarding the shelf-life, complexity and high cost are still present. Compared with biomolecules, non-bio recognition elements assure lower-cost, long shelf-life, inherent stability, and comparable sensitivity and specificity <sup>[229]</sup>. Teng et al. <sup>[203]</sup> functionalized exfoliated graphite (EG) with zincon, a molecule with high ability of complexation to zinc ions. By taking advantage of the  $\pi$ - $\pi$  interaction, zincon was conjugated with EG and dropped on screen-printed electrodes (SPE) for the detection of mobile zinc ions in the early diagnostic of prostate cancer. By DPV, the system presented LOD of 5 ng.ml<sup>-1</sup> and range of detection of 250 to 1500 ng.ml<sup>-1</sup> in tris HCl buffer solution. The system was also performed in serum samples from mouse prostatic cancer showing low sensitivity of 2500 ng.ml<sup>-1</sup>.

An emerging strategy on the electrochemical detection of metal-containing proteins is the use of non-bio inhibitor molecules that react with the proteins, resulting in changes in the electrochemical

response. Using a GCE, Moradi et al<sup>[230]</sup> monitored the current signal of the interaction of carbonic anhydrase (CA) with three different inhibitory drugs (acetazolamide, dorzolamide and methazolamide). Methazolamide drug was the most potent inhibitor among the drugs and for this reason it was used to measure CA concentration. By chronoamperometry, in a tris-buffered saline solution containing both the drug and the enzyme (pH 7.4), the system showed a decrease in the current upon addition of the CA, confirming the binding of the drug with the enzyme molecules. The inhibitory strategy showed current response when varying CA concentration from 0 to 600 ng.ml<sup>-1</sup> and LOD of 6 ng.ml<sup>-1</sup>. The system showed stability over 3 months.

**Table 1.6** Recognition elements-based electrodes for zinc ion sensing

Electrode	Recognition element	Analyte	Solution	LOD (ng.ml <sup>-1</sup> )	Range (ng.ml <sup>-1</sup> )	Method	Limitations	Ref
Carbon-GOx - Poly(red) film	Enzyme	Zinc ion	PBS (pH 7.0)	9	410 to 14500	Chrono-amperometry	Low range of detection for biofluids	[191]
MMP-9 antibody on AuNPs-PDA-Silica	Antibody	MMP-9	KCL in Fe(CN) <sub>6</sub> <sup>3-/4-</sup> (pH 7.0)	0.06	0.1 to 150	CV	High cost of antibodies	[213]
MMP-2 antibody on AuNPs-rGO	Antibody	MMP-2	PBS (pH 7.4)	0.00011	0.0005 to 50	DPV	High cost of antibody and limited range of detection	[214]
MMP-1 antibody on AuNP/PEI/rGO	Antibody	MMP-1	PBS (pH 7.4)	0.22	1 to 50	DPV	High cost of antibody and limited range of detection	[215]
GCE-AuNPs-CCPGCGDGE	Peptide	Zinc ion	KCL in Fe(CN) <sub>6</sub> <sup>3-/4-</sup>	0.68	1.4 to 68	EIS	Limited range of detection	[197]
Au-Oxytocin	Peptide (Hormone)	Zinc ion	KCL in Fe(CN) <sub>6</sub> <sup>3-/4-</sup>	Not informed	0.01 to 20.000	EIS	Need validation in biofluids	[201]
CNT-AuNPs-Peptide	Peptide	MMP-7	PBS (pH 7.4)	0.006	0.01 to 1000	DPV	One-time use and fluctuation on the signal	[219]
Au/Peptide/Dextran	Peptide	MMP-9	Tris-buffer (pH 7.5)	15	50 to 400	EIS	Complex synthesis, one-time use	[223]
rGO-MOF-G-quadruplex	Nucleic Acid	Zinc ion	PBS (pH 7.0)	0.004	0.02 to 950	DPV	Complex synthesis	[198]
AuNP-decorated graphene-DNA	Nucleic Acid	p53	PBS (pH 7.4)	0.000006	0.0001 to 0.1	EIS	Limited range of detection for biofluids	[224]
Au-Graphene-PSE	Aptamer	MMP-9 and MMP-2	PBS (pH 7.4)	0.0092 and 0.95	Not informed	DPV	Complex synthesis	[228]
Functionalized Zincon-graphite SPE	Non bioelement	Zinc ion	Tris HCl buffer (pH 7.5)	5	250 to 1500	DPV	Low sensitivity in serum samples	[203]
GCE	Non bioelement	Carbonic anhydrase	TBS buffer (pH 7.4)	6	0-600	Chrono-amperometry	No nanostructured surface was studied.	[230]

## 6. Conclusion and Future perspectives

The present review described the recent innovations in the field of electrochemical detection of zinc-related biomarkers present in cancer related fluids. Different strategies for improving sensitivity and selectivity of electrochemical sensors towards quantitative detection of zinc and zinc-containing proteins are available in a variety of environmental and biological fluids. Functionalized-nanostructured materials demonstrated incredible ability to boost sensors' performance with fast, accurate, and sensitive detection of zinc-related biomarkers. A detailed analysis has confirmed that the sensitivity of electrochemical sensors can be significantly superior through various paths, including the use of nanocarbon, nanometal, and recognition elements on the electrode surfaces. However, further development in this research field must be made to be able to address the major challenges, including: i) satisfactory stability and controlled synthesis of sensors' surfaces; ii) proper immobilization of recognition elements on nanostructures; iii) design of novel non-bio recognition elements-based electrodes; iv) better sample validation, including biofluids not only buffer solutions; v) cross interference within the similar elements present in biofluids; vi) real clinical scenario validation; and vii) storage capability. In addition, it is essential to better understand the electrochemical behavior in the complex biological samples, such as serum, urine, and saliva. The translation of electrochemical systems presenting high sensitivity and specificity to the clinical practice is still a challenge because of the nonspecific adsorption of numerous biomolecules present in the biofluids at the electrode surface. This can drastically block the electrochemical signal, increasing the background noise and decreasing the specificity of the sensor. The use of nanostructures it is one of the strategies in place to overcome biofouling, however, if it is not sufficient, few directions must be conducted as the design of polymer antifouling layers, nano porous membranes, and hydrogels. Furthermore, the miniaturization of

electrochemical sensors to desirable portable devices may be developed through efficient connectivity and integration between distinct areas of research, ensuring large scale production, accessibility, and cost reduction.

## References

- [1] A. I. Anzellotti, N. P. Farrell, *Chem. Soc. Rev.* **2008**, *37*, 1629.
- [2] A. S. Prasad, O. Kucuk, *Cancer Metastasis Rev.* **2002**, *21*, 291.
- [3] A. S. Prasad, F. W. Beck, D. C. Snell, O. Kucuk, *Nutr. Cancer* **2009**, *61*, 879.
- [4] E. Ho, *J. Nutr. Biochem.* **2004**, *15*, 572.
- [5] B. J. Grattan, H. C. Freake, *Nutrients* **2012**, *4*, 648.
- [6] C. T. Chasapis, P.-S. A. Ntoupa, C. A. Spiliopoulou, M. E. Stefanidou, *Arch. Toxicol.* **2020**, *94*.
- [7] M. Murakami, T. Hirano, *Cancer Sci.* **2008**, *99*, 1515.
- [8] J. Wang, H. Zhao, Z. Xu, X. Cheng, *Cancer Biol. Med.* **2020**, *17*, 612.
- [9] H. Tapiero, K. D. Tew, *Biomed. Pharmacother.* **2003**, *57*, 399.
- [10] L. C. Costello, R. B. Franklin, *Pancreat. Disord. Ther.* **2013**.
- [11] M. J. Jackson, in *Zinc Hum. Biol.*, Springer, **1989**, pp. 1–14.
- [12] N. C. Lim, H. C. Freake, C. Brückner, *Chem.- Eur. J.* **2005**, *11*, 38.
- [13] J. Hrabeta, T. Eckschlager, M. Stiborova, Z. Heger, S. Krizkova, V. Adam, *J. Mol. Med.* **2016**, *94*, 1199.
- [14] F. Chen, J. Wang, J. Chen, L. Yan, Z. Hu, J. Wu, X. Bao, L. Lin, R. Wang, L. Cai, *Oral Dis.* **2019**, *25*, 80.
- [15] B. K. Ayinampudi, M. Narsimhan, *J. Oral Maxillofac. Pathol. JOMFP* **2012**, *16*, 178.
- [16] N. Kagara, N. Tanaka, S. Noguchi, T. Hirano, *Cancer Sci.* **2007**, *98*, 692.
- [17] K. M. Taylor, P. Vichova, N. Jordan, S. Hiscox, R. Hendley, R. I. Nicholson, *Endocrinology* **2008**, *149*, 4912.
- [18] L. Jouybari, F. Kiani, A. Akbari, A. Sanagoo, F. Sayehmiri, J. Aaseth, M. S. Chartrand, K. Sayehmiri, S. Chirumbolo, G. Bjørklund, *J. Trace Elem. Med. Biol.* **2019**, *56*, 90.
- [19] K. Schilling, R. E. Moore, K. V. Sullivan, M. S. Capper, M. Rehkämper, K. Goddard, C. Ion, R. C. Coombes, L. Vesty-Edwards, A. D. Lamb, *Metallomics* **2021**, *13*, mfab020.
- [20] B. X. Hoang, B. Han, D. G. Shaw, M. Nimni, *Eur. J. Cancer Prev.* **2016**, *25*, 457.

- [21] L. C. Costello, R. B. Franklin, *Arch. Biochem. Biophys.* **2016**, *611*, 100.
- [22] R. B. Franklin, P. Feng, B. Milon, M. M. Desouki, K. K. Singh, A. Kajdacsy-Balla, O. Bagasra, L. C. Costello, *Mol. Cancer* **2005**, *4*, 1.
- [23] L. C. Costello, R. B. Franklin, *JBIC J. Biol. Inorg. Chem.* **2011**, *16*, 3.
- [24] P. Christudoss, R. Selvakumar, J. J. Fleming, G. Gopalakrishnan, *Indian J. Urol. IJU J. Urol. Soc. India* **2011**, *27*, 14.
- [25] V. C. Wakwe, E. P. Odum, C. Amadi, *Investig. Clin. Urol.* **2019**, *60*, 162.
- [26] M. Li, Y. Zhang, Z. Liu, U. Bharadwaj, H. Wang, X. Wang, S. Zhang, J. P. Liuzzi, S.-M. Chang, R. J. Cousins, *Proc. Natl. Acad. Sci.* **2007**, *104*, 18636.
- [27] S. Krizkova, M. Ryzolova, J. Hrabeta, V. Adam, M. Stiborova, T. Eckschlager, R. Kizek, *Drug Metab. Rev.* **2012**, *44*, 287.
- [28] M. Baharvand, S. Manifar, R. Akkafan, H. Mortazavi, S. Sabour, *Biomed J* **2014**, *37*, 331.
- [29] Y. Wang, Z. Sun, A. Li, Y. Zhang, *World J. Surg. Oncol.* **2019**, *17*, 1.
- [30] A. Sadat, M. I. Hossain, M. K. Hossain, M. S. Reza, Z. Nahar, S. K. N. Islam, A. Hasnat, *J. Appl. Reliab.* **2008**, *8*, 24.
- [31] C. T. Supuran, A. Scozzafava, *J. Enzym. Inhib.* **2000**, *15*, 597.
- [32] M. Benej, S. Pastorekova, J. Pastorek, *Carbonic Anhydrase Mech. Regul. Links Dis. Ind. Appl.* **2014**, 199.
- [33] P. C. McDonald, J.-Y. Winum, C. T. Supuran, S. Dedhar, *Oncotarget* **2012**, *3*, 84.
- [34] H. M. Becker, *Br. J. Cancer* **2020**, *122*, 157.
- [35] B. Wang, *Drug Design of Zinc-Enzyme Inhibitors: Functional, Structural, and Disease Applications*, John Wiley & Sons, **2009**.
- [36] C. P. S. Potter, A. L. Harris, *Br. J. Cancer* **2003**, *89*, 2.
- [37] S. Mondal, N. Adhikari, S. Banerjee, S. A. Amin, T. Jha, *Eur. J. Med. Chem.* **2020**, *194*, 112260.
- [38] M. Egeblad, Z. Werb, *Nat. Rev. Cancer* **2002**, *2*, 161.
- [39] K. Kessenbrock, V. Plaks, Z. Werb, *Cell* **2010**, *141*, 52.
- [40] K. J. Isaacson, M. M. Jensen, N. B. Subrahmanyam, H. Ghandehari, *J. Controlled Release* **2017**, *259*, 62.

- [41] E. Gobin, K. Bagwell, J. Wagner, D. Mysona, S. Sandirasegarane, N. Smith, S. Bai, A. Sharma, R. Schleifer, J.-X. She, *BMC Cancer* **2019**, *19*, 1.
- [42] G. Gonzalez-Avila, B. Sommer, D. A. Mendoza-Posada, C. Ramos, A. A. Garcia-Hernandez, R. Falfan-Valencia, *Crit. Rev. Oncol. Hematol.* **2019**, *137*, 57.
- [43] B. Ma, R. Ran, H.-Y. Liao, H.-H. Zhang, *Biomed. Pharmacother.* **2021**, *141*, 111899.
- [44] S.-M. Sheen-Chen, H.-S. Chen, H.-L. Eng, C.-C. Sheen, W.-J. Chen, *Cancer Lett.* **2001**, *173*, 79.
- [45] S. Patel, G. Sumitra, B. C. Koner, A. Saxena, *Clin. Biochem.* **2011**, *44*, 869.
- [46] G. Giannelli, E. Fransvea, F. Marinosci, C. Bergamini, A. Daniele, S. Colucci, A. Paradiso, M. Quaranta, S. Antonaci, *Biochem. Biophys. Res. Commun.* **2002**, *292*, 161.
- [47] A. Acar, A. Onan, U. Coskun, A. Uner, U. Bagriacik, F. Atalay, D. K. Unsal, H. Guner, *Med. Oncol.* **2008**, *25*, 279.
- [48] B. Schmalfeldt, D. Prechtel, K. Härting, K. Späthe, S. Rutke, E. Konik, R. Fridman, U. Berger, M. Schmitt, W. Kuhn, *Clin. Cancer Res.* **2001**, *7*, 2396.
- [49] K. Gohji, N. Fujimoto, I. Hara, A. Fujii, A. Gotoh, H. Okada, S. Arakawa, S. Kitazawa, H. Miyake, S. Kamidono, *Int. J. Cancer* **1998**, *79*, 96.
- [50] G. Morgia, M. Falsaperla, G. Malaponte, M. Madonia, M. Indelicato, S. Travali, M. C. Mazarino, *Urol. Res.* **2005**, *33*, 44.
- [51] M. Stearns, M. E. Stearns, *Oncol. Res. Featur. Preclin. Clin. Cancer Ther.* **1996**, *8*, 69.
- [52] F. Riedel, K. Götte, J. Schwalb, K. Hörmann, *Anticancer Res.* **2000**, *20*, 3045.
- [53] B.-K. Lee, M.-J. Kim, H.-S. Jang, H.-R. Lee, K.-M. Ahn, J.-H. Lee, P.-H. Choung, M.-J. Kim, *In Vivo* **2008**, *22*, 593.
- [54] Y. Kanoh, T. Abe, N. Masuda, T. Akahoshi, *Oncol. Rep.* **2013**, *29*, 469.
- [55] P. Iniesta, A. Morán, C. De Juan, A. Gómez, F. Hernando, C. García-Aranda, C. Frías, A. Díaz-López, F.-J. Rodríguez-Jiménez, J.-L. Balibrea, *Oncol. Rep.* **2007**, *17*, 217.
- [56] E. S. Gershtein, D. N. Kushlinsky, N. V. Levkina, I. V. Tereshkina, V. B. Nosov, K. P. Laktionov, L. V. Adamyan, *Bull. Exp. Biol. Med.* **2011**, *151*, 449.
- [57] J. Maurel, C. Nadal, X. Garcia-Albeniz, R. Gallego, E. Carcereny, V. Almendro, M. Mármol, E. Gallardo, J. Maria Augé, R. Longarón, *Int. J. Cancer* **2007**, *121*, 1066.
- [58] R. Gallego, J. Codony-Servat, X. Garcia-Albeniz, E. Carcereny, R. Longaron, A. Oliveras, M. Tosca, J. M. Auge, P. Gascon, J. Maurel, *Endocr. Relat. Cancer* **2009**, *16*, 311.

- [59] I. Dimitrova, T. Tacheva, I. Mindov, B. Petrov, E. Aleksandrova, S. Valkanov, M. Gulubova, T. Vlaykova, *Biotechnol. Biotechnol. Equip.* **2019**, *33*, 881.
- [60] Y. Miyata, T. Iwata, K. Ohba, S. Kanda, M. Nishikido, H. Kanetake, *Clin. Cancer Res.* **2006**, *12*, 6998.
- [61] C. Niedworok, F. Vom Dorp, S. Tschirdewahn, H. Rübber, H. Reis, M. Szucs, T. Szarvas, *Int. Urol. Nephrol.* **2016**, *48*, 355.
- [62] T. Shiomi, Y. Okada, *Cancer Metastasis Rev.* **2003**, *22*, 145.
- [63] J. H. Kristensen, L. Larsen, B. Dasgupta, C. Brodmerkel, M. Curran, M. A. Karsdal, J. M. B. Sand, N. Willumsen, A. J. Knox, C. E. Bolton, *Clin. Biochem.* **2015**, *48*, 1083.
- [64] D. Liu, J. Nakano, S. Ishikawa, H. Yokomise, M. Ueno, K. Kadota, M. Urushihara, C. Huang, *Lung Cancer* **2007**, *58*, 384.
- [65] D. C. Jinga, A. Blidaru, I. Condrea, C. Ardeleanu, C. Dragomir, G. Szegli, M. Stefanescu, C. Matache, *J. Cell. Mol. Med.* **2006**, *10*, 499.
- [66] K.-P. Guan, H.-Y. Ye, Z. Yan, Y. Wang, S.-K. Hou, *Urology* **2003**, *61*, 719.
- [67] S. Ricci, D. Bruzzese, A. Di Carlo, *Oncol. Lett.* **2015**, *10*, 2527.
- [68] S. T. Reis, K. R. M. Leite, L. F. Piovesan, J. Pontes-Junior, N. I. Viana, D. K. Abe, A. Crippa, C. M. Moura, S. P. Adonias, M. Srougi, *BMC Urol.* **2012**, *12*, 1.
- [69] S. T. Reis, J. Pontes-Junior, A. A. Antunes, J. M. de Sousa-Canavez, M. F. Dall'Oglio, C. C. Passerotti, D. K. Abe, A. Crippa, J. A. S. Da Cruz, L. M. Timoszczuk, *Int. J. Biol. Markers* **2011**, *26*, 255.
- [70] A. E. Stanciu, A. Zamfir-Chiru-Anton, M. M. Stanciu, C. R. Popescu, D. C. Gheorghe, *Clin. Lab.* **2016**, *62*, 1569.
- [71] E. Laack, A. Köhler, C. Kugler, T. Dierlamm, C. Knuffmann, G. Vohwinkel, A. Niestroy, N. Dahlmann, A. Peters, J. Berger, *Ann. Oncol.* **2002**, *13*, 1550.
- [72] Z.-P. Yang, D.-Y. Ling, Y.-H. Xie, W.-X. Wu, J.-R. Li, J. Jiang, J.-L. Zheng, Y.-H. Fan, Y. Zhang, *Dis. Markers* **2015**, *2015*.
- [73] R. González de Vega, D. Clases, M. L. Fernández-Sánchez, N. Eiró, L. O. González, F. J. Vizoso, P. A. Doble, A. Sanz-Medel, *Anal. Bioanal. Chem.* **2019**, *411*, 639.
- [74] L. Pang, D.-W. Wang, N. Zhang, D.-H. Xu, X.-W. Meng, *Cancer Biomark.* **2016**, *16*, 599.
- [75] C.-J. Xu, F. Xu, *Int. J. Clin. Exp. Med.* **2014**, *7*, 2883.
- [76] D. Yan, H. Dai, J.-W. Liu, *BMC Cancer* **2011**, *11*, 1.

- [77] Z.-S. Zhao, Y.-Q. Chu, Z.-Y. Ye, Y.-Y. Wang, H.-Q. Tao, *Hum. Pathol.* **2010**, *41*, 686.
- [78] C.-H. Hsin, M.-K. Chen, C.-H. Tang, H.-P. Lin, M.-Y. Chou, C.-W. Lin, S.-F. Yang, *PloS One* **2014**, *9*, e113129.
- [79] C.-H. Hsin, Y.-E. Chou, S.-F. Yang, S.-C. Su, Y.-T. Chuang, S.-H. Lin, C.-W. Lin, *Oncotarget* **2017**, *8*, 32783.
- [80] H. Yang, P. Jiang, D. Liu, H.-Q. Wang, Q. Deng, X. Niu, L. Lu, H. Dai, H. Wang, W. Yang, *Mol. Ther.-Oncolytics* **2019**, *14*, 82.
- [81] T. J. Delebecq, H. Porte, F. Zerimech, M.-C. Copin, V. Gouyer, E. Dacquembronne, M. Balduyck, A. Wurtz, G. Huet, *Clin. Cancer Res.* **2000**, *6*, 1086.
- [82] P. Laudański, J. Swiatecka, L. Kozłowski, M. Leśniewska, M. Wojtukiewicz, S. Wołczyński, *Folia Histochem. Cytobiol.* **2010**, *48*, 101.
- [83] D. Di, L. Chen, Y. Guo, L. Wang, H. Wang, J. Ju, *Oncol. Lett.* **2018**, *15*, 5020.
- [84] R. Kaimal, R. Aljumaily, S. L. Tressel, R. V. Pradhan, L. Covic, A. Kuliopulos, C. Zarwan, Y. B. Kim, S. Sharifi, A. Agarwal, *Cancer Res.* **2013**, *73*, 2457.
- [85] A. A. Kamat, M. Fletcher, L. M. Gruman, P. Mueller, A. Lopez, C. N. Landen, L. Han, D. M. Gershenson, A. K. Sood, *Clin. Cancer Res.* **2006**, *12*, 1707.
- [86] Z. Dong, X. Sun, J. Xu, X. Han, Z. Xing, D. Wang, J. Ge, L. Meng, X. Xu, *Med. Sci. Monit. Int. Med. J. Exp. Clin. Res.* **2019**, *25*, 7770.
- [87] S. Ogawa, H. Kubo, Y. Murayama, T. Kubota, M. Yubakami, T. Matsumoto, T. Ohashi, K. Okamoto, Y. Kuriki, K. Hanaoka, *Photodiagnosis Photodyn. Ther.* **2021**, *35*, 102420.
- [88] H. Zhang, M. Liu, Y. Sun, J. Lu, *Eur. Arch. Otorhinolaryngol.* **2009**, *266*, 1427.
- [89] Y. Wang, K. Wu, A. Wu, Z. Yang, J. Li, Y. Mo, M. Xu, B. Wu, Z. Yang, *Tumor Biol.* **2014**, *35*, 9815.
- [90] D. B. Woods, K. H. Vousden, *Exp. Cell Res.* **2001**, *264*, 56.
- [91] S. N. Loh, *Metallomics* **2010**, *2*, 442.
- [92] T. Ozaki, A. Nakagawara, *Cancers* **2011**, *3*, 994.
- [93] G. Zhu, C. Pan, J.-X. Bei, B. Li, C. Liang, Y. Xu, X. Fu, *Front. Oncol.* **2020**, 2418.
- [94] L. A. Donehower, T. Soussi, A. Korkut, Y. Liu, A. Schultz, M. Cardenas, X. Li, O. Babur, T.-K. Hsu, O. Lichtarge, *Cell Rep.* **2019**, *28*, 1370.
- [95] K. Somasundaram, W. S. El-Deiry, *Front Biosci* **2000**, *5*, D424.

- [96] C. Kandoth, M. D. McLellan, F. Vandin, K. Ye, B. Niu, C. Lu, M. Xie, Q. Zhang, J. F. McMichael, M. A. Wyczalkowski, *Nature* **2013**, *502*, 333.
- [97] M. J. Duffy, N. C. Synnott, J. Crown, *Eur. J. Cancer* **2017**, *83*, 258.
- [98] M. Cassandri, A. Smirnov, F. Novelli, C. Pitolli, M. Agostini, M. Malewicz, G. Melino, G. Raschellà, *Cell Death Discov.* **2017**, *3*, 1.
- [99] D. Munro, D. Ghersi, M. Singh, *PLoS Comput. Biol.* **2018**, *14*, e1006290.
- [100] J. M. Berg, D. L. Merkle, *J. Am. Chem. Soc.* **1989**, *111*, 3759.
- [101] J. Jen, Y.-C. Wang, *J. Biomed. Sci.* **2016**, *23*, 1.
- [102] S. S. Krishna, I. Majumdar, N. V. Grishin, *Nucleic Acids Res.* **2003**, *31*, 532.
- [103] S. Iuchi, *Cell. Mol. Life Sci. CMLS* **2001**, *58*, 625.
- [104] K. J. Brayer, D. J. Segal, *Cell Biochem. Biophys.* **2008**, *50*, 111.
- [105] J. Caramel, M. Ligier, A. Puisieux, *Cancer Res.* **2018**, *78*, 30.
- [106] M. Pieraccioli, S. Nicolai, A. Antonov, J. Somers, M. Malewicz, G. Melino, G. Raschella, *Oncogene* **2016**, *35*, 2592.
- [107] X.-H. Gao, Q.-Z. Liu, W. Chang, X.-D. Xu, Y. Du, Y. Han, Y. Liu, Z.-Q. Yu, Z.-G. Zuo, J.-J. Xing, *Cancer* **2013**, *119*, 2212.
- [108] S. E. Theocharis, A. P. Margeli, A. Koutselinis, *Int. J. Biol. Markers* **2003**, *18*, 162.
- [109] M. Si, J. Lang, *J. Hematol. Oncol. J Hematol Oncol* **2018**, *11*, 1.
- [110] P. Dziegiel, B. Pula, C. Kobierzycki, M. Stasiolek, M. Podhorska-Okolow, **2016**.
- [111] H. Wei, M. M. Desouki, S. Lin, D. Xiao, R. B. Franklin, P. Feng, *Mol. Cancer* **2008**, *7*, 1.
- [112] S.-S. Lee, S.-F. Yang, Y.-C. Ho, C.-H. Tsai, Y.-C. Chang, *Oral Oncol.* **2008**, *44*, 180.
- [113] M. Dutsch-Wicherek, A. Lazar, R. Tomaszewska, W. Kazmierczak, L. Wicherek, *Cell Tissue Res.* **2013**, *352*, 341.
- [114] B. Tariha, T. Živković, N. Krasnići, V. F. Marijić, M. Erk, M. Gamulin, M. Grgić, A. Pizent, *Cancer Chemother. Pharmacol.* **2015**, *75*, 813.
- [115] A. Nakayama, H. Fukuda, M. Ebara, H. Hamasaki, K. Nakajima, H. Sakurai, *Biol. Pharm. Bull.* **2002**, *25*, 426.
- [116] P. R. Srinivas, B. S. Kramer, S. Srivastava, *Lancet Oncol.* **2001**, *2*, 698.

- [117] V. S. A. Jayanthi, A. B. Das, U. Saxena, *Biosens. Bioelectron.* **2017**, *91*, 15.
- [118] J. D. Wulfkuhle, L. A. Liotta, E. F. Petricoin, *Nat. Rev. Cancer* **2003**, *3*, 267.
- [119] L. Wu, X. Qu, *Chem. Soc. Rev.* **2015**, *44*, 2963.
- [120] B. J. Bolann, R. Rahil-Khazen, H. Henriksen, R. Isrenn, R. J. Ulvik, *Scand. J. Clin. Lab. Invest.* **2007**, *67*, 353.
- [121] A. C. Davis, P. Wu, X. Zhang, X. Hou, B. T. Jones, *Appl. Spectrosc. Rev.* **2006**, *41*, 35.
- [122] V. A. Lemos, A. L. de Carvalho, *Environ. Monit. Assess.* **2010**, *171*, 255.
- [123] S. N. Topkaya, M. Azimzadeh, M. Ozsoz, *Electroanalysis* **2016**, *28*, 1402.
- [124] H. G. Gika, G. A. Theodoridis, R. S. Plumb, I. D. Wilson, *J. Pharm. Biomed. Anal.* **2014**, *87*, 12.
- [125] J. J. Pitt, *Clin. Biochem. Rev.* **2009**, *30*, 19.
- [126] A. C. Sun, D. A. Hall, *Electroanalysis* **2019**, *31*, 2.
- [127] F. Cui, Z. Zhou, H. S. Zhou, *J. Electrochem. Soc.* **2019**, *167*, 037525.
- [128] M. R. Hasan, M. S. Ahommed, M. Daizy, M. S. Bacchu, M. R. Ali, M. R. Al-Mamun, M. A. S. Aly, M. Z. H. Khan, S. I. Hossain, *Biosens. Bioelectron. X* **2021**, *8*, 100075.
- [129] J. Yu, R. M. A. Hahne, in *Encycl. Anal. Sci. Second Ed.* (Eds.: P. Worsfold, A. Townshend, C. Poole), Elsevier, Oxford, **2005**, pp. 48–55.
- [130] C. M. Hussain, R. Keçili, in *Mod. Environ. Anal. Tech. Pollut.* (Eds.: C. M. Hussain, R. Keçili), Elsevier, **2020**, pp. 199–222.
- [131] F. R. Simões, M. G. Xavier, in *Nanosci. Its Appl.* (Eds.: A. L. Da Róz, M. Ferreira, F. de Lima Leite, O. N. Oliveira), William Andrew Publishing, **2017**, pp. 155–178.
- [132] H. Teymourian, A. Barfidokht, J. Wang, *Chem. Soc. Rev.* **2020**, *49*, 7671.
- [133] A. Nsabimana, X. Ma, F. Yuan, F. Du, A. Abdussalam, B. Lou, G. Xu, *Electroanalysis* **2019**, *31*, 177.
- [134] F. McEachern, E. Harvey, G. Merle, *Biotechnol. J.* **2020**, *15*, 2000140.
- [135] Y. Ou, A. M. Buchanan, C. E. Witt, P. Hashemi, *Anal. Methods* **2019**, *11*, 2738.
- [136] H. S. Magar, R. Y. Hassan, A. Mulchandani, *Sensors* **2021**, *21*, 6578.
- [137] S. Andreescu, O. A. Sadik, *Methods* **2005**, *37*, 84.

- [138] M. Labib, E. H. Sargent, S. O. Kelley, *Chem. Rev.* **2016**, *116*, 9001.
- [139] B. Bansod, T. Kumar, R. Thakur, S. Rana, I. Singh, *Biosens. Bioelectron.* **2017**, *94*, 443.
- [140] X. Huang, Y. Zhu, E. Kianfar, *J. Mater. Res. Technol.* **2021**, *12*, 1649.
- [141] A. Bogomolova, E. Komarova, K. Reber, T. Gerasimov, O. Yavuz, S. Bhatt, M. Aldissi, *Anal. Chem.* **2009**, *81*, 3944.
- [142] K. Beaver, A. Dantanarayana, S. D. Minter, *J. Phys. Chem. B* **2021**, *125*, 11820.
- [143] N. Wongkaew, M. Simsek, C. Griesche, A. J. Baeumner, *Chem. Rev.* **2018**, *119*, 120.
- [144] H. Karimi-Maleh, F. Karimi, M. Alizadeh, A. L. Sanati, *Chem. Rec.* **2020**, *20*, 682.
- [145] C. Zhu, G. Yang, H. Li, D. Du, Y. Lin, *Anal. Chem.* **2015**, *87*, 230.
- [146] A. de la Escosura-Muñiz, A. Merkoçi, *Expert Opin. Med. Diagn.* **2010**, *4*, 21.
- [147] A. C. Power, B. Gorey, S. Chandra, J. Chapman, *Nanotechnol. Rev.* **2018**, *7*, 19.
- [148] C. Yang, M. E. Denno, P. Pyakurel, B. J. Venton, *Anal. Chim. Acta* **2015**, *887*, 17.
- [149] J. Kudr, L. Richtera, L. Nejd, K. Xhaxhiu, P. Vitek, B. Rutkay-Nedecky, D. Hynek, P. Kopel, V. Adam, R. Kizek, *Materials* **2016**, *9*, 31.
- [150] A. J. Saleh Ahammad, J.-J. Lee, M. A. Rahman, *sensors* **2009**, *9*, 2289.
- [151] C. B. Jacobs, M. J. Peairs, B. J. Venton, *Anal. Chim. Acta* **2010**, *662*, 105.
- [152] A. A. Dias, C. L. Chagas, H. de A. Silva-Neto, E. O. Lobo-Junior, L. F. Sgobbi, W. R. de Araujo, T. R. Paixão, W. K. Coltro, *ACS Appl. Mater. Interfaces* **2019**, *11*, 39484.
- [153] X. Guo, Y. Yun, V. N. Shanov, H. B. Halsall, W. R. Heineman, *Electroanalysis* **2011**, *23*, 1252.
- [154] N. Ruecha, N. Rodthongkum, D. M. Cate, J. Volckens, O. Chailapakul, C. S. Henry, *Anal. Chim. Acta* **2015**, *874*, 40.
- [155] N. Behnia, M. Asgari, A. Feizbakhsh, *J. Environ. Chem. Eng.* **2015**, *3*, 271.
- [156] M. Pacios, I. Martín-Fernández, R. Villa, P. Godignon, M. Del Valle, J. Bartrolí, M. J. Esplandiú, in *Carbon Nanotub.-Growth Appl.*, IntechOpen, **2011**.
- [157] J. Wang, *Analyst* **2005**, *130*, 421.
- [158] S. Gupta, A. Irihamye, *AIP Adv.* **2015**, *5*, 037106.
- [159] J. N. Tiwari, V. Vij, K. C. Kemp, K. S. Kim, *ACS Nano* **2016**, *10*, 46.

- [160] S. Sawan, R. Maalouf, A. Errachid, N. Jaffrezic-Renault, *TrAC Trends Anal. Chem.* **2020**, *131*, 116014.
- [161] G. March, T. D. Nguyen, B. Piro, *Biosensors* **2015**, *5*, 241.
- [162] P. S. Jensen, C. Engelbrekt, K. H. Sørensen, J. Zhang, Q. Chi, J. Ulstrup, *J. Mater. Chem.* **2012**, *22*, 13877.
- [163] L. Liu, D. Deng, W. Sun, X. Yang, S. Yang, S. He, *Int J Electrochem Sci* **2018**, *13*, 10496.
- [164] E. Valera, A. Hernández-Albors, M.-P. Marco, *TrAC Trends Anal. Chem.* **2016**, *79*, 9.
- [165] J. M. Pingarrón, P. Yanez-Sedeno, A. González-Cortés, *Electrochimica Acta* **2008**, *53*, 5848.
- [166] P. Jothimuthu, R. A. Wilson, J. Herren, X. Pei, W. Kang, R. Daniels, H. Wong, F. Beyette, W. R. Heineman, I. Papautsky, *Electroanalysis* **2013**, *25*, 401.
- [167] S. A. Younis, T. A. Ali, P. Serp, *J. Environ. Chem. Eng.* **2021**, *9*, 106186.
- [168] Q.-X. Zhang, H. Wen, D. Peng, Q. Fu, X.-J. Huang, *J. Electroanal. Chem.* **2015**, *739*, 89.
- [169] M. Baghayeri, H. Alinezhad, M. Fayazi, M. Tarahomi, R. Ghanei-Motlagh, B. Maleki, *Electrochimica Acta* **2019**, *312*, 80.
- [170] S. P. Akanji, O. M. Ama, S. S. Ray, P. O. Osifo, in *Nanostructured Met.-Oxide Electrode Mater. Water Purif.*, Springer, **2020**, pp. 113–126.
- [171] Y. Shao, Y. Dong, L. Bin, L. Fan, L. Wang, X. Yuan, D. Li, X. Liu, S. Zhao, *Microchem. J.* **2021**, *170*, 106726.
- [172] X. Hui, M. Sharifuzzaman, S. Sharma, X. Xuan, S. Zhang, S. G. Ko, S. H. Yoon, J. Y. Park, *ACS Appl. Mater. Interfaces* **2020**, *12*, 48928.
- [173] P. R. de Oliveira, A. C. Lamy-Mendes, J. L. Gogola, A. S. Mangrich, L. H. M. Junior, M. F. Bergamini, *Electrochimica Acta* **2015**, *151*, 525.
- [174] A. A. Ensafi, F. Rezaloo, B. Rezaei, *Electroanalysis* **2017**, *29*, 2839.
- [175] W. Song, L. Zhang, L. Shi, D.-W. Li, Y. Li, Y.-T. Long, *Microchim. Acta* **2010**, *169*, 321.
- [176] J. Kudr, H. V. Nguyen, J. Gumulec, L. Nejd, I. Blazkova, B. Ruttkay-Nedecky, D. Hynek, J. Kynicky, V. Adam, R. Kizek, *Sensors* **2014**, *15*, 592.
- [177] N. Wang, E. Kanhere, A. G. P. Kottapalli, J. Miao, M. S. Triantafyllou, *Microchim. Acta* **2017**, *184*, 3007.
- [178] X. Pei, W. Kang, W. Yue, A. Bange, W. R. Heineman, I. Papautsky, *J. Electrochem. Soc.* **2014**, *161*, B3160.

- [179] H. Li, J. Zhao, S. Zhao, G. Cui, *Microchem. J.* **2021**, *168*, 106390.
- [180] N. M. Thanh, N. Van Hop, N. D. Luyen, N. H. Phong, T. T. Tam Toan, *Adv. Mater. Sci. Eng.* **2019**, *2019*.
- [181] S. Lee, J. Oh, D. Kim, Y. Piao, *Talanta* **2016**, *160*, 528.
- [182] S. Cinti, B. De Lellis, D. Moscone, F. Arduini, *Sens. Actuators B Chem.* **2017**, *253*, 1199.
- [183] F. O. Omokhodion, J. M. Howard, *Clin. Chim. Acta* **1994**, *231*, 23.
- [184] J. Kim, W. R. de Araujo, I. A. Samek, A. J. Bandothkar, W. Jia, B. Brunetti, T. R. Paixao, J. Wang, *Electrochem. Commun.* **2015**, *51*, 41.
- [185] X. Xuan, X. Hui, H. Yoon, S. Yoon, J. Y. Park, *Microchim. Acta* **2021**, *188*, 1.
- [186] X. Zhu, B. Liu, L. Li, L. Wu, S. Chen, L. Huang, J. Yang, S. Liang, K. Xiao, J. Hu, *Microchim. Acta* **2019**, *186*, 1.
- [187] M. Marton, P. Michniak, M. Behul, V. Rehacek, A. V. Stanova, R. Redhammer, M. Vojs, *Vacuum* **2019**, *167*, 182.
- [188] H. Yin, H. He, T. Li, M. Hu, W. Huang, Z. Wang, X. Yang, W. Yao, F. Xiao, Y. Wu, *Anal. Chim. Acta* **2023**, *1239*, 340730.
- [189] N. J. Ronkainen, H. B. Halsall, W. R. Heineman, *Chem. Soc. Rev.* **2010**, *39*, 1747.
- [190] A. M. Stortini, M. A. Baldo, G. Moro, F. Polo, L. M. Moretto, *Sensors* **2020**, *20*, 6800.
- [191] M. E. Ghica, C. M. Brett, *Microchim. Acta* **2008**, *163*, 185.
- [192] W. da Silva, M. E. Ghica, C. M. Brett, *Talanta* **2020**, *208*, 120427.
- [193] A. M. Ashrafi, M. Sýs, E. Sedláčková, A. Shaaban Farag, V. Adam, J. Příbyl, L. Richtera, *Sensors* **2019**, *19*, 2939.
- [194] T. Kokab, A. Shah, F. J. Iftikhar, J. Nisar, M. S. Akhter, S. B. Khan, *ACS Omega* **2019**, *4*, 22057.
- [195] K. C. Honeychurch, *Insciences J* **2012**, *2*, 1.
- [196] J. J. Gooding, D. B. Hibbert, W. Yang, *Sensors* **2001**, *1*, 75.
- [197] T. Liu, J. Yin, Y. Wang, P. Miao, *J. Electroanal. Chem.* **2016**, *783*, 304.
- [198] L. Li, Y. Zhang, L. Zhang, S. Ge, M. Yan, J. Yu, *Sci. Bull.* **2017**, *62*, 1114.
- [199] A. Khan, E.-S. Salama, Z. Chen, H. Ni, S. Zhao, T. Zhou, Y. Pei, R. K. Sani, Z. Ling, P. Liu, *Biosens. Bioelectron.* **2020**, *147*, 111763.

- [200] S. Ravikumar, I. Ganesh, I. Yoo, S. H. Hong, *Process Biochem.* **2012**, *47*, 758.
- [201] E. Mervinetsky, I. Alshanski, K. K. Tadi, A. Dianat, J. Buchwald, R. Gutierrez, G. Cuniberti, M. Hurevich, S. Yitzchaik, *J. Mater. Chem. B* **2020**, *8*, 155.
- [202] K. K. Tadi, I. Alshanski, E. Mervinetsky, G. Marx, P. Petrou, K. M. Dimitrios, C. Gilon, M. Hurevich, S. Yitzchaik, *ACS Omega* **2017**, *2*, 8770.
- [203] Y. Teng, C. K. Singh, O. Sadak, N. Ahmad, S. Gunasekaran, *J. Electroanal. Chem.* **2019**, *833*, 269.
- [204] Z. H. Ibupoto, S. M. Usman Ali, C. O. Chey, K. Khun, O. Nur, M. Willander, *J. Appl. Phys.* **2011**, *110*, 104702.
- [205] S. Mondal, C. Subramaniam, *ACS Sustain. Chem. Eng.* **2019**, *7*, 14569.
- [206] A. Touati, M. Benounis, K.-E. Boudjemaa, H. Barhoumi, *Sens. Lett.* **2016**, *14*, 1138.
- [207] M. Vestergaard, K. Kerman, E. Tamiya, *Sensors* **2007**, *7*, 3442.
- [208] K. Velusamy, S. Periyasamy, P. S. Kumar, G. Rangasamy, J. M. N. Pauline, P. Ramaraju, S. Mohanasundaram, D.-V. N. Vo, *Food Chem. Toxicol.* **2022**, 113307.
- [209] A. Syahir, K. Usui, K. Tomizaki, K. Kajikawa, H. Mihara, *Microarrays* **2015**, *4*, 228.
- [210] X. Yu, D. Xu, Q. Cheng, *Proteomics* **2006**, *6*, 5493.
- [211] X. Dai, S. Wu, S. Li, *J. Chin. Adv. Mater. Soc.* **2018**, *6*, 91.
- [212] A. G. E. Saum, R. H. Cumming, F. J. Rowell, *Biosens. Bioelectron.* **1998**, *13*, 511.
- [213] S. Jing, B. Yu, H. Qiao, Y. Huang, X. Liao, *Int J Electrochem Sci* **2017**, *12*, 5233.
- [214] G. Yang, L. Li, R. K. Rana, J.-J. Zhu, *Carbon* **2013**, *61*, 357.
- [215] X. Liu, L.-Y. Lin, F.-Y. Tseng, Y.-C. Tan, J. Li, L. Feng, L. Song, C.-F. Lai, X. Li, J.-H. He, *Analyst* **2021**, *146*, 4066.
- [216] Q. Hu, L. Su, Y. Mao, S. Gan, Y. Bao, D. Qin, W. Wang, Y. Zhang, L. Niu, *Biosens. Bioelectron.* **2021**, *178*, 113010.
- [217] J. Lee, J. Y. Yun, W. C. Lee, S. Choi, J. Lim, H. Jeong, D.-S. Shin, Y. J. Park, *Sens. Actuators B Chem.* **2017**, *240*, 735.
- [218] X. Xi, M. Wen, S. Song, J. Zhu, W. Wen, X. Zhang, S. Wang, *Chem. Commun.* **2020**, *56*, 6039.
- [219] Q. Palomar, X. Xu, R. Selegård, D. Aili, Z. Zhang, *Sens. Actuators B Chem.* **2020**, *325*, 128789.

- [220] V. Vanova, K. Mitrevska, V. Milosavljevic, D. Hynek, L. Richtera, V. Adam, *Biosens. Bioelectron.* **2021**, *180*, 113087.
- [221] Y. Zheng, Z. Ma, *Biosens. Bioelectron.* **2018**, *108*, 46.
- [222] J. Puy-Llovera, C. Pérez-Ràfols, N. Serrano, J. M. Díaz-Cruz, C. Ariño, M. Esteban, *Talanta* **2017**, *175*, 501.
- [223] A. Biela, M. Watkinson, U. C. Meier, D. Baker, G. Giovannoni, C. R. Becer, S. Krause, *Biosens. Bioelectron.* **2015**, *68*, 660.
- [224] H. Imran, P. N. Manikandan, D. Prabhu, V. Dharuman, J. Jeyakanthan, J. H. Hahn, *Sens. Bio-Sens. Res.* **2019**, *23*, 100261.
- [225] M. Hasanzadeh, N. Shadjou, M. de la Guardia, *TrAC Trends Anal. Chem.* **2017**, *89*, 119.
- [226] L. He, R. Huang, P. Xiao, Y. Liu, L. Jin, H. Liu, S. Li, Y. Deng, Z. Chen, Z. Li, *Chin. Chem. Lett.* **2021**, *32*, 1593.
- [227] A. V. Lakhin, V. Z. Tarantul, L. Gening, *Acta Naturae Англоязычная Версия* **2013**, *5*, 34.
- [228] V. Mishyn, M. Aslan, A. Hugo, T. Rodrigues, H. Happy, R. Sanyal, W. Knoll, F. Baudoux, V. Bouchiat, R. O. Bilyy, *Sens. Diagn.* **2022**, *1*, 739.
- [229] K. Y. Goud, S. K. Kailasa, V. Kumar, Y. F. Tsang, K. V. Gobi, K.-H. Kim, *Biosens. Bioelectron.* **2018**, *121*, 205.
- [230] A. Moradi, H. Adibi, V. Akbari, A. R. Jalalvand, *Sens. Bio-Sens. Res.* **2022**, *37*, 100516.

## **Chapter 2. Zincon-Modified CNTs Electrochemical Tool for Salivary and Urinary Zinc Detection**

This chapter includes a published peer-reviewed paper. The bibliographic details of the coauthored paper, including all authors, are:

*Daniela Vieira*, Jérôme Allard, Kathleen Taylor, Edward J Harvey, Geraldine Merle

Published in: *Nanomaterials* 2022, 12(24), 4431; <https://doi.org/10.3390/nano12244431>

My contributions to the paper involved: Experimental design, implementation, and performance; Data collection and analysis; Preparation of the manuscript.

The chapter II “*Zincon-Modified CNTs Electrochemical Tool for Salivary and Urinary Zinc Detection*” shows the ability of a simple molecule to assure high selectivity for the electrochemical detection of mobile zinc in a variety of media, including a buffer solution containing important bio metals, and two artificial biofluids, urine and saliva. The simple molecule, zincon, was covalently attached to CNTs increasing its stability and improving the electron transfer capability between the electrode surface and zinc ions. The designed zincon-CNT system presented great ability on the detection of mobile zinc, showing LOD of 20 and 30 ng·ml<sup>-1</sup> in urine and saliva, respectively, and efficacy of ~70% after 1 year storage at room temperature.

## Zincon-Modified CNTs Electrochemical Tool for Salivary and Urinary Zinc Detection

*D. Vieira*<sup>1</sup>, *J. Allard*<sup>2</sup>, *K. Taylor*<sup>2,3</sup>, *E. Harvey*<sup>1</sup> and *G. Merle*<sup>1,2,\*</sup>

<sup>1</sup> McGill University, Faculty of Medicine, Department of Experimental Surgery, 1650 Cedar Avenue, A7-117 Montreal, QC H3G 1A4, Canada; daniela.vieira@mail.mcgill.ca (D.V.); edward.harvey@mcgill.ca (E.H.)

<sup>2</sup> Polytechnique Montreal, Department of Chemical Engineering, J.-A.-Bombardier Building, Office 2067, Montreal, QC H3C 3A7, Canada; jerome.allard@polymtl.ca (J.A.); ktaylorh@comcast.net (K.T.)

<sup>3</sup> Georgia Institute of Technology, Department of Chemical and Biomolecular Engineering, 311 Ferst Dr, Atlanta, GA 30318, USA

**Abstract:** Recently, the abnormal level of zinc emerged as a powerful indicator or risk factor for metabolic, endocrine, neurodegenerative, and cardiovascular diseases, including cancer. Electrochemical detection has been explored to quantify zinc in a precise, rapid, and non-expensive way; however, most of the current electrochemical systems lack in specificity. In this work we studied a highly selective and sensitive electrochemical method to detect quickly and reliably free zinc ions ( $Zn^{2+}$ ). The surface of the working electrode was modified with zincon electropolymerized on carbon nanotube (CNT) to enable the binding of zinc in complex body fluids. After being physicochemically characterized, the performances of the zincon-CNT complex were electrochemically assessed. Square Wave Voltammetry (SWV) was used to determine the calibration curve and the linear range of zinc quantification in artificial saliva and urine. This zincon- CNT system could specifically quantify mobile  $Zn^{2+}$  in salivary and urinary matrices with a sensitivity of  $\sim 100 \text{ ng.ml}^{-1}$  and a limit of detection (LOD) of  $\sim 20 \text{ ng.ml}^{-1}$ . Zincon-modified CNT presented as a desirable candidate for the detection and quantification of free zinc in easily body fluids that potentially can become a diagnostic non-invasive testing platform.

**Keywords:** electrochemical detection; carbon nanotube; zinc quantification; zincon; complexation; saliva; urine.

## 1. Introduction

Metallomics is a systematic study on the identification and concentration of essential metals for life processes. It is becoming fundamental for the understanding of biological systems. Metals are crucial for bodily function and are directly involved on a variety of biochemical processes such as osmotic regulation, catalysis, metabolism, and cell signaling<sup>[1-3]</sup>. Despite their vital role, metal deficiency or overexpression are associated with several health conditions. The monitoring of the concentration of some essential metals may help to identify, track progression, and evaluate the impact of therapeutic agents in a variety of diseases <sup>[2-5]</sup>.

Zinc (Zn) is one of the most abundant trace elements in the body and it is essential for more than 300 enzyme functionalities <sup>[6-8]</sup>. Zinc plays a crucial role to intracellular communication, immune system, homeostasis, apoptosis, DNA repair and replication, balancing oxidative stress, and the aging process <sup>[7,9,10]</sup>. The deficiency or excess of zinc is potentially a powerful indicator of risk factor for various health issues, including metabolic, endocrine, neurodegenerative, cardiovascular diseases, and cancer <sup>[4,5,11]</sup>. Salivary and/or urinary zinc level is abnormal in a variety of cancer <sup>[8,12]</sup>, including prostate <sup>[13-15]</sup>, oral <sup>[16,17]</sup>, breast <sup>[15,18-21]</sup>, pancreatic <sup>[15,22]</sup>, brain <sup>[23]</sup>, lung<sup>[24]</sup> and bladder <sup>[25]</sup> (**Table 2.1**).

**Table 2.1** - Some examples of abnormal expression of salivary and urinary zinc for different types of cancer.

Cancer	Salivary Zinc (ng.ml <sup>-1</sup> )		Urinary Zinc (ng.ml <sup>-1</sup> )		Reference(s)
	Healthy*	Unhealthy*	Healthy*	Unhealthy*	
<b>Prostate</b>	~270	~630	~400	~675	[13–15,26]
<b>Oral</b>	~360	~150	-	-	[16,17]
<b>Breast</b>	~600	~1010	~320	~602	[15,18–21]
<b>Pancreatic</b>	-	-	~400	~945	[15,22]
<b>Brain</b>	~540	~410	-	-	[23]
<b>Lung</b>	-	-	~570	~1500	[24]
<b>Bladder</b>	-	-	~470	~1000	[25]

\* Mean values. Note the concentration may change depending on sex, age, and stage of the disease; —no data found in the literature.

The detection and quantification of zinc through saliva and/or urine is ideal because it enables non-invasive sampling, high volume collection, and ease repeatability of measurements when compared to blood, plasma, or tissues specimens [15,27]. Common applied methods to quantify zinc involve atomic absorption spectroscopy, inductively coupled plasma mass spectrometry, and Raman spectroscopy [4,28]; however most tests utilize sizable machinery and highly qualified personnel, are time consuming, and costly. Salivary and urinary zinc could be easily accessible through electrochemical techniques with a user-friendly, precise, and specific quantification without invasive or costly testing.

The most common electrochemical systems applied to detect and quantify zinc involve mercury and bismuth electrodes [28–32]. Besides their great ability to detect zinc, mercury is extremely toxic, and bismuth is usually applied as a co-deposited film, being invalid for many applications [29–31]. Other materials such as carbon-based electrodes (carbon nanoparticles, carbon nanotube e, graphene), show very low limit of detection (LOD), reaching nM [28,29,33]; however, carbon alone

does not present specificity and barely have been tested in body fluids for zinc detection and quantification. One of the emergent strategies to assure the specificity of carbon-based electrodes towards zinc detection is through the functionalization of carbon with molecules that allow complexation with zinc [34,35]. EDTA [36], amino acids [37] and zincon [26] are promising mediators for electron transfer by complexing and de-complexing zinc [34,35]. In this way, zincon stands out as metal chelator (Pb, Cu and Zn) and demonstrates great ability on the detection of metallic content in environmental and biological samples by colorimetric methods [26,38,39]. Recently, zincon has been explored as a complex agent in electrochemical systems for heavy metals quantification (Zn and Pb) [26,39]. Most of studies applied zincon electro-polymerization to modify the carbon-based electrodes [40–43], which must be extremely well controlled to avoid the blockage of the active sites [44,45]. A zincon exfoliated graphite electrode, to quantify free zinc ions in prostate fluid, was built via the  $\pi$ - $\pi$  stacking interaction [26]. Unfortunately, this novel system presented a high LOD and poor stability probably because of the instability of the non-covalent bind between the ink and the exfoliated graphite. New alternatives must be investigated to ensure stability and conductivity of zincon carbon-based electrodes.

In this work, we engineered a fast, non-invasive, precise, and specific electrochemical zinc sensor based on the covalent grafting of zincon on multi-walled carbon nanotubes (CNTs). CNTs offer excellent intrinsic properties such as high surface area, chemical stability and high electrical conductivity ( $10^6$ – $10^7$  S/m)<sup>[46]</sup>, becoming one of the most attractive nanomaterials in electrochemical sensing [47–49]. Through a better immobilization and stabilization of zincon on CNTs, we hypothesized that the system's performance will be strongly enhanced and that the electron transfer will be facilitated leading to an increased LOD and specificity and a minimization of interferences— a critical feature given bodily fluids have thousands of metabolites<sup>[26,50]</sup>. Among

the different immobilization methods <sup>[49]</sup>, the covalent grafting was chosen via an in situ radical polymerization using potassium persulfate as a radical initiator, followed by refluxing with concentrated hydrochloric acid <sup>[47]</sup>. The resulting zincon-modified CNT sensor was physiochemically characterized and tested in buffer and artificial biofluids, i.e., saliva and urine, demonstrating great ability to quantify zinc when simulating its concentration for different types of cancer.

## 2. Materials and Methods

### *2.1 Materials and Chemicals*

Zincon monosodium salt and glassy carbon electrodes (GCE) were purchased from Alfa Aesar, Haverhill, MA, USA. Copper sulfate (99.99%), magnesium sulphate (99.99%), manganese chloride (97%), iron sulfate heptahydrate (98%), calcium chloride (93%), anhydrous, cobalt chloride hexahydrate (98%), and nickel sulfate hexahydrate (99%) were purchased from Sigma Aldrich. Carbon nanotubes (CNTs) were purchased from Sigma-Aldrich, Darmstadt, Germany. Artificial saliva (#1700-0305) was purchased from Pickering laboratories, Park Way, Mountain View, CA, USA. Artificial urine (control #IS5080) was purchased from Aldon Corporation, Avon, NY, USA (Table 2.2). All the other chemicals and materials used in this work were purchased from Fisher Scientific, Scotia Court, ON, Canada.

**Table 2.2** - Chemical composition of commercial artificial urine and saliva.

Artificial Saliva (g.l <sup>-1</sup> ) [51]		Artificial Urine (g.l <sup>-1</sup> ) [52]	
Sodium Chloride	1.594	Urea	25
Ammonium Nitrate	0.328	Sodium Chloride	9
Potassium Phosphate	0.636	Disodium Hydrogen orthophosphate	2.5
Potassium Chloride	0.202	Potassium dihydrogen orthophosphate	2.5
Potassium Citrate	0.308	Ammonium chloride	3
Uric Acid Sodium Salt	0.021	Creatinine	2
Urea	0.198	Sodium sulphite	3
Lactic Acid Sodium Salt	0.146		
Mucin	5		

### 2.2 Zincon-Modified CNT

Zincon-modified CNT was prepared adapting the protocol of Zhang et al. [47]. Briefly, 1 g of zincon monosodium salt (100%, Alfa Aesar, Haverhill, MA, USA) was dissolved in 100 mL of ultrapure water (Milli-Q, Merck, Darmstadt, Germany), and then 50 mg of multi walled carbon nanotubes (CNTs) (>98%, Sigma-Aldrich, Oakville, ON, Canada) was added. After sonication for 1 h, the black solution was stirred for another 3 h at room temperature. Afterwards, the mixture was purged with nitrogen gas for 30 min to remove oxygen and 0.25 g of potassium persulfate (>99%, Fisher Scientific, Scotia Court, ON, Canada) was added into as a radical initiator. The solution was stirred continuously at 70 °C for 3 h, followed by at 85 °C for 1 h. The solution was filtered through a 0.22µm nylon membrane (GVS, Fisher Scientific, Scotia Court, ON, Canada), washed several times with ultrapure water and redissolved in concentrated hydrochloric acid (HCl) (35–39%, Fisher Scientific, Scotia Court, ON, Canada) for 12 h at 100 °C. Finally, after being filtered through a 0.22µm nylon membrane, the zincon-modified CNT product was washed several times with ultrapure water until pH 7 is reached. The black powder was dried overnight at 45 °C in incubator (Blue M 100A, Blue Island, IL, USA). Solution containing 1 mg.ml<sup>-1</sup> zincon-modified CNT in ethanol (89–91%, Fisher Scientific, Scotia Court, ON, Canada) were prepared and stored.

Solutions containing 1 mg.ml<sup>-1</sup> of pristine CNT was also prepared. Glassy carbon electrodes (GCE) (5 mm, Alfa Aesar, Haverhill, MA, USA) were polished with 0.05µm Al<sub>2</sub>O<sub>3</sub> (Fisher Scientific, Scotia Court, ON, Canada) suspension to achieve a shiny surface. GCEs were cleaned by sonication in 10% H<sub>2</sub>SO<sub>4</sub> (98%, Fisher Scientific, Scotia Court, ON, Canada), 50% acetone (≥ 99.5%, Fisher Scientific, Scotia Court, ON, Canada) and ultrapure water each for 10 min, successively. The electrodes were dried at room temperature. Finally, 10 µL of the zincon-modified CNT solution was dropped onto the cleaned GCE and dried at room temperature. Pristine CNT was also performed following the same procedure.

### *2.3 Materials Characterization*

The morphology of CNT and zincon-modified CNT electrodes was investigated by Scanning Electron Microscopy (SEM, Inspect F50, FEI Company, Hillsboro, OR, USA). ImageJ software (National Institutes of Health, Stapleton, New York, United States) was applied to measure the diameter of CNT and zincon-modified CNT ( $n = 10$ ). Fourier transform infrared spectroscopy (FT-IR—PerkinElmer) was carried out in the wavenumber range of 4000 to 400 cm<sup>-1</sup> to confirm the grafting of zincon on CNT. Electrochemical experiments were performed using a potentiostat (VersaSTAT 4, Princeton Applied Research, Oak Ridge, TN, USA) with a three-electrode system cell, where GCE, CNT, zincon-modified CNT were used as work electrodes, Pt wire as counter electrode and saturated calomel electrode (SCE) as reference electrode. The electrochemical behavior was tested in different solutions, such as, 1 mM K<sub>4</sub>Fe (CN)<sub>6</sub> in a 0.1 M KCl (99%, Fisher Scientific, Scotia Court, ON, Canada), buffer (0.1 M Tris-HCl pH 7.5), artificial saliva (Pickering laboratories, Park Way, Mountain View, CA, USA) and artificial urine (Aldon Corporation, Avon, NY, USA) solutions in presence and/or absence of zinc (Zinc acetate, anhydrous, >99.9%, Fisher

Scientific, Scotia Court, ON, Canada). Note that saliva and urine solutions were diluted by 50% with buffer (pH 7.5). Cyclic voltammetry (CV) was carried out in the presence and absence of zinc. The potential was scanned from  $-0.8$  V to  $-1.3$  V (vs. SCE) at scan rate of  $50 \text{ mV}\cdot\text{s}^{-1}$ . Square wave stripping voltammetry (SWV) was performed to characterize the electrochemical detection of Zn using CNT and zincon-modified CNT electrodes. The potential of deposition was selected at  $-1.40$  V (vs. SCE), applied for 300 s, and followed by a SWV, from  $-1.4$  V to  $-0.7$  V (vs. SCE), at 10 Hz, amplitude of 25 mV, and step potential of 40 mV. A pre time (adsorption time) of 180 s was applied (with no potential applied, electrical connections were disconnected to the electrode). All analysis were performed in triplicates ( $n = 3$ ). Linear fit was obtained using OriginPro (OriginLab Corporation, version 2018G, Northampton, MA, USA) software. Different parameters of zinc deposition (time and potential) were studied to verify the best performance. Zincon-modified CNT electrodes were tested using different concentrations of zinc solutions (from 0 to  $1000 \text{ ng}\cdot\text{mL}^{-1}$ ). Experiments were performed in triplicates.

Limit of detection (LOD) was calculated according to the Formula (1):

$$\text{LOD} = 3 \times (\text{SD}/\text{S}) \quad (1)$$

where, SD is the standard error intercept and the S is the slope of the calibration curve (S), both extracted from origin software after linear regression.

## 2.4 Statistics

The data were analyzed using OriginPro (OriginLab Corporation, version 2018G) and presented as mean  $\pm$  SD. Repeatability standard deviation was obtained by the square foot of the variance. Stability was calculated according to Formula (2):

$$\text{Stability} = 100\% - |\text{Relative deviation}| \quad (2)$$

where  $\text{relative deviation} = \left( \frac{\text{different time detection value} - \text{baseline}}{\text{baseline}} \right) \times 100$ .

## 3. Results and Discussion

### 3.1 Materials Characterizations

In this work, we proposed a covalent polymerization of zincon on CNTs to maximize the specificity and ability of the modified CNTs for the quantification of free zinc. As noted above the synthesis was performed in water solution, adding potassium persulfate (KPS) as a free radical initiator, followed by HCl reflux. Zincon not only acted as a reaction monomer but also as a dispersant of pristine CNT in water because of the presence of hydrophilic and hydrophobic chains, dismissing the use of additional dispersants<sup>[47,53]</sup>. CNTs tend to agglomerate due to the van der Waals forces. Here, the presence of sulfonated group in zincon assures hydrophilicity and electrostatic repulsion to overcome the van der Waals attraction of CNT, while the hydrophobic part form  $\pi$ - $\pi$  stacking interaction with the CNT<sup>[47]</sup>. The covalent functionalization enables strong interfacial interactions on CNTs. In addition, it is expected a better dispersion, facilitating the flow of electrons and enhancing the interaction between the analyte and the electrode surface<sup>[54,55]</sup>. The suggested mechanism of the covalent grafting facilitated by KPS and, the morphology of CNT and

zincon-modified CNT is demonstrated in **Figure 2.1A**. The surface morphologies of zincon-modified CNT, and CNT electrodes are shown in **Figures 2.1B,C**. Low magnification SEM analysis showed a higher quality dispersion of CNT onto electrodes as less aggregates are observed on the zincon-modified CNT electrode surface. As mentioned, this is probably the result of the sulfonic groups on benzene ring that ensure adequate electrostatic repulsions<sup>[47,53]</sup>. In **Figure 2.1B**, the coating appears to be denser for CNT- compared to the zincon-modified CNTs coating. The pristine CNTs are tangled together, due to the van der Waals attractions between tubes. After grafted with zincon, the materials because of the sulfonic group of the zincon, have a much better dispersibility than pristine CNTs. At higher magnification, the morphology of the CNTs appears to be unchanged, confirming that after the zincon polymerization treatment, no obvious alterations of the tubular structure of CNTs could be observed (**Figure 2.1B**). The CNT fiber's diameter was measured using ImageJ software ( $n = 10$ ). Untreated CNTs and zincon-modified CNTs presented similar diameters of  $18.07 \pm 3.15$  nm and  $18.54 \pm 1.42$  nm, respectively, indicating that the graft of zincon does not affect the tubular structure of CNTs. Similar effect has been already observed using same chemical treatment to graft poly(*p*-styrenesulfonic acid) onto multi-walled carbon nanotubes<sup>[47]</sup>.

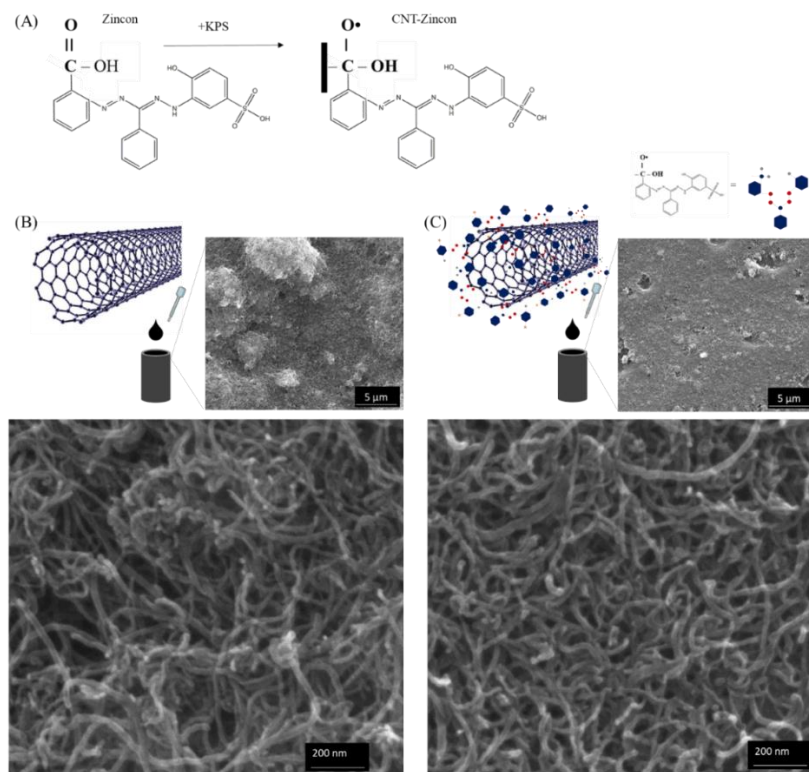


**Figure 2.1** - (A) Suggested mechanism of covalent grafting facilitated by KPS and, schematic of (B) CNT and (C) zincon-modified CNT followed by SEM images (low and high magnitude), where hexagon, gray dots, blue dots, red dots, and star represent aromatic group, oxygen element, carbon element, nitrogen element and Sulfonic acid, respectively.

The successful grafting of zincon on CNT was confirmed by FT-IR (**Figure 2.2A**) and cyclic voltammetry (CV) (**Figure 2.2B**). The FT-IR spectrum of zincon-modified CNT (**Figure 2.2A**) showed, as expected, additional peaks compared to pristine CNTs at  $\sim 1660\text{ cm}^{-1}$  and at  $\sim 1530\text{ cm}^{-1}$  are attributed to C=N stretching and N=N stretching, respectively. The peaks at  $\sim 1500\text{ cm}^{-1}$  and  $\sim 1350\text{ cm}^{-1}$  are due to the benzene ring vibration of the zincon<sup>[40,56,57]</sup>. The broad band in the region at  $\sim 1250\text{ cm}^{-1}$  to  $750\text{ cm}^{-1}$  could be attributed to the stretching of C-C and C-O in the carbon after the treatment with concentrated hydrochloric acid for 12 h<sup>[56]</sup>. It should be noticed

that the as-received CNTs were purified by the manufacturer and partial oxidation during purification by the manufacturer can result in the presence of groups on the surface of pristine carbon nanotube. The peak  $\sim 3700\text{ cm}^{-1}$ , for both CNT and zincon-modified CNT, could be related to the absorption of water molecules as a result of an O-H stretching mode of hydroxyl groups [47,56]. The peaks at  $\sim 2670\text{ cm}^{-1}$ ,  $2320\text{ cm}^{-1}$ ,  $2097\text{ cm}^{-1}$ , and at  $1990\text{ cm}^{-1}$  could be attributed to the C=C asymmetric stretching in graphite-like CNT structure [58].

The cyclic voltammogram of zincon-modified CNT (**Figure 2.2B**) clearly showed the reduction ( $\sim 0\text{ V}$  and  $-0.6\text{ V}$  vs. SCE) and oxidation ( $-0.4\text{ V}$  and  $\sim 0.1\text{ V}$  vs. SCE) peaks for zincon [43] and demonstrated a good stability after 10 cycles of CV (**Figure 2.2.C**).

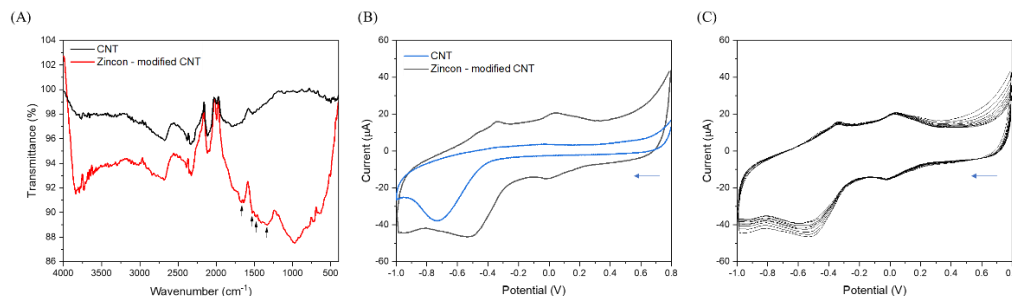


**Figure 2.2** - (A) FTIR spectrum of CNT and zincon–modified CNT, where black arrows show the zincon peaks. (B) CV showing the reduction and oxidation peaks of zincon present on CNT after grafting process. The zincon–modified CNT showed good stability after (C) 10 CVs on tris–HCl (pH 7.5), scan rate 10 mV/s. The blue arrows mean the direction of the CV from + to -.

Carbon structures have been previously modified with zincon through the electropolymerisation of poly-zincon films [40–43] or  $\pi$ - $\pi$  stacking interaction [26]. However, as mentioned before, both techniques may suffer from loss of conductivity because of the enclosed surface and/or the zincon attachment instability- signal loss after few measurements if the polymer attachment is not well

controlled [44,45]. The covalent polymerization grafting process assures a more robust and stable connection between the zincon compound and the CNTs in comparison to noncovalent procedures, generating a more effective electrode interface [59–62].

### 3.2 Electrochemical Behavior

Cyclic voltammetry of the ferrocyanide/ferricyanide redox couple ( $\text{Fe}(\text{CN})_6^{3-/4-}$ ) was used to verify the grafting of zincon on CNT (**Figure 2.3A**). As expected, an increase of  $\sim 42\%$  in peak current density ( $I_{\text{pa}} = \sim 10 \mu\text{A}$ ), and a decrease of  $\sim 53\%$  in peak width ( $\Delta E_{\text{p}} = \sim 77 \text{ mV}$ ) can be observed in the  $\text{Fe}(\text{CN})_6^{3-/4-}$  voltammograms (**Figure 2.3A**), after deposition of CNTs on GCE because of the electron transport kinetics at the electrode. Successive attachment of zincon onto CNTs leads to a drop of  $\sim 58\%$  in peak current density ( $I_{\text{pa}} = \sim 7 \mu\text{A}$ ) and growing of  $\sim 47\%$  in peak width ( $\Delta E_{\text{p}} = \sim 145 \text{ mV}$ ), attributed to a loss of conductivity. These results were consistent with FTIR and previous CV, confirming the successful grafting of zincon on CNT.

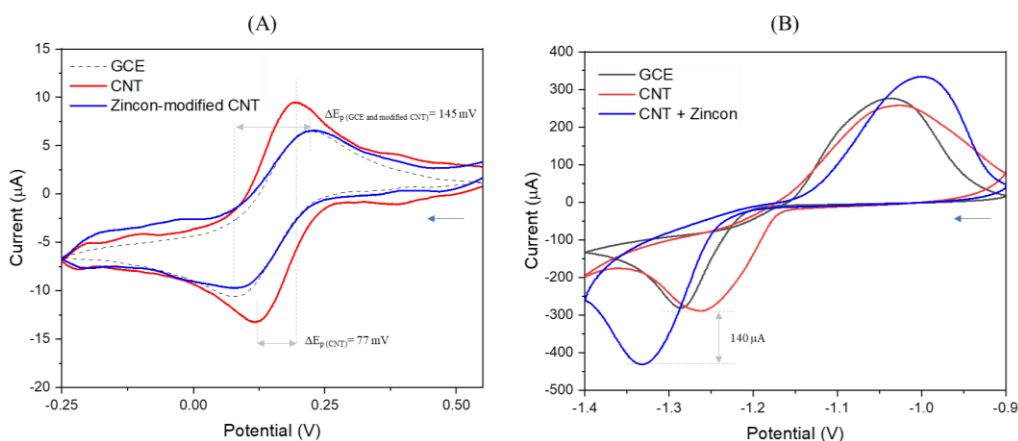


**Figure 2.3** - CVs for GCE, CNT and zincon–modified CNT in (A) 1 mM  $\text{K}_4\text{Fe}(\text{CN})_6$  in a 0.1 M KCl and (B) tris HCl (pH 7.5) containing  $0.5 \text{ mg} \cdot \text{ml}^{-1}$  of zinc. The blue arrows mean the direction of the CV from + to -.

Besides the reduction of the redox currents when compared to CNTs, in **Figure 2.3B** it is clear that zincon-modified CNT influences the quantification of zinc. CVs response in buffer for GCE, CNT and zincon-modified CNT showed an increase on both reduction and oxidation peaks when zincon was applied. A shift in the reduction potential was observed for the different electrodes (**Figure 3B**). The unmodified GCE and pristine CNT showed reduction peaks at  $\sim -1.3$  V and  $\sim -1.25$  V, respectively; whereas the zincon-modified CNT showed reduction peak at  $\sim -1.34$  V. Pristine CNT electrode showed the lowest peak separation ( $\sim 0.23$  V), indicating higher reversibility of  $\text{Zn}^0/\text{Zn}^{+2}$  and higher number of active sites <sup>[63]</sup>. However, the peak current intensity is lower than zincon-modified CNT. The reduction current intensity increased by  $\sim 140\mu\text{A}$  for the modified electrode when compared to pristine CNT, suggesting the greater capability of the compound for the quantification of zinc.

The mechanism behind the detection is probably attributed to the zincon quadridentate ligand property, coordinating zinc ions with two oxygens (OH and COOH) and two nitrogens (N=N and NH) <sup>[26,50,64]</sup>. Further, the complexed  $\text{Zn}^{+2}$  is preconcentrated onto the electrode surface at  $-1.4$  V (vs. SCE) for 300 s, allowing the reduction for  $\text{Zn}^0$ . Followed by a potential scan (from  $-1.3$  V to  $-0.7$  V), the zinc stripped back to the solution ( $\text{Zn}^0 \rightarrow \text{Zn}^{+2}$ ) and the current intensity is measured in function of concentration of zinc (**Figure 2.4**). Note that the pH is a very important parameter to assure the complexation. Zincon can also complex with other metals, such copper, iron, cobalt, and nickel; however, the optimized pH for these metals and zincon complexation is at  $\text{pH} \sim 5$  <sup>[64,65]</sup>. The optimized zincon-zinc complexes occur in  $\text{pH} > 7.0$ , being inefficient for  $\text{pH} < 6.0$  <sup>[26,64]</sup>. To ensure the complexation between zincon-zinc, a pre-time of 180 s was used before metal deposition and the stripping steps.

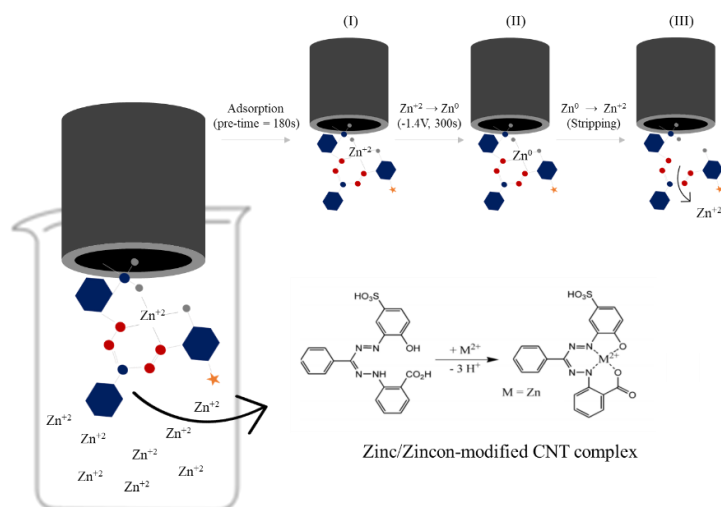


**Figure 2.4** - Schematic of complexation mechanism of zincon–modified CNT and  $Zn^{+2}$ ; (I) adsorption, (II) reduction and (III) stripping step. The hexagon, gray dots, blue dots, red dots, and star represent aromatic group, oxygen element, carbon element, nitrogen element and sulfonic acid, respectively.

We first studied the ability of zincon-modified CNT on the quantification of free zinc in a buffer setup. The linear range and limit of detection (LOD) of zinc by zincon-modified CNT was determined by square wave voltammetry (SWV), varying the concentration of zinc from 0 to 1000  $ng.ml^{-1}$ , in a Tris HCl (pH 7.5) buffer solution. Figure 2.5 shows the increase of the ability for the quantification of zinc when zincon was grafted on CNT.

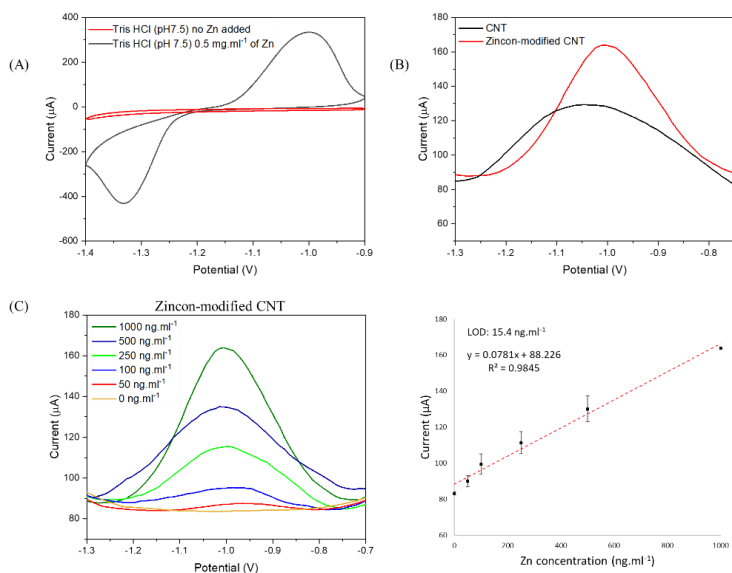


**Figure 2.5** - . Study of the electrochemical detection of Zn<sup>+2</sup> on 0.1 M Tris–HCl (pH 7.5) solution. (A) CV in absence and presence of 0.5 mg.ml<sup>-1</sup> of Zn<sup>+2</sup>. (B) SWV showing the increase of current after grafting of zincon on CNT in Tris–HCl solution containing concentration of Zn<sup>+2</sup> = 1 μg.ml<sup>-1</sup>, and (C) SWV of zincon–modified CNT varying Zn<sup>+2</sup> concentration from 0 to 1000 ng.ml<sup>-1</sup> and its linear fit (n = 3).

**Figure 2.5A** shows the CV of zincon-modified CNT in presence and absence of zinc. The zinc reduction and oxidation peaks, at ~-1.3 V and ~-1 V (vs. SCE), respectively, were found in a well-defined shape. As expected, no peaks were found in buffer without addition of zinc. In order to confirm the improvement of zinc detection by the complexation mechanism with zincon, we compared the current responses for CNT and zincon-modified CNT in presence of 1 μg.ml<sup>-1</sup> of zinc (**Figure 2.5B**). The zincon-modified CNT electrode showed more efficacy for the detection of zinc, where the current intensity enhanced by ~40 μA when compared to pristine CNT (160 μA and 120 μA, respectively). Further, LOD was determined by SWV for zincon-modified CNT in a buffer solution varying the concentration of zinc. **Figure 2.5C** shows the linear response of current

intensity in function of the concentration of zinc. Zincon-modified CNT system was able to quantify  $50 \text{ ng}\cdot\text{ml}^{-1}$  of zinc and presented a LOD of  $15.4 \text{ ng}\cdot\text{ml}^{-1}$ . A zincon-modified exfoliated graphite electrode based on  $\pi$  stacking was designed in order to quantify free zinc in prostate fluids [50]. The system could only quantify  $250 \text{ ng}\cdot\text{ml}^{-1}$  of free zinc whereas our electrode could quantify  $50 \text{ ng}\cdot\text{ml}^{-1}$ , 5-fold less than the  $\pi$  stacking system, probably attributed to the stronger connection between zincon and carbon structure via a covalent in situ polymerization. It has been previously shown using UV-vis spectroscopy that zincon in solution with same quantity of bivalent metals such as Zn, Cu, Cd, Pb, Co, Ca, Ni, Ba, Mg and Mn, only changes in color with  $\text{Cu}^{2+}$  similarly to  $\text{Zn}^{2+}$ . Based on this observation [26], an interference study was performed on the zincon-modified CNT electrode (**Figure 2.6**). We chose Ca, Cu, Co, Mg, Mn, and Fe since they are the most common metals in body and quite often presented in body fluid samples [5,66] and may interfere with  $\text{Zn}^{2+}$  detection. The detection of these bivalent metals was performed using CV and SWV, and as it can be seen, peak of  $\text{Zn}^{2+}$  (about potential  $-1 \text{ V}$ ) is well separated from other metals (**Figure 2.6**).

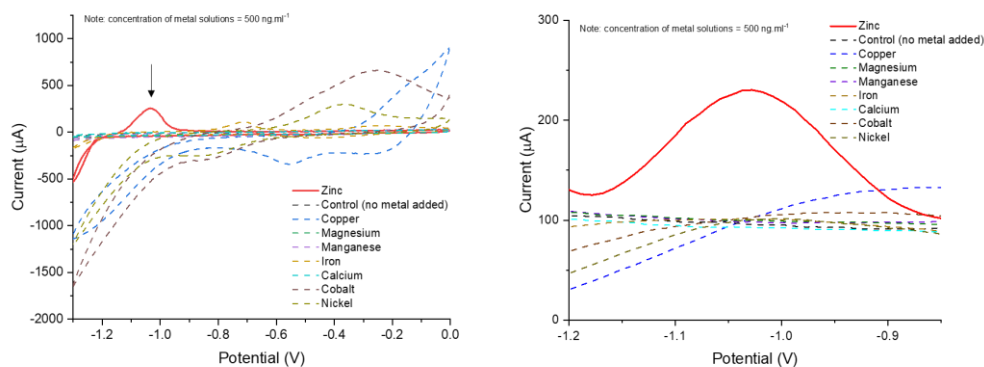


**Figure 2.6** - CV in absence and presence of  $0.5 \text{ mg} \cdot \text{ml}^{-1}$  of bivalent metals in  $0.1 \text{ M}$  Tris-HCl (pH 7.5) solution. SWV showing the increase of current after grafting of zincon on CNT in Tris-HCl solution containing concentration of  $\text{Zn}^{+2}$  and other metals at a concentration of  $0.5 \text{ mg} \cdot \text{ml}^{-1}$ .

SWVs showed that the presence of other metals did not affect the peak heights, confirming that all the tested metallic ions exhibited no apparent interference in  $\text{Zn}^{+2}$  detection. To further study, interferences and contaminants, the viability of the zincon system reported here as a sensor was verified in 2 different artificial body fluids—urine, and saliva. Urine and saliva have been specifically explored as diagnostic fluids, because they are a source of biomarkers, allowing non-invasive analysis<sup>[15,27]</sup>. **Figure 2.7** shows the CV and SWV for zincon-modified CNT in artificial urine and saliva solutions.

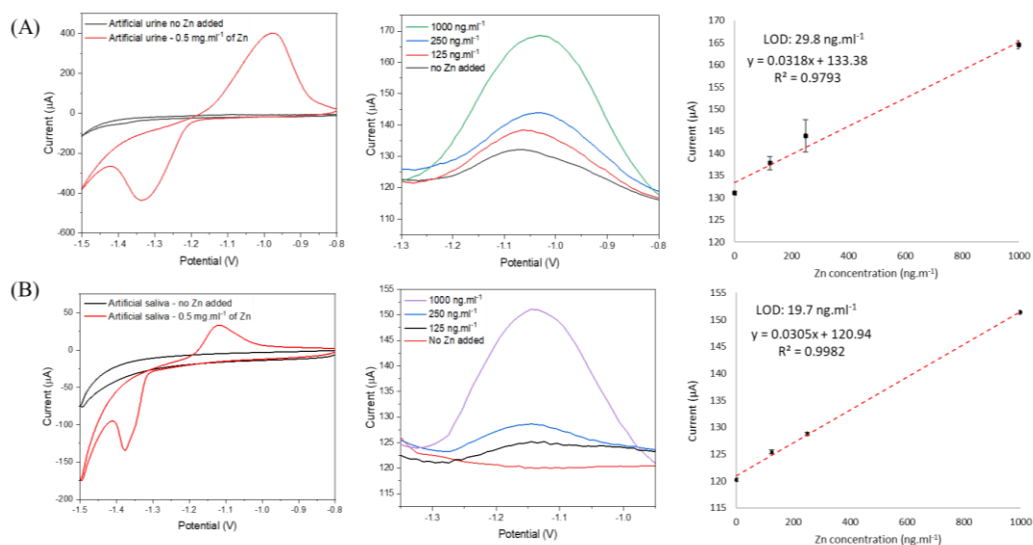


**Figure 2.7** - Salivary and urinary zinc quantification using zincon-modified CNT electrode. CV in absence and presence of zinc and SWV varying zinc concentration from 0 to 1000 ng·ml<sup>-1</sup> in artificial (A) urine and (B) saliva, respectively (n = 3).

The ability of zinc quantification in body fluids was studied by CV and SWV. In artificial urine (**Figure 2.7A**) a background reduction peak (at ~-1.4 V) was observed when zinc was absent, this is probably because of the elements present in the artificial urine (**Table 2.2**). Stronger and well-defined reduction and oxidation peaks were observed in presence of 0.5 mg·ml<sup>-1</sup> of zinc. Same behavior could be seen by SWV, where in absence of added zinc a background current was observed, increasing the intensity as the concentration of zinc increased. Similar behavior was observed in artificial saliva with the increase of concentration of zinc; however, no background signals were found in absence of zinc (**Figure 2.7B**). The zincon-modified CNT showed affinity for the detection and quantification of free zinc when simulating both body fluids, presenting linear detection from 125 ng·ml<sup>-1</sup> and LOD of ~30 ng·ml<sup>-1</sup> and ~20 ng·ml<sup>-1</sup> for urine and saliva, respectively. We have tested repeatability of the system by the repeatability standard deviation,

which can be measured by the square root of the variance. For the buffer, saliva and urine, the repeatability standard deviation was  $\pm 7.07 \mu\text{A}$ ,  $\pm 0.55 \mu\text{A}$  and  $\pm 3.28 \mu\text{A}$ , respectively. The system showed stability of  $\sim 65\%$  after 1 year. The designed zincon-modified CNT system not only showed considerable sensitivity but also presented the advantages of simplicity and lower LOD.

Salivary and/or urinary zinc levels are a powerful indicator of risk factor for a variety of cancer as shown in **Table 2.1**. The designed zincon-modified CNT system could quantify zinc in various circumstances, being an additional possible source of information for both the diagnosis and judgement of treatment efficacy. When compared to different works in the literature (**Table 2.3**), the zincon-modified CNT showed great potential to be applied as zinc sensor. Investigating current studies, only a few were able to quantify zinc in saliva or urine, and most of them were performed in serum or other fluids, needing an invasive procedure. Our system also presented competitive results when compared to commercial colorimetric zinc rapid test for biological fluids, including urine and saliva, where the quantification is from  $200 \text{ ng}\cdot\text{ml}^{-1}$  (Zinc Assay Kit—abcam 102507),  $\sim 2$ -fold lower than the zincon-modified CNT demonstrated here. Our engineered electrode demonstrated simplicity, low-cost, specificity and great ability to detect and quantify free Zinc.

**Table 2.3** - Comparison of reported electrochemical quantification of zinc in different body fluids.

Strategy	Range of Detection (ng.ml <sup>-1</sup> )	LOD (ng.ml <sup>-1</sup> )	Disadvantages	Sample	Ref.
Bismuth-Graphene Oxide	20–8000	6 (buffer)	In situ bismuth co-deposition/Zinc needs extra extraction steps	Seminal Fluid	[67]
Zincon exfoliated graphite	250–1500	5 (buffer)	Zinc needs extra extraction steps	Serum	[26]
Nafion-Gold electrode	180–2500	18 (buffer)	Zinc needs extra extraction steps	Serum	[68]
Polyethyleneimine, poly (sodium 4-styrenesulfonate), and mercury nitrate on Carbon fibers	20–2000	9 (buffer)	Use of mercury compound (toxic)	Blood and Urine	[69]
Zincon-modified CNT	<b>125–1000</b>	<b>15 (buffer)</b> <b>20 (urine)</b> <b>30 (saliva)</b>		Saliva and Urine	This work

#### 4. Conclusions

Here, we report a new generation of organic/inorganic nanocarbon based sensing material using a striking synthetic approach capable of quantify mobile zinc ions in biofluids, i.e., saliva and urine. Currently, time consuming, and costly techniques requiring highly qualified personnel and sizable machines are available to measure and monitor metal level. Given the specific binding between zincon and zinc, and that a cheap and practical biosensing platform is preferred, carbon nanotubes were chosen and chemically modified to attach zincon onto the inert and conductive surface. The electro-capability of this sensing materials for zinc quantification was unprecedented with a LOD of ~20 and 30 ng·ml<sup>-1</sup> in urine and saliva, respectively, a linear range of detection of 125–1000 ng·ml<sup>-1</sup> and proven to be selective towards this bivalent cation. The zincon-modified CNT system is a specific, fast, simple, and non-expensive alternative for the quantification of zinc in easily body fluids. Given the clinical importance of measuring free zinc ions, the development of this

composite nanomaterials points the way to removing a key technical bottleneck for easy, low cost and fast detection of disease biomarkers and could offer a route to cost reduction and lowering hurdles to more widespread adaptation of point of care testing.

## References

- [1] H. Haraguchi, *Metallomics* **2017**, 3.
- [2] J. Szpunar, *Analytical and Bioanalytical Chemistry* **2004**, 378, 54.
- [3] S. Mounicou, J. Szpunar, R. Lobinski, *Chemical Society Reviews* **2009**, 38, 1119.
- [4] X. Zheng, W. Cheng, C. Ji, J. Zhang, M. Yin, *Reviews in Analytical Chemistry* **2020**, 39, 231.
- [5] M. A. Zoroddu, J. Aaseth, G. Crisponi, S. Medici, M. Peana, V. M. Nurchi, *Journal of inorganic biochemistry* **2019**, 195, 120.
- [6] A. I. Anzellotti, N. P. Farrell, *Chemical Society Reviews* **2008**, 37, 1629.
- [7] A. S. Prasad, O. Kucuk, *Cancer and metastasis Reviews* **2002**, 21, 291.
- [8] B. J. Grattan, H. C. Freake, *Nutrients* **2012**, 4, 648.
- [9] M. J. Jackson, in *Zinc in Human Biology*, Springer, **1989**, pp. 1–14.
- [10] C. T. Chasapis, P.-S. A. Ntoupa, C. A. Spiliopoulou, M. E. Stefanidou, *Archives of toxicology* **2020**, 94.
- [11] J. Wang, H. Zhao, Z. Xu, X. Cheng, *Cancer biology & medicine* **2020**, 17, 612.
- [12] M. Murakami, T. Hirano, *Cancer science* **2008**, 99, 1515.
- [13] H. Farahani, M. Alaei, J. Amri, M.-R. Baghinia, M. Rafiee, *Laboratory medicine* **2020**, 51, 243.
- [14] Z. Medarova, S. K. Ghosh, M. Vangel, R. Drake, A. Moore, *American journal of cancer research* **2014**, 4, 385.
- [15] K. Schilling, R. E. Moore, K. V. Sullivan, M. S. Capper, M. Rehkämper, K. Goddard, C. Ion, R. C. Coombes, L. Vesty-Edwards, A. D. Lamb, *Metallomics* **2021**, 13, mfab020.
- [16] S. R. Shetty, S. Babu, S. Kumari, P. Shetty, S. Hegde, A. Karikal, *Journal of cancer research and therapeutics* **2015**, 11, 146.
- [17] M. M. Khalil, S. Zraiki, M. I. Khayat, *Journal of Indian Academy of Oral Medicine and Radiology* **2019**, 31, 293.
- [18] M. ABDUL-MOUNTHER, *IMPACT: International Journal of Research in Applied, Natural and Social Sciences (IMPACT: IJRANSS)* **2016**, 4, 191.
- [19] C. Burton, Y. Dan, A. Donovan, K. Liu, H. Shi, Y. Ma, C. P. Bosnak, *Clinica Chimica Acta* **2016**, 452, 142.

- [20] E. C. Porto-Mascarenhas, D. X. Assad, H. Chardin, D. Gozal, G. D. L. Canto, A. C. Acevedo, E. N. S. Guerra, *Critical reviews in oncology/hematology* **2017**, *110*, 62.
- [21] Y. Feng, J.-W. Zeng, Q. Ma, S. Zhang, J. Tang, J.-F. Feng, *Journal of Trace Elements in Medicine and Biology* **2020**, *62*, 126629.
- [22] K. Schilling, F. Larner, A. Saad, R. Roberts, H. M. Kocher, O. Blyuss, A. N. Halliday, T. Crnogorac-Jurcevic, *Metallomics* **2020**, *12*, 752.
- [23] S. Mirlohi, S. E. Duncan, M. Harmon, D. Case, G. Lesser, A. M. Dietrich, *Clinical oral investigations* **2015**, *19*, 127.
- [24] B. Callejón-Leblic, A. Arias-Borrego, A. Pereira-Vega, J. L. Gómez-Ariza, T. García-Barrera, *International journal of molecular sciences* **2019**, *20*, 778.
- [25] C.-N. Lin, L.-H. Wang, K.-H. Shen, *Journal of clinical laboratory analysis* **2009**, *23*, 192.
- [26] Y. Teng, C. K. Singh, O. Sadak, N. Ahmad, S. Gunasekaran, *Journal of Electroanalytical Chemistry* **2019**, *833*, 269.
- [27] J. Liu, Y. Duan, *Oral oncology* **2012**, *48*, 569.
- [28] J. Kudr, L. Richtera, L. Nejdil, K. Xhaxhiu, P. Vitek, B. Rutkay-Nedecky, D. Hynek, P. Kopel, V. Adam, R. Kizek, *Materials* **2016**, *9*, 31.
- [29] X. Guo, W. H. Lee, N. Alvarez, V. N. Shanov, W. R. Heineman, *Electroanalysis* **2013**, *25*, 1599.
- [30] G. March, T. D. Nguyen, B. Piro, *Biosensors* **2015**, *5*, 241.
- [31] S. K. Pandey, P. Singh, J. Singh, S. Sachan, S. Srivastava, S. K. Singh, *Electroanalysis* **2016**, *28*, 2472.
- [32] J. Wang, *Electroanalysis: An International Journal Devoted to Fundamental and Practical Aspects of Electroanalysis* **2005**, *17*, 1341.
- [33] X. Guo, Y. Yun, V. N. Shanov, H. B. Halsall, W. R. Heineman, *Electroanalysis* **2011**, *23*, 1252.
- [34] G. Aragay, A. Merkoçi, *Electrochimica Acta* **2012**, *84*, 49.
- [35] A. Waheed, M. Mansha, N. Ullah, *TrAC Trends in Analytical Chemistry* **2018**, *105*, 37.
- [36] A. Touati, M. Benounis, K.-E. Boudjemaa, H. Barhoumi, *Sensor Letters* **2016**, *14*, 1138.
- [37] T. Kokab, A. Shah, F. J. Iftikhar, J. Nisar, M. S. Akhter, S. B. Khan, *ACS omega* **2019**, *4*, 22057.
- [38] C. E. Säbel, J. M. Neureuther, S. Siemann, *Analytical biochemistry* **2010**, *397*, 218.

- [39] S. Vasanthi, M. Devendiran, S. S. Narayanan, *Applied Surface Science* **2017**, 422, 138.
- [40] M. H. Aliabadi, N. Esmaeili, H. S. Jahromi, *Applied Nanoscience* **2020**, 10, 597.
- [41] W. Qin, X. Liu, H. Chen, J. Yang, *Analytical Methods* **2014**, 6, 5734.
- [42] S. Vasanthi, K. K. Kumar, S. S. Narayanan, *IJSRST* **2018**, 4, 751.
- [43] A. A. Ensafi, F. Rezaei, B. Rezaei, *Electroanalysis* **2017**, 29, 2839.
- [44] J. L. W. Ling, S. Ab Ghani, *Journal of Solid State Electrochemistry* **2013**, 17, 681.
- [45] M. Lo, N. Ktari, D. Gningue-Sall, A. Madani, S. E. Aaron, J.-J. Aaron, Z. Mekhalif, J. Delhalle, M. M. Chehimi, *Emergent Materials* **2020**, 1.
- [46] B. Marinho, M. Ghislandi, E. Tkalya, C. E. Koning, G. de With, *Powder technology* **2012**, 221, 351.
- [47] X.-H. Zhang, Q.-Q. Tang, D. Yang, W.-M. Hua, Y.-H. Yue, B.-D. Wang, X.-H. Zhang, J.-H. Hu, *Materials Chemistry and Physics* **2011**, 126, 310.
- [48] Z. Zhu, *Nano-micro letters* **2017**, 9, 1.
- [49] C. Gao, Z. Guo, J.-H. Liu, X.-J. Huang, *Nanoscale* **2012**, 4, 1948.
- [50] Y. Teng, Z. Ren, Y. Zhang, Z. Wang, Z. Pan, K. Shao, Y. She, *Talanta* **2020**, 209, 120569.
- [51] J. Pytko-Polonczyk, A. Jakubik, A. Przeklasa-Bierowiec, B. Muszynska, *J. Physiol. Pharmacol* **2017**, 68, 807.
- [52] Safety Data Sheet—Urine-Artificial. Available online: <https://www.aldon-chem.com/sds/urine-artificial-set-of-4.pdf> (accessed on 30 November 2021).
- [53] S. Qin, D. Qin, W. T. Ford, J. E. Herrera, D. E. Resasco, S. M. Bachilo, R. B. Weisman, *Macromolecules* **2004**, 37, 3965.
- [54] R. Atif, F. Inam, *Beilstein journal of nanotechnology* **2016**, 7, 1174.
- [55] Y. Zhou, Y. Fang, R. P. Ramasamy, *Sensors* **2019**, 19, 392.
- [56] M. Ghanei-Motlagh, M. Fayazi, M. A. Taher, E. Darezereshki, E. Jamalizadeh, R. Fayazi, *RSC advances* **2015**, 5, 100039.
- [57] Z. Li, X. Chang, Z. Hu, X. Huang, X. Zou, Q. Wu, R. Nie, *Journal of Hazardous Materials* **2009**, 166, 133.
- [58] P. J. Wibawa, M. Nur, M. Asy'ari, H. Nur, *Heliyon* **2020**, 6, e03546.
- [59] X. Luo, J. J. Davis, *Chemical Society Reviews* **2013**, 42, 5944.

- [60] C. Klumpp, K. Kostarelos, M. Prato, A. Bianco, *Biochimica et Biophysica Acta (BBA)-Biomembranes* **2006**, 1758, 404.
- [61] V. Țucureanu, A. Matei, A. M. Avram, *Critical reviews in analytical chemistry* **2016**, 46, 502.
- [62] K. Balasubramanian, M. Burghard, *small* **2005**, 1, 180.
- [63] Y. Munaiah, S. Suresh, S. Dheenadayalan, V. K. Pillai, P. Ragupathy, *The Journal of Physical Chemistry C* **2014**, 118, 14795.
- [64] Y. Yan, B. Kou, L. Yan, *Analytical Methods* **2015**, 7, 8757.
- [65] A. Karatepe, M. Soylak, L. Elçi, *Clean–Soil, Air, Water* **2011**, 39, 502.
- [66] M. Herman, M. Golasik, W. Piekoszewski, S. Walas, M. Napierala, M. Wyganowska-Swiatkowska, A. Kurhanska-Flisykowska, A. Wozniak, E. Florek, *Biological trace element research* **2016**, 173, 275.
- [67] W. Seanghirun, K. Samoson, S. Cotchim, S. Kongkaew, W. Limbut, *Microchemical Journal* **2020**, 157, 104958.
- [68] W. Yue, A. Bange, B. L. Riehl, J. M. Johnson, I. Papautsky, W. R. Heineman, *Electroanalysis* **2013**, 25, 2259.
- [69] K. G. Nikolaev, E. V. Kalmykov, D. O. Shavronskaya, A. A. Nikitina, A. A. Stekolshchikova, E. A. Kosareva, A. A. Zenkin, I. S. Pantiukhin, O. Y. Orlova, A. V. Skalny, *ACS omega* **2020**, 5, 18987.

### **Chapter 3. Stripping metalloprotein with bismuth nanomaterials tethered on carbon surface.**

This chapter includes a published peer-reviewed paper. The bibliographic details of the coauthored paper, including all authors, are:

*Daniela Vieira*, Edward J Harvey, Geraldine Merle

Published in: Applied surface Science 2023, Volume 635, 157636;

<https://doi.org/10.1016/j.apsusc.2023.157636>

My contributions to the paper involved: Experimental design, implementation, and performance; Data collection and analysis; Preparation of the manuscript.

In the previous chapter II, we introduced how a non bio recognition element could replace bioelements to assure specificity without losing the sensitivity. However, mobile zinc is more accessible and easier to transfer electrons with the electrode surface when compared to zinc-containing proteins. For the following chapters, we will verify the selectivity of non bio recognition element towards the detection of zinc-containing proteins, where the isolated active site gives a great challenge to overcome. The chapter III “*Stripping metalloprotein with bismuth nanomaterials tethered on carbon surface*” shows how a designed structured system could bring many advantages towards the detection of carbonic anhydrase I (CA-I), a zinc-containing protein. By taking advantage of a longer sulfonic structure and its inhibitory effect, combined to the high conductivity of carbon, and the selectivity of bismuth we successfully reached the buried redox center of the protein. The result is a system able to detect CA I in buffer and in artificial saliva, showing LOD of 11 ng.ml<sup>-1</sup>.

## Stripping metalloprotein with bismuth nanomaterials tethered on carbon surface

*D. Vieira<sup>1</sup>, E. Harvey<sup>1</sup>, G. Merle<sup>\*1,2</sup>*

<sup>1</sup> McGill University, Faculty of Medicine, Department of Experimental Surgery

<sup>2</sup> Polytechnique Montreal, Department of Chemical Engineering

*\*Corresponding author*

*Email. Geraldine.merle@polymtl.ca*

### **Abstract**

An increasing number of metalloproteins has shown to play essential roles in physiological processes. The Zn(II)-dependent metalloprotein, carbonic anhydrase (CA), is a hallmark of metabolic change in cancer cells. Being able to evaluate CA expression is crucial for the early detection of malignant tissues. The fabrication of sensor based on bismuth nanomaterials tethered on mesoporous carbon through a conductive spacer arm is reported. By coupling this hybrid material with stripping analysis, its functionality in measuring CA levels in body fluids is validated. Notably, the zinc finger metalloprotein biosensor system successfully and reliably tunnels zinc within the protein shell allowing the detection of increased concentrations of metalloproteins in saliva. The sensor displays high specificity, sensitivity, repeatability, and most of all a limit of detection of  $4.8 \text{ ng}\cdot\text{ml}^{-1}$  for zinc ions and  $11 \text{ ng}\cdot\text{ml}^{-1}$  for CA metalloprotein. Given the clinical significance of carbonic anhydrase in tumour development, these findings are the first step towards fast, low cost and stable sensor technology and will revolutionize the field of cancer diagnosis.

**Keywords:** bismuth nanoparticles, spacer arm, zinc-containing protein, stripping analysis, carbonic anhydrase, cancer biomarker

## 1. Introduction

Bismuth-film electrodes have gained much interest and recognition in the last decade to replace the mercury-based electrodes to monitor trace of heavy metals and organic compounds. With a wide negative potential window, Bi has the ability to synergistically interact with metallic ions such as zinc with reduction potential more positive and thus allowing their detection. These exceptional properties make them attractive for electrochemical sensing free metallic ions in environmental analysis but also could possess a tremendous potential for biomedical applications. An efficient detection platform with high selectivity and sensitivity for metalloproteins would have immense significance in the fields of clinical diagnostics. Metalloproteins are a special class of proteins with a metal ion cofactor, which play a central role in energy conversion based cellular processes [1-3]. Because they catalyse efficiently the most important biological reactions such as structural stabilization or signal transduction, sensitive feedbacks such as concentration, function and conformation about these metallic redox center in the metalloproteins within biological samples could give valuable insights and relevance to human diseases [2,3].

Carbonic anhydrase (CA) represents an attractive zinc-containing protein, which has been established to be involved in different pathophysiological processes [4,5], notably in the development and progression of cancers [6-11]. This zinc metalloenzyme catalyzes the reversible hydration of carbon dioxide to bicarbonate ions and protons ( $\text{CO}_2 + \text{H}_2\text{O} \leftrightarrow \text{HCO}_3^- + \text{H}^+$ ) [4,5,12,13]. It provides bicarbonate ions to neutralize the intracellular pH, whereas protons acidify the extracellular microenvironment (pH 6.2 to 6.5)<sup>[12,14]</sup>. As a result, the extracellular matrix degrades, causing the migration and invasion of cancerous cells [4,5,12]. Given that only limited information can be obtained via biochemical assays at high costs, electrochemical sensors represent promising candidates for future clinical diagnostics [15-18]. Currently, electrochemical detection of metalloprotein is done via the binding to a recognition molecule such as immunological compound

or aptamer<sup>[18,19]</sup>. Despite being extremely specific to detect target molecules, these platforms are expensive and do not allow continuous measurement, thereby their transition to a non-research environment has been hampered. Other strategy to detect continuously relevant molecules is to measure directly the electrochemical signal of the metalloproteins generated directly by the reduction and oxidation of metallic redox center in the structures when a redox potential is applied<sup>[3,20]</sup>. Unfortunately, it is usually embedded within the protein shell, at few nanometres from the surface of the enzyme. Taking into account that the maximum distance electron can travel is up to 20 Å<sup>[3,21]</sup>, a functional working-electrode design is needed to achieve an efficient electronic coupling between metalloprotein and electrode surface. Efforts to maximize charge transfer have been focusing on protein engineering<sup>[3,20]</sup>, immobilization of the biocatalysts on the electrode<sup>[22–24]</sup> to minimize the tunneling distance and finally the use of nanostructures as electrodes to increase enzyme concentration and reduce tunneling.

Given the large success of bismuth electrodes to detect zinc in water sample analysis<sup>[25–27]</sup>, the advantageous role of Bi electrodes have been further applied to detect free zinc ions in body fluids<sup>[28,29][30] [31] [32]</sup> but also bound in metallothionein protein down to 1 µg.ml<sup>-1</sup><sup>[33]</sup>. The immense potential of nanoscale dimensional materials has been well documented to maximize enzyme/electrode interaction and minimize tunneling distance for efficient charge transfer. However, no work has been reported to examine the combining effect of bismuth with nanoscale materials in the detection of zinc-containing protein. Herein, we demonstrate for the first time, the importance of modified Bi nanostructures for the construction of zinc-containing protein-based sensor. Significance of each component as well as the performance of this biosensor in buffer and simulated body fluid were examined and its viability for applications in real sample analysis proven.

## 2. Materials and Methods

### *Functionalization of Carbon nanoparticles (S-CN)*

Mesoporous carbon nanoparticles (CN) were sulfonated following Wahab et al (2011) [34]. Briefly, 4 mmol of sulfanilic acid (98+%, Alfa Aesar™) was mixed in 5 ml of ultrapure water (Milli-Q, Merck) containing 0.2 g of mesoporous CN (<500 nm particle size, Sigma Aldrich). The resultant solution was cooled down by an ice-bath in a three-neck flask. Then, 5 ml of 0.27 g sodium nitrate (Sigma Aldrich) was mixed in 5 ml of ultrapure water and added to the first cooled solution. The mixture was stirred until the solution became deep orange. After, 9.9 mmol of Sodium borohydride (Sigma Aldrich) was mixed with 5 ml of pure water and added dropwise to the solution and stirred for 1h in an ice-bath. At the end, the sulfonated carbon nanoparticles (S-CN) were filtered, and the retained particles were washed using a nylon filter membrane (pore size 0.22 μm, Sigma Aldrich) with ultrapure water, followed by 1% wt/wt NaOH (Fisher Scientific), acetone (Fisher Scientific), ethanol (Fisher Scientific) and, finally, methanol (Fisher Scientific). Cleaned S-CN were dried in an oven overnight at 60 °C and stored at room temperature. S-CN solutions was prepared for future use adding 1 mg of S-CN in 1 ml of ethanol + 100 μL of Nafion (1%, Dupont). The resultant solution was ultrasonicated for 30 min.

### *Preparation of sulfonated carbon nanoparticles bismuth electrodes (S-CN-Bi)*

Bismuth ions were electroreduced on S-CN. Briefly, a glassy carbon electrode (GCE) (5mm diameter, Amatek) was well hand-polished with alumina solution (MasterPrep™ polishing suspension 0.05 μm – Buehler) and rinsed with ultrapure water. Afterwards, 10 μL of S-CN in ethanol/nafion solution was dropped on GCE surface and dried at room temperature. The S-CN electrode was immersed in an aqueous solution of 0.01 M Bi (NO<sub>3</sub>)<sub>3</sub> (Sigma Aldrich) for 3h,

allowing the chemical bound between  $\text{Bi}^{+3}$  ions and  $\text{SO}^{-3}$  groups presented in S-CN [35]. The electrode was rinsed with ultrapure water to remove unbound materials. Lastly,  $\text{Bi}^{3+}$  ions were electroreduced to Bi at potential of -0.6V (vs SCE) for 400s in an aqueous solution of 0.5 M boric acid (Sigma Aldrich), resulting in S-CN-Bi electrode. Different parameters of Bi reduction (time and potential) were studied to verify the best performance of the electrode.

#### *Physicochemical properties*

The morphology of CN, S-CN and S-CN-Bi electrodes was investigated by Scanning Electron Microscopy (SEM, Inspect F50, FEI Company, Hillsboro, OR, USA) and by transmission electron microscopy (STEM/TEM, FEI Tecnai F20, 200 kV). Crystalline behavior was examined using an X-Ray diffractometer (Bruker D8 Discovery Instrument) operating at a voltage of 40 kV and a current of 20 mA with  $\text{CuK}\alpha$  ( $\lambda = 1.5406 \text{ \AA}$ ) radiation and a programmable divergent slit. Samples were scanned in the  $2\theta$  range  $10^\circ$ – $90^\circ$  with a scanning speed of  $2^\circ \text{ min}^{-1}$ .

#### *Electrochemical performance*

Electrochemical experiments were performed using a potentiostat (VersaSTAT 4) with a three-electrode system cell, where GCE, CN, S-CN and S-CN-Bi were used as work electrodes, Pt wire as counter electrode and saturated calomel electrode (SCE) as reference electrode. The electrodes were tested in zinc solutions to verify the ability of  $\text{Zn}^{+2}$  detection. Cyclic voltammetry (CV) was carried out in 0.1 M tris-HCl (pH: 4.5) aqueous solution, in the presence and absence of zinc ions. The potential was scanned from  $-0.8 \text{ V}$  to  $-1.3 \text{ V}$  (vs SCE) at scan rate of  $10 \text{ mV}\cdot\text{s}^{-1}$ . Square wave stripping voltammetry (SWV) was performed to characterize the electrochemical detection of  $\text{Zn}^{+2}$  using S-CN-Bi electrodes. The potential of deposition was selected at  $-1.40 \text{ V}$  (vs. SCE), applied for 300s, and followed by a SWV, from  $-1.4\text{V}$  to  $-1\text{V}$  (vs SCE), at 25Hz, amplitude of 25 mV, and

step potential of 0.2 mV in 0.1M tris-HCl (pH 4.5). Different parameters of Zn deposition (time and potential) were studied to verify the best performance. S-CN-Bi electrodes were tested using different concentrations of  $Zn^{+2}$  solutions (from 0 to 1000 ng.ml<sup>-1</sup>).

Cyclic voltammetry (CV) was carried out in phosphate-buffered saline (PBS) solution (pH 6.0) aqueous solution in presence and absence of carbonic anhydrase (CA). The potential was scanned from -1 V to -1.7 V (vs SCE) at scan rate of 5 mVs<sup>-1</sup>. Chronoamperometry was performed at -1.7V (vs SCE), during 300s, varying the concentration of CA, from 0 to 1000 ng.ml<sup>-1</sup>. CV and chronoamperometry were applied to verify the specificity of S-CN-Bi to detect CA when simulating the cancerous environment. CV was carried out in PBS solution (pH 6) in presence and absence of CA, Collagenase and CA + Collagenase. The potential was scanned from -1 V to -1.7 V (vs SCE) at scan rate of 5 mV.s<sup>-1</sup>. Chronoamperometry was performed at -1.7V (vs SCE), varying the concentration of proteins from 0 to 500 ng.ml<sup>-1</sup>. In order to study the electrode sensitivity to salivary CA, CV was performed in a PBS (pH 6) solution containing 50% of artificial saliva, in presence and absence of CA applying the same parameters used in the PBS experiment. Limit of detection (LOD) was calculated according to the Formula (1):

$$LOD = 3 \times (SD/S) \quad (1)$$

where, SD is the standard error intercept and the S is the slope of the calibration curve (S), both extracted from origin software after linear regression.

### *Statistics*

The data were analyzed using OriginPro (OriginLab Corporation, version 2018G) and presented as mean  $\pm$  SD. A one-way ANOVA and Tukey test were performed to evaluate statistical significance. *P*-value smaller than 0.05 means significant difference.

### 3. Results and discussion

In this work, the synergistic interaction between bismuth nanostructures and carbonic anhydrase via a direct electron transfer was studied. The zinc metalloprotein sensor was constructed after the deposition of sulfonated carbon nanostructures followed by bismuth grafting and electroreduction as illustrated in **Figure 1**.

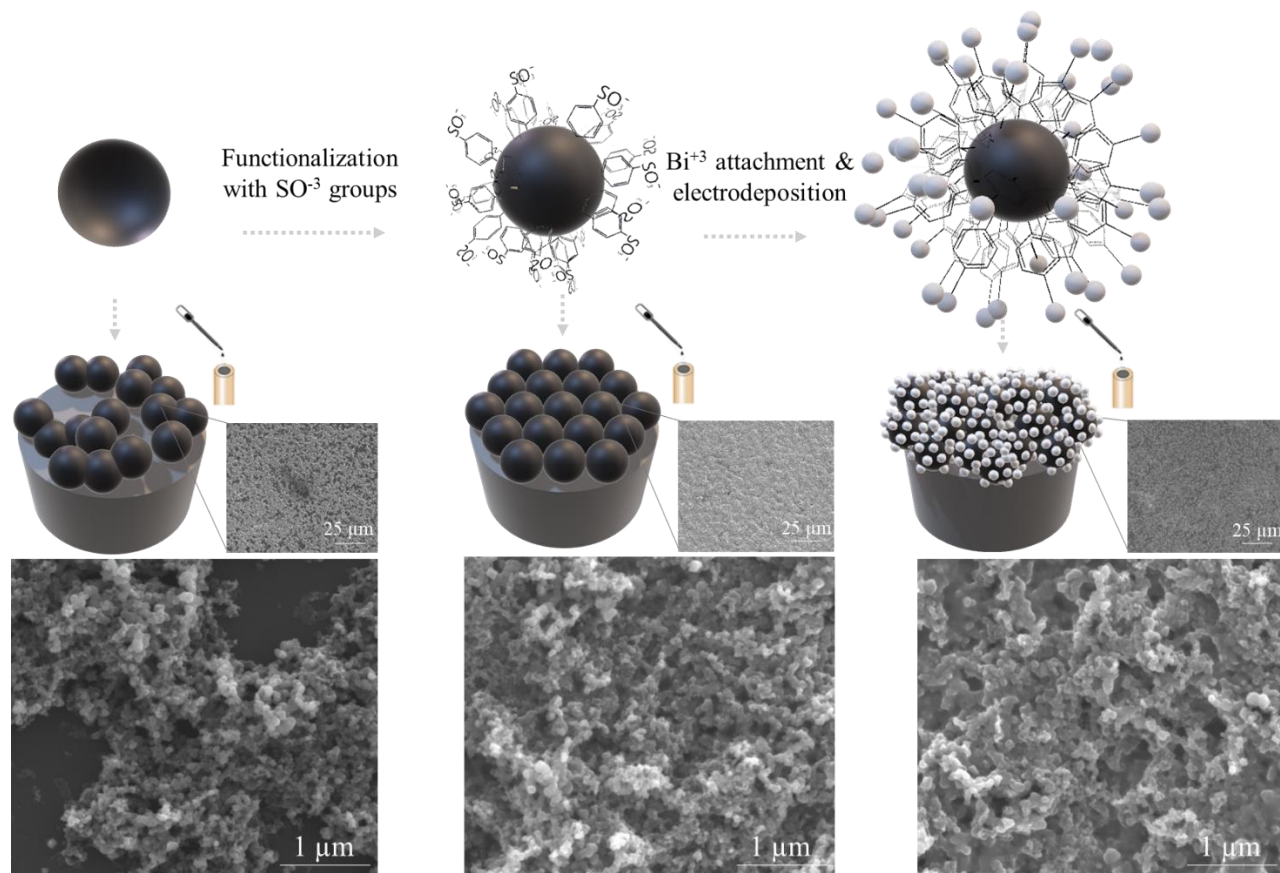


**Figure 8-** Schematic of particles on GCE surface and SEM pictures (low and high magnification) showing particles distribution for carbon nanoparticles (CN), sulfonated-carbon nanoparticles (S-CN) and bismuth deposited on sulfonated-carbon nanoparticles (S-CN-Bi), respectively.

The most common approach to functionalize carbon is through high concentrated sulfuric acid combined with high temperature, however this usually leads to oxidative destruction, increasing

surface defects and harming the amount of sulfonated group in the final material [36–39]. In this work, sulfonated carbon was functionalized using diazonium salts at low temperature and the sulfonated carbon nanoparticles (S-CN) were obtained after chemical reduction using sodium borohydride [34]. Nanoscale carbon was employed to increase the surface to volume ratio and also to ensure higher electrical properties[40], whereas the sulfonated group served to increase the surface adhesion and dispersion of the nanocarbon (**Figure 1**), and enabled the bismuth ions to attach at the surface of the carbon. In **Supplementary information S1** it is possible to observe the effect of the functionalization by sulfates groups on carbon nanoparticles. In water solution, charged particles were better dispersed than non-functionalized particles. SEM pictures showed similar effect, where non functionalized particles were agglomerated, and sulfonated carbon nanoparticles presented a homogeneous distribution on GCE surface (**Figure 1**). This effect may be explained due to the hydrophilic characteristics gave by the sulfonated groups on the CN, dispersing them much better when compared to non-functionalized particles [34,40]. The electrovalent bond between the pendant sulfonic acid groups ( $-\text{SO}^{-3}$ ) on the carbon and  $\text{Bi}^{+3}$  occurred after immersing the S-CN electrode in  $\text{Bi}(\text{NO}_3)_3$  aqueous solution. Finally,  $\text{Bi}^{+3}$  ions were electrochemically reduced into  $\text{Bi}^0$  to form bismuth nanoparticles around S-CN particles [35]. TEM and STEM pictures (**Figure 2C-D**) showed the presence of well distributed bismuth nanoparticles with a diameter of  $\sim 2$  nm on the nanocarbon support. Note that in Figure 2D, the STEM mode efficiently showed the high contrast of bismuth particles when compared to TEM as expected in the dark-field imaging. This was also confirmed with EDS (**Supplementary information S2**) and XRD analysis (**Figure 2E**). The diffraction peaks at  $2\theta \approx 25^\circ$  and  $44^\circ$  were presented in all samples and represent the carbon structure (002) and (101) plan, respectively [41,42]. The well-defined shape presented in (101) plane for carbon (non-sulfonated) could be related to

the existence of the  $a$  axis present in the graphite structure, indicating a high degree of carbonization [41,42]. For S-CN we observed a weaker and larger diffraction peak in (101) plane, showing the presence of amorphous carbon structure that may be consisted of polycyclic aromatic carbon ring [42].

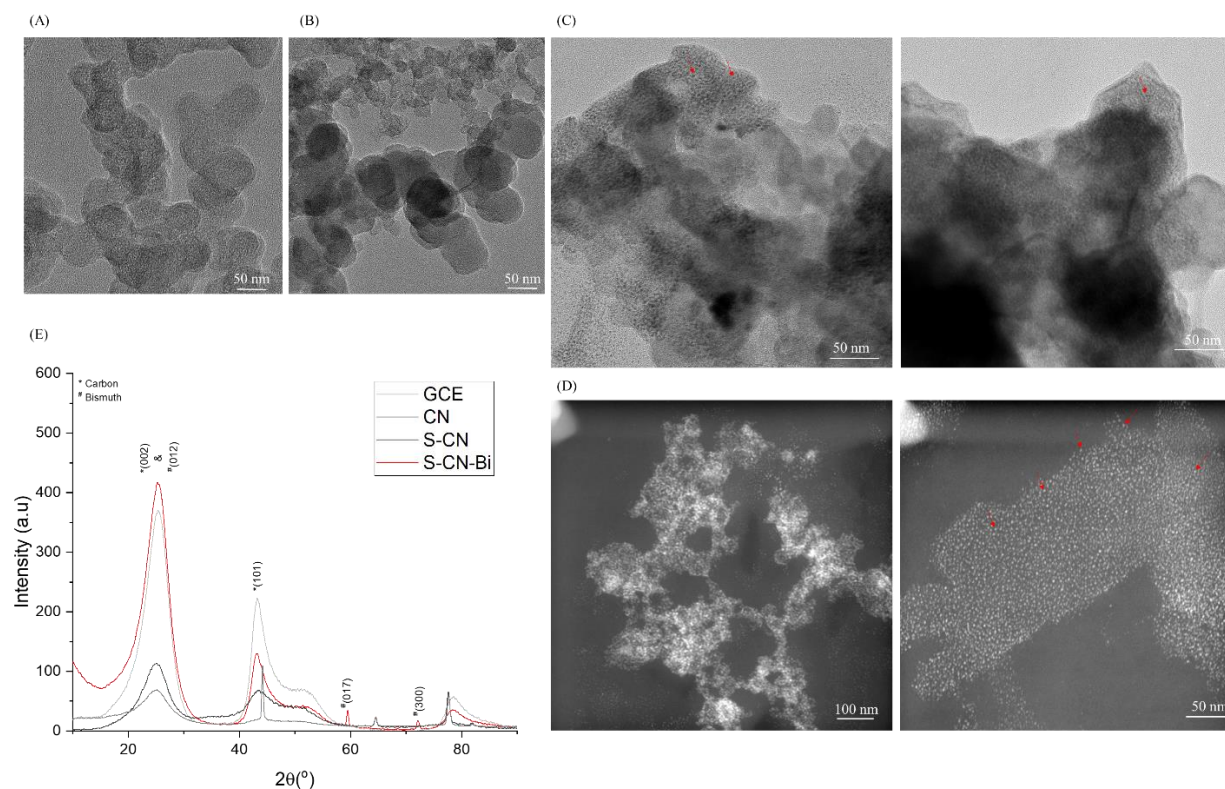


**Figure 9** – TEM images of (A) CN, (B) S-CN and (C) S-CN-Bi materials. The contrast and size of Bi nanoparticles was determined via STEM at low and high magnification (D). Note that the red arrows indicate few bismuth nanoparticles. XRD patterns (E) of GCE, CN, S-CN and S-CN-Bi electrodes. Bi rhombohedral structure was identified without any impurities or oxides.

The pattern for S-CN-Bi shows two diffractions peaks at  $2\theta \approx 60^\circ$  (017) and  $72^\circ$  (300), representing the Bi rhombohedral structure (JCPDS card No. 5-519) [43–45] compared to the bare and S-CN electrodes (**Figure 2D**). The high intensity of the C (002) peak related to carbon structure is believed to conceal the characteristic diffraction peak of Bi structure at  $2\theta \approx 25^\circ$  (012). A crystallite

size of  $1.38 \pm 1.19$  nm for bismuth nanoparticles was obtained from XRD pattern based on Scherrer equation and showed similarity to the size obtained by TEM. No other diffraction peaks corresponding to an oxide, or an impurity were observed from the XRD pattern indicating crystallized Bi with a high purity.

Successful deposition of each coating of material was further confirmed with heterogenous electron transfer studies using cyclic voltammetry (**Supplementary information S3**). The redox peaks of the ferri/ferrocyanide couple are identified at 0.236 V and +0.059V at the bare GC electrode. The impact of mesoporous carbon as a surface area and conductivity enhancer is evident as an increased redox current and decreased  $\Delta E_p$  between the redox peak potentials is observed. With the subsequent deposition of the sulfonated organic layer, a lower redox current combined with increased in  $\Delta E_p$  is observed. Finally, the electrodeposition of Bi nanoparticles led to a slight increase in redox current and a lower  $\Delta E_p$  (**Supplementary information S3-C**) indicating a superior electron transfer [46,47].

To verify the interactions of Bi nanomaterials with zinc ions, square wave voltammetry (SWV) response of S-CN-Bi electrode was studied toward decreased concentrations of  $Zn^{2+}$ . **Figure 3** shows the stripping behavior and the linear function of Zn concentration vs current, respectively. The optimized parameters of  $Bi^{+3}$  reduction was determined by setting the potential of reduction at -0.6 V (vs SCE) for 400s; and for  $Zn^{+2}$  the potential of deposition selected was -1.4V (vs SCE) for 300s (**Supplementary information S4 and S5**).

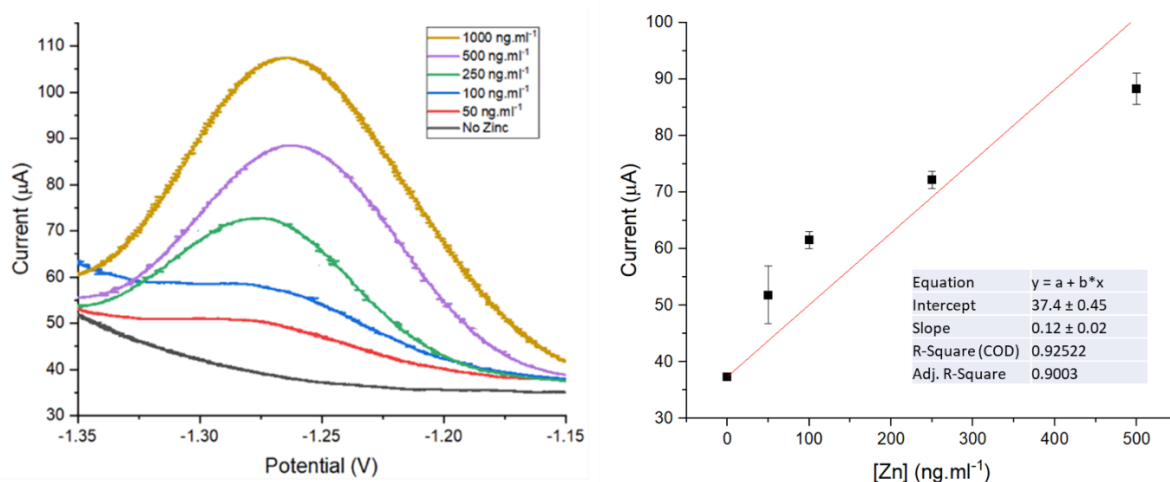


**Figure 10** - (A) SWV response for S-CN-Bi electrodes in different concentrations of zinc solutions, from 0 ng.ml<sup>-1</sup> to 500 ng.ml<sup>-1</sup>, using potential of deposition of zinc at -1.40V (vs SCE), for 300s and (B) linear function of zinc concentration and the current response, showing LOD of ~4.8 ng.ml<sup>-1</sup>, (n=3).

The most common way to build bismuth electrodes consists of the *in-situ* method, where simultaneous plating of Bi<sup>0</sup> and the target metal (as such Zn, Pb, Cd) occurs on the electrode surface, whereas in the *ex situ* method, bismuth is plated separated and before target metal detection [26,48]. Although *in situ* method presented a better detection threshold than *ex situ*, it becomes inadequate for a point-of-care system, where free Bi ions are evidently not available in saliva, blood or tissues samples. [49,50]. With the *ex situ* method, the S-CN-Bi electrode showed a limit of detection of ~4.8 ng.ml<sup>-1</sup> comparable to previously published zinc sensors using carbon as substrate for plating *ex situ* bismuth (~5 and 40 ng.ml<sup>-1</sup>) [50–52]. Other zinc sensors using gold [28,53] and graphene [21,54] offer a high conductivity with a poor limit of detection of μg.ml<sup>-1</sup>.

Following the optimization of S-CN-Bi electrodes with  $Zn^{2+}$ , we further studied the analytical parameters of the S-CN-Bi sensor in the presence of carbonic anhydrase. CVs of GCE, CN, S-CN and S-CN-Bi electrodes in presence and absence of  $0.5 \text{ mg}\cdot\text{ml}^{-1}$  CA in PBS (pH 6) were performed (**Figure 4A**). The current response in function of protein concentration was studied by chronoamperometry and it is illustrated in **Figure 4B**. Note that CA presented better detection at low pHs (5.5 and 6) (**Supplementary information S6**). However, pH 6 was selected because of its similarity to body fluids, such as saliva pH [55].

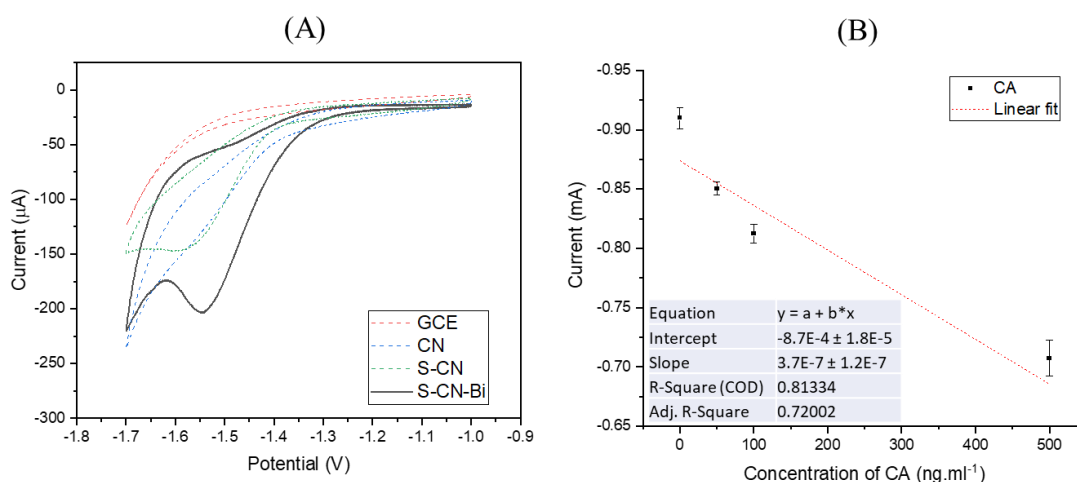


**Figure 11** – (A) CVs showing the ability of S-CN-Bi electrode to detect CA in  $0.5 \text{ mg}\cdot\text{ml}^{-1}$  CA/PBS, pH=6, scan rate  $5 \text{ mV}\cdot\text{s}^{-1}$ ) and (B) current response of S-CN-Bi electrode in function of CA concentration at  $-1.7\text{V}$  (vs SCE), from  $0 \text{ ng}\cdot\text{ml}^{-1}$  to  $500 \text{ ng}\cdot\text{ml}^{-1}$ . ( $n=2$ ,  $p\text{-value} < 0.05$ ), significant difference between current response for respective concentrations.

While no reduction and oxidation peaks of CA were detected at GCE and CN electrode, a slight reduction peak appeared at S-CN electrode at around  $\sim -1.55\text{V}$  (vs SCE). A stronger and more defined reduction peak was observed at the S-CN-Bi electrode only in the presence of CA (**Figure 4A**). The apparent reduction potential of CA at  $\sim -1.5\text{V}$  (vs SCE) appears to be similar to the reduction potential of zinc and might be attributed to the reduction of  $Zn^{+2}$  to  $Zn^0$  within the CA.

To understand the synergistic interactions between Bi and CA, chronoamperometric response of the S-CN-Bi electrode toward CA concentration was studied. A decrease in reduction currents is observed with increasing concentrations of CA (**Figure 4B**), presenting LOD of  $\sim 11 \text{ ng.ml}^{-1}$ . Note no coherent response was observed for CN and S-CN electrodes (**Supplementary information S7**). It has been already established that aromatic sulfonamide and some anions such as  $\text{SO}^{-3}$  [56] have an inhibitory effect on CA [56–58]. Recent work [58] has showed that the inhibition of CA by sulfonamides results in a diminution of the current intensity as the concentration of CA increased. The study attributed this effect to the synergistic interaction and the complex formation that occurred between the sulfonamide and CA, and not to the hindrance of the electrode surface to the enzyme. Another study also found similar current response in function of protein concentration when applying CA inhibitory drugs in the electrochemical detection of CA [59]. The decrease of the current response was attributed to the binding of the drugs with CA and formation of a bulky complex. The study showed that the complex species were electroactive due to the unfolding structure of the CA upon its binding with the drugs, providing some routes for the electrochemical reaction of the electroactive amino acid residues at the sensor surface. In this work, three combined effects are believed to positively act towards CA electrochemical detection: i) the complex formation between  $\text{SO}^{-3}$  and CA, giving that the same current behavior at increased CA concentration was observed by Khodarahmi et al (2019); ii) a higher affinity of Zn towards Bi; and iii) the length of linker of S-CN-Bi nanostructure which may allow a better electron tunneling from CA to the electrode surface. The distance created by adding the S-CN link was simulated and calculated by comparing C-Bi and S-CN-Bi structures using MarvinSketch software (**Supplementary information S8**). S-CN-Bi structure (11 Å) appeared to be  $\sim 50\%$  longer than C-Bi structure (5Å). As the zinc core inside CA is  $\sim 20\text{Å}$  distance from the protein surface [21], a

longer structure may facilitate the access to  $Zn^{2+}$ , and thereby improve the electron transfer process – which usually occurs at  $15\text{\AA}$  [60]. Through these combined effects, S-CN-Bi electrodes has demonstrated a great ability to electrochemical detect CA.

Moreover, it is crucial to assess the selectivity of the S-CN-Bi electrode towards CA, as it is based on metal affinity and electrochemical signature. To demonstrate the good selectivity of this advanced material, a mixed zinc-protein PBS solution (pH 6), simulating cancerous environment was used to perform electrochemical characterization (**Figure 5**).

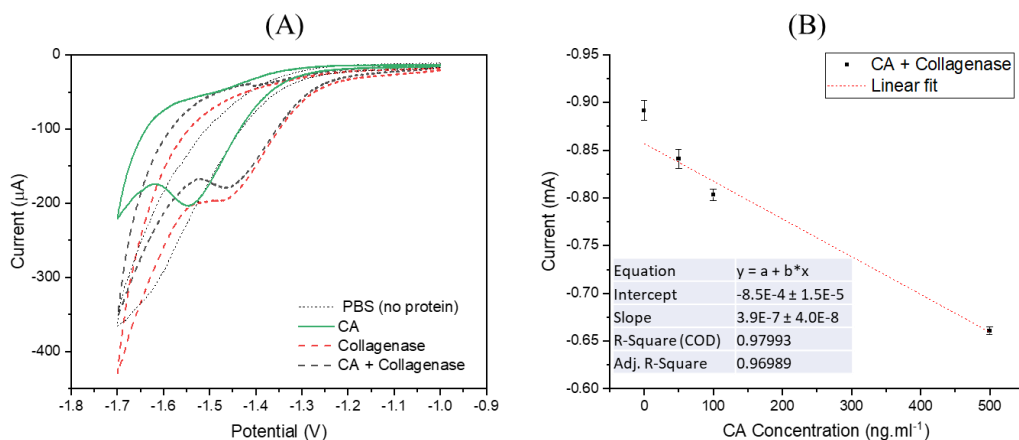


**Figure 12** - CVs of S-CN-Bi electrode in absence and presence of CA, collagenase, and both proteins ( $0.5 \text{ mg.ml}^{-1}$  of each protein in PBS, pH=6, scan rate  $5 \text{ mV.s}^{-1}$ ) and (B) current response of S-CN-Bi electrode in function of CA concentration at  $-1.7\text{V}$  (vs SCE), from  $0 \text{ ng.ml}^{-1}$  to  $500 \text{ ng.ml}^{-1}$  when collagenase was present in the solution ( $n=2$ ,  $p\text{-value} < 0.05$ ), significant difference between current response for respective concentrations. No peak could be detected in absence of protein. Note there was no significant difference when compared to only CA, meaning the collagenase did not interfere in the CA detection.

In the presence of the two zinc finger proteins, two reduction peaks at -1.5V and -1.45V were observed for CA and collagenase, respectively. In the mixed solution the peaks are overlapped and more defined. **Figure 5B** shows the current response as a function of mixed-protein concentration. The dependence of electrochemical response of S-CN-Bi electrode in the protein cocktail to CA concentration is clearly observed and similar to findings obtained in absence of collagenase (**Figure 4B**). It is worthwhile noticing that no response was obtained in solution containing only collagenase (**Supplementary information S9**). These behaviours were expected as  $\text{SO}^{-3}$  have an inhibitory effect only in CA and not in collagenase. Besides collagenase could be detected by CV due to the Bi-Zinc affinity, there was not a complex formation between  $\text{SO}^{-3}$  and collagenase, not affecting the current response at -1.7V. The sensor showed stability over 1 year of the study. No further analysis were performed related to the sensor's stability.

Previous electrochemical characterisations were performed in buffer and therefore did not complete replicate a real biological system as they do not have for instance the same composition, viscosity, or ionic strength. In order to investigate the voltammetry response from a more biological aspect, we employed artificial saliva – as salivary CA is an alternative source for monitoring a variety of cancers, including head and neck (HNSCC) [61,62], breast [63–65] and lung [66]. In addition, saliva testing is a non-invasive and cost-effective approach for diagnostic approaches [55]. Similar to previous experiments carried out previously, CV was taken in a mixture of artificial saliva and CA (**Figure 6A**). Comparison was made between the voltametric responses derived from buffer and artificial media, a similar reduction peak at around -1.55V is observed in presence of CA, with a decrease as CA concentration increases, presenting LOD of  $8 \mu\text{l.ml}^{-1}$ . In this study, S-CN-Bi system showed great ability in the detection of CA, presenting LOD of  $\sim 11 \text{ ng.ml}^{-1}$  in PBS (pH 6). Besides of the higher LOD in saliva, probably because of its higher viscosity

and impurities, this work brings a new avenue in the strategies applied to detect protein in body fluids and could be applied as a fast and non-invasive tool in the early detection or monitoring of cancer over the salivary CA concentration (**Figure 6B**).

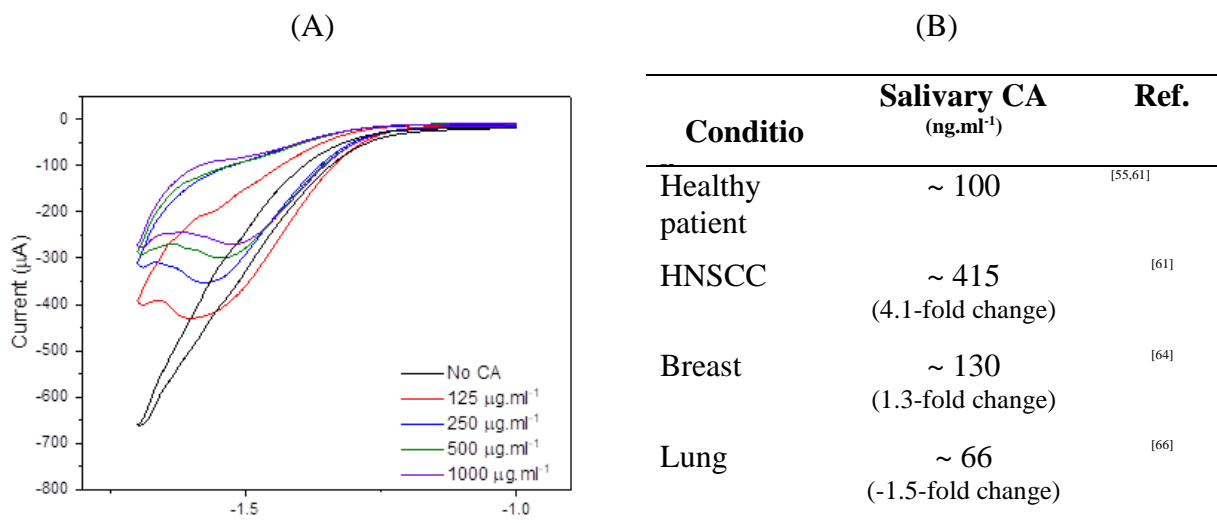


**Figure 13** – (A) CVs of S-CN-Bi electrodes in artificial saliva in presence and absence of CA, from -1V to -1.7V (vs SCE) at scan rate of 5mV.s<sup>-1</sup> and (B) Concentration of CA in a healthy and cancerous saliva

#### 4. Conclusion

To summarize, this study showed that Zn(II)-dependent metalloprotein concentration in saliva could be detected via the traditional stripping analysis using Bi nanoparticles tethered on carbon surface with a flexible and conjugated spacer arm. As the metalloprotein sensor is developed by simple chemical synthesis and electrochemical fabrication techniques, it strongly reduces variability and could easily be scaled up. The sensing material was specifically designed by attaching ~ 2nm bismuth particles (Bi) on an arm to reach the 20Å distance of the Zinc coordination site to the electrode surface. The great ability of S-CN-Bi electrode towards CA detection was supported based on three effects: the complex formation between SO<sup>-3</sup> and CA; the stronger

affinity of Bi with zinc; and the nanostructured length allowing better electron tunneling from CA to the electrode surface. Through these combined effects, the S-CN-Bi electrode demonstrated excellent ability on the electrochemical detection of CA in a low LOD of 11 ng.ml<sup>-1</sup> in a mixed protein PBS solution, being selective and sensitive to this protein. The S-CN-Bi electrode could also present signal of detection when simulating salivary CA. Via an easy and fast way, we have demonstrated that CA may be detectable by S-CN-Bi electrode in a non-invasive method, including a variety of samples as such saliva, blood, urine and sweat. The S-CN-Bi electrode presented as a promising clinical diagnostic and prognostic sensor for the detection of CA.

### **Acknowledgements**

The present work was funded by Fonds de recherche du Québec (FRQ) et Natural Sciences and Engineering Research Council of Canada (NSERC) discovery grants.

**Supplementary information:** Stripping metalloprotein with bismuth nanomaterials tethered on carbon surface

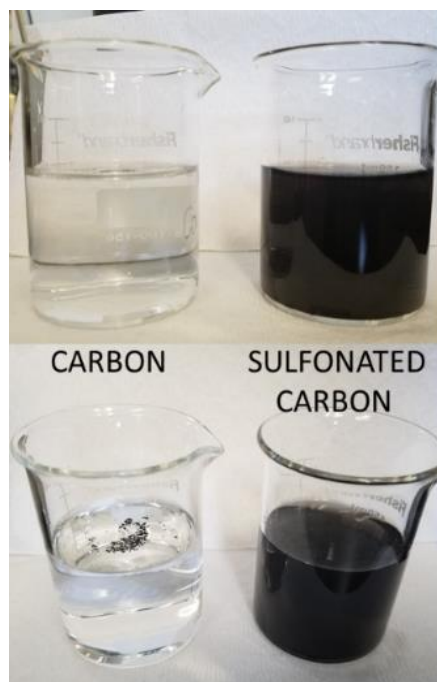


**Figure S 4.1** - CN and S-CN in ultrapure water. Clearly S-CN presented better dispersion of particles in water when compared with CN



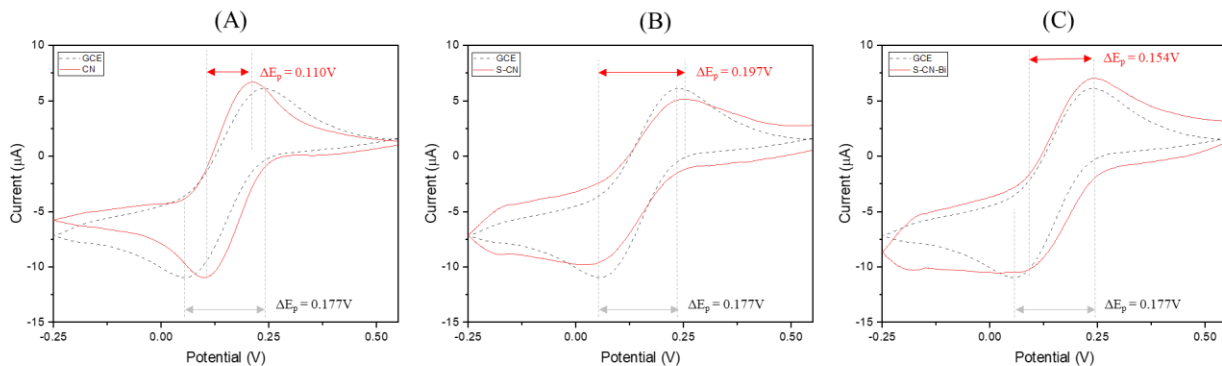


**Figure S 4.3** - Cyclic voltammograms in 1 mM  $K_4Fe(CN)_6$  in a 0.1 M KCl at 10 mV/s for GCE (dashed line), (A) CN, (B) S-CN and (C) S-CN-Bi, respectively

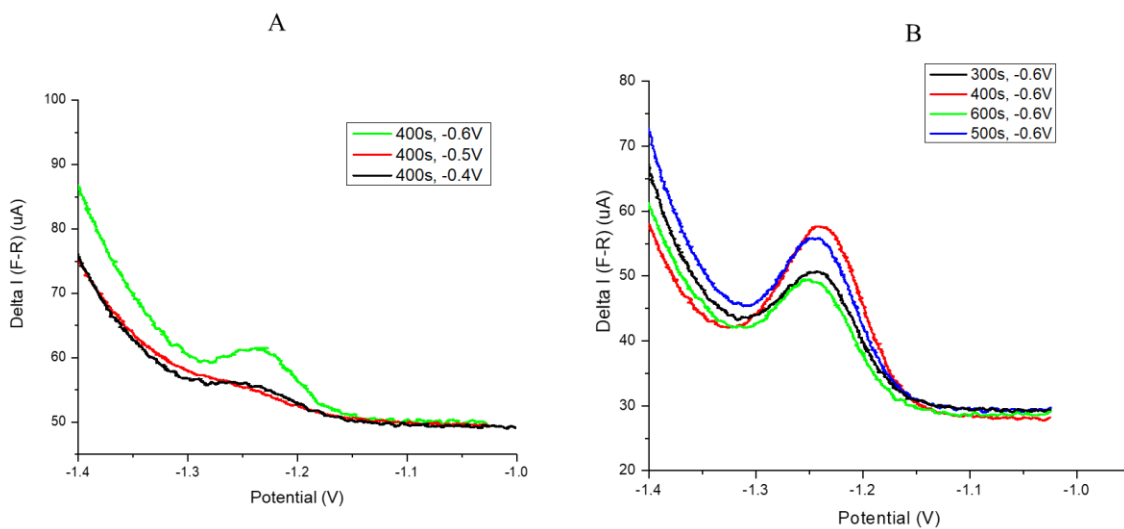


**Figure S 4.4** - Study of different parameters to electroreduced Bi ions in  $0.5 \mu\text{g}\cdot\text{ml}^{-1}$  of Zinc + 0.1M tris HCl. (A) The potential of deposition was varied from -0.4V to -0.6V (vs SCE), setting  $t=400\text{s}$ , and (B) the time of reduction was analysed from 300s to 600s, setting  $U= -0.6\text{V}$  (vs SCE). The best condition found to electroreduced Bi ions was -0.6V (vs SCE) for 400s.

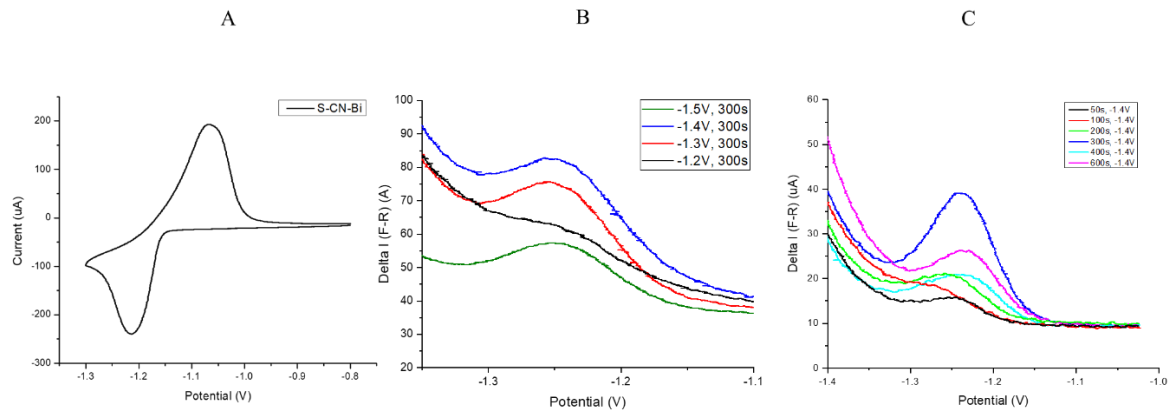


**Figure S 4.5** – Study of different parameters to detect Zn ions in  $0.5 \mu\text{g}\cdot\text{ml}^{-1}$  of Zinc +  $0.1\text{M}$  tris HCl. (A) CV of S-CN-Bi electrode in  $1 \text{ mg}\cdot\text{ml}^{-1}$  Zn Acetate +  $0.1\text{M}$  ABS (pH=4.5) aqueous solution, from  $-0.8\text{V}$  to  $-1.3\text{V}$  (vs SCE) at scan rate  $10\text{mV/s}$ . (B) The potential of deposition was varied from  $-1.2\text{V}$  to  $-1.5\text{V}$  (vs SCE), setting  $t=300\text{s}$ , and (C) The time of reduction was analysed from  $50\text{s}$  to  $600\text{s}$ , setting  $U= -1.4 \text{ V}$  (vs SCE). The best condition found to detect Zn ions was  $-1.4\text{V}$  (vs SCE) for  $300\text{s}$ .

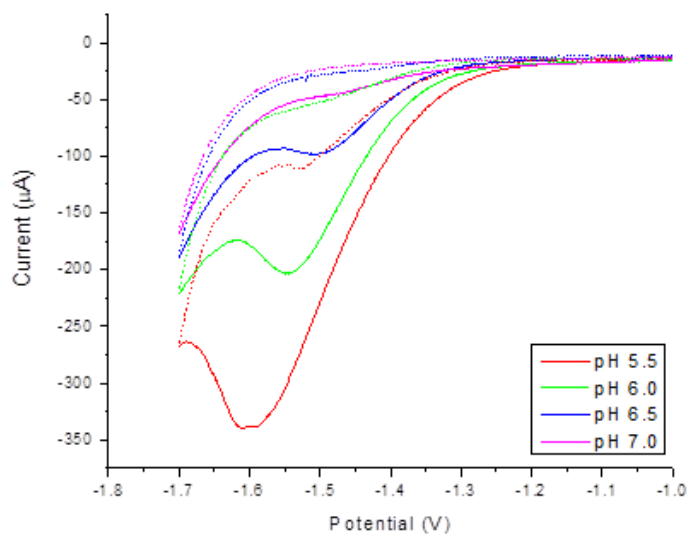


**Figure S 4.6** - Study of the best pH in PBS to detect CA

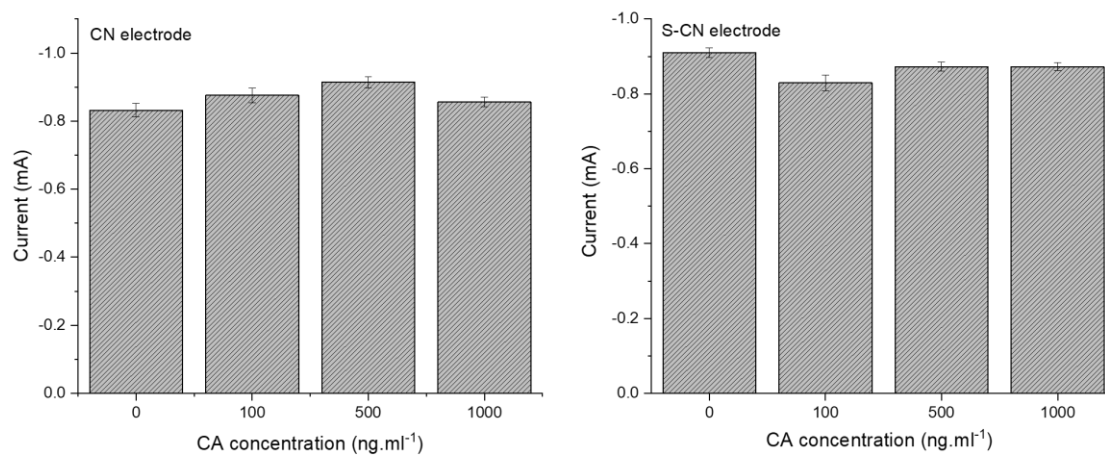


**Figure S 4.7** - Incoherent current response of CN and S-CN electrode in function of CA concentration at -1.7V (vs SCE), from 0 ng.ml<sup>-1</sup> to 500 ng.ml<sup>-1</sup>, respectively (PBS, pH 6).

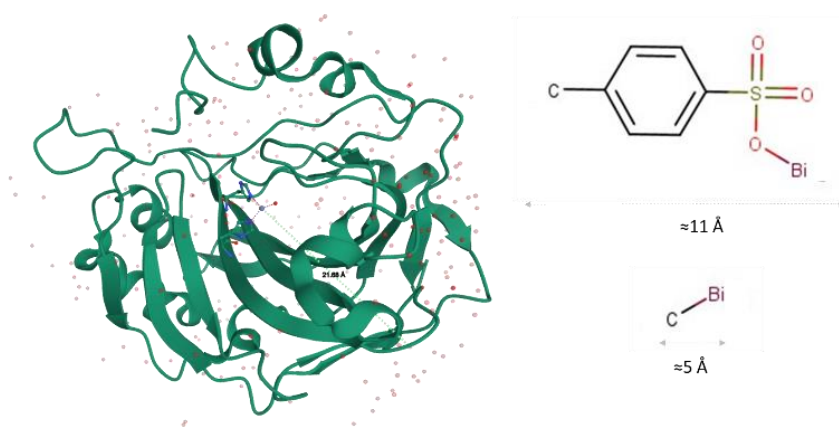


**Figure S 4.8** - Schematic of (A) CA and (B) Structural length of S-CN-Bi and C-Bi structures.

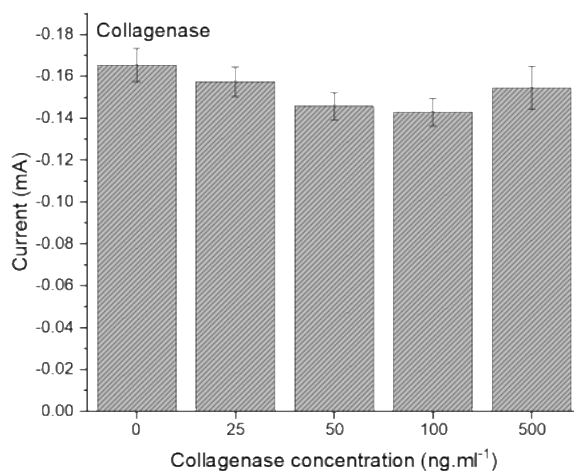


Figure S 4.9 - Incoherent current response of S-CN-Bi electrode in function of collagenase concentration at -1.7V (vs SCE), from 0 ng.ml<sup>-1</sup> to 500 ng.ml<sup>-1</sup> (PBS, pH 6).

## References

- [1] J. S. Garcia, C. S. de Magalhães, M. A. Z. Arruda, *Talanta* **2006**, *69*, 1.
- [2] D. Fu, L. Finney, *Expert Rev. Proteomics* **2014**, *11*, 13.
- [3] S. Prabhulkar, H. Tian, X. Wang, J.-J. Zhu, C.-Z. Li, *Antioxid. Redox Signal.* **2012**, *17*, 1796.
- [4] J.-S. Yang, C.-W. Lin, Y.-H. Hsieh, M.-H. Chien, C.-Y. Chuang, S.-F. Yang, *Oncotarget* **2017**, *8*, 83088.
- [5] Y.-H. Chu, C.-W. Su, Y.-S. Hsieh, P.-N. Chen, C.-W. Lin, S.-F. Yang, *Cells* **2020**, *9*, 704.
- [6] I. Gkouveris, N. G. Nikitakis, J. Aseervatham, N. Rao, K. U. Ogbureke, *Met. Med.* **2017**, *4*, 47.
- [7] S. Blatt, M. Krüger, T. Ziebart, K. Sagheb, E. Schiegnitz, E. Goetze, B. Al-Nawas, A. M. Pabst, *J. Cranio-Maxillofac. Surg.* **2017**, *45*, 722.
- [8] A. W. Eckert, S. Horter, D. Bethmann, J. Kotrba, T. Kaune, S. Rot, M. Bache, U. Bilkenroth, W. Reich, T. Greither, *Int. J. Mol. Sci.* **2019**, *20*, 375.
- [9] F. J. Huizing, J. Garousi, J. Lok, G. Franssen, B. A. Hoeben, F. Y. Frejd, O. C. Boerman, J. Bussink, V. Tolmachev, S. Heskamp, *Sci. Rep.* **2019**, *9*, 1.
- [10] I. J. Hoogsteen, H. A. Marres, K. I. Wijffels, P. F. Rijken, J. P. Peters, F. J. van den Hoogen, E. Oosterwijk, A. J. van der Kogel, J. H. Kaanders, *Clin. Cancer Res.* **2005**, *11*, 97.
- [11] M. I. Koukourakis, S. M. Bentzen, A. Giatromanolaki, G. D. Wilson, F. M. Daley, M. I. Saunders, S. Dische, E. Sivridis, A. L. Harris, *J. Clin. Oncol.* **2006**, *24*, 727.
- [12] M. Y. Mboge, B. P. Mahon, R. McKenna, S. C. Frost, *Metabolites* **2018**, *8*, 19.
- [13] K. M. Merz Jr, M. A. Murcko, P. A. Kollman, *J. Am. Chem. Soc.* **1991**, *113*, 4484.
- [14] B. A. Webb, M. Chimenti, M. P. Jacobson, D. L. Barber, *Nat. Rev. Cancer* **2011**, *11*, 671.
- [15] S. Tonello, F. Stradolini, G. Abate, D. Uberti, M. Serpelloni, S. Carrara, E. Sardini, *Sci. Rep.* **2019**, *9*, 1.
- [16] S. Campuzano, P. Yáñez-Sedeño, J. M. Pingarrón, *TrAC Trends Anal. Chem.* **2017**, *86*, 14.
- [17] G. Maduraiveeran, M. Sasidharan, V. Ganesan, *Biosens. Bioelectron.* **2018**, *103*, 113.
- [18] M. Vestergaard, K. Kerman, E. Tamiya, *Sensors* **2007**, *7*, 3442.
- [19] M. Pacios, I. Martín-Fernández, R. Villa, P. Godignon, M. Del Valle, J. Bartrolí, M. J. Esplandiu, in *Carbon Nanotub.-Growth Appl.*, IntechOpen, **2011**.

- [20] P. Hosseinzadeh, Y. Lu, *Biochim. Biophys. Acta BBA-Bioenerg.* **2016**, 1857, 557.
- [21] R. P. D. Bank, “RCSB PDB: Homepage,” can be found under <https://www.rcsb.org/>, **n.d.**
- [22] Z. Zhou, M. Hartmann, *Top. Catal.* **2012**, 55, 1081.
- [23] C. Ley, D. Holtmann, K.-M. Mangold, J. Schrader, *Colloids Surf. B Biointerfaces* **2011**, 88, 539.
- [24] Z. S. Aghamiri, M. Mohsennia, H.-A. Rafiee-Pour, *Talanta* **2018**, 176, 195.
- [25] S. Lee, S.-K. Park, E. Choi, Y. Piao, *J. Electroanal. Chem.* **2016**, 766, 120.
- [26] V. Jovanovski, S. B. Hočevcar, B. Ogorevc, *Curr. Opin. Electrochem.* **2017**, 3, 114.
- [27] A. Dueraning, P. Kanatharana, P. Thavarungkul, W. Limbut, *Electrochimica Acta* **2016**, 221, 133.
- [28] P. Jothimuthu, R. A. Wilson, J. Herren, X. Pei, W. Kang, R. Daniels, H. Wong, F. Beyette, W. R. Heineman, I. Papautsky, *Electroanalysis* **2013**, 25, 401.
- [29] B. Liu, L. Lu, M. Wang, Y. Zi, *Electroanal. Int. J. Devoted Fundam. Pract. Asp. Electroanal.* **2008**, 20, 2363.
- [30] A. T. Maghasi, H. B. Halsall, W. R. Heineman, H. L. R. Rilo, *Anal. Biochem.* **2004**, 326, 183.
- [31] J. Kim, W. R. de Araujo, I. A. Samek, A. J. Bandodkar, W. Jia, B. Brunetti, T. R. Paixão, J. Wang, *Electrochem. Commun.* **2015**, 51, 41.
- [32] M. de la Gala Morales, M. R. P. Marín, L. C. Blázquez, E. P. Gil, *Anal. Methods* **2014**, 6, 8668.
- [33] M. Yang, Z. Zhang, Z. Hu, J. Li, *Talanta* **2006**, 69, 1162.
- [34] M. F. Wahab, C. A. Pohl, C. A. Lucy, *Analyst* **2011**, 136, 3113.
- [35] S. Wu, W. Lu, Q. Kang, D. Shen, D. Pan, *Micro Nano Lett.* **2012**, 7, 1260.
- [36] R. Xing, Y. Liu, Y. Wang, L. Chen, H. Wu, Y. Jiang, M. He, P. Wu, *Microporous Mesoporous Mater.* **2007**, 105, 41.
- [37] L. Peng, A. Philippaerts, X. Ke, J. Van Noyen, F. De Clippel, G. Van Tendeloo, P. A. Jacobs, B. F. Sels, *Catal. Today* **2010**, 150, 140.
- [38] Y. Wei, X. Ling, L. Zou, D. Lai, H. Lu, Y. Xu, *Colloids Surf. Physicochem. Eng. Asp.* **2015**, 482, 507.
- [39] A. P. Koskin, Y. V. Larichev, I. V. Mishakov, M. S. Mel’gunov, A. A. Vedyagin, *Microporous Mesoporous Mater.* **2020**, 110130.

- [40] S. Mallakpour, S. Soltanian, *RSC Adv.* **2016**, *6*, 109916.
- [41] X.-Y. Liu, M. Huang, H.-L. Ma, Z.-Q. Zhang, J.-M. Gao, Y.-L. Zhu, X.-J. Han, X.-Y. Guo, *Molecules* **2010**, *15*, 7188.
- [42] I. M. Lokman, U. Rashid, Y. H. Taufiq-Yap, *Arab. J. Chem.* **2016**, *9*, 179.
- [43] W. Giurlani, M. Cavallini, R. A. Picca, N. Cioffi, M. Passaponti, C. Fontanesi, A. Lavacchi, M. Innocenti, *ChemElectroChem* **2020**, *7*, 299.
- [44] G.-J. Lee, H.-M. Lee, C.-K. Rhee, *Electrochem. Commun.* **2007**, *9*, 2514.
- [45] Y. Gao, H. Niu, C. Zeng, Q. Chen, *Chem. Phys. Lett.* **2003**, *367*, 141.
- [46] Y. He, Z. Wang, L. Ma, L. Zhou, Y. Jiang, J. Gao, *RSC Adv.* **2020**, *10*, 27697.
- [47] B. Li, M. Gu, Z. Nie, Y. Shao, Q. Luo, X. Wei, X. Li, J. Xiao, C. Wang, V. Sprenkle, *Nano Lett.* **2013**, *13*, 1330.
- [48] J. Wang, *Electroanal. Int. J. Devoted Fundam. Pract. Asp. Electroanal.* **2005**, *17*, 1341.
- [49] G. Kefala, A. Economou, A. Voulgaropoulos, *Analyst* **2004**, *129*, 1082.
- [50] R. Pauliukaitė, C. M. Brett, *Electroanal. Int. J. Devoted Fundam. Pract. Asp. Electroanal.* **2005**, *17*, 1354.
- [51] N. Serrano, J. M. Díaz-Cruz, C. Ariño, M. Esteban, *Electroanalysis* **2010**, *22*, 1460.
- [52] M. Á. G. Rico, M. Olivares-Marín, E. P. Gil, *Talanta* **2009**, *80*, 631.
- [53] W. Kang, X. Pei, W. Yue, A. Bange, W. R. Heineman, I. Papautsky, *Electroanalysis* **2013**, *25*, 2586.
- [54] P. K. Sahoo, B. Panigrahy, S. Sahoo, A. K. Satpati, D. Li, D. Bahadur, *Biosens. Bioelectron.* **2013**, *43*, 293.
- [55] K. E. Kaczor-Urbanowicz, F. Wei, S. L. Rao, J. Kim, H. Shin, J. Cheng, M. Tu, D. T. Wong, Y. Kim, *Biochim. Biophys. Acta BBA-Rev. Cancer* **2019**, *1872*, 49.
- [56] D. Vullo, S. Isik, S. Del Prete, V. De Luca, V. Carginale, A. Scozzafava, C. T. Supuran, C. Capasso, *Bioorg. Med. Chem. Lett.* **2013**, *23*, 1636.
- [57] C. T. Supuran, A. Scozzafava, *J. Enzym. Inhib.* **2000**, *15*, 597.
- [58] R. Khodarahmi, S. Khateri, H. Adibi, V. Nasirian, M. Hedayati, E. Faramarzi, S. Soleimani, H. C. Goicoechea, A. R. Jalalvand, *Int. J. Biol. Macromol.* **2019**, *136*, 377.
- [59] A. Moradi, H. Adibi, V. Akbari, A. R. Jalalvand, *Sens. Bio-Sens. Res.* **2022**, *37*, 100516.

- [60] M. Kuss-Petermann, O. S. Wenger, *J. Am. Chem. Soc.* **2016**, *138*, 1349.
- [61] J.-S. Yu, Y.-T. Chen, W.-F. Chiang, Y.-C. Hsiao, L. J. Chu, L.-C. See, C.-S. Wu, H.-T. Tu, H.-W. Chen, C.-C. Chen, *Proc. Natl. Acad. Sci.* **2016**, *113*, 11549.
- [62] T. T. H. Nguyen, B. Sodnom-Ish, S. W. Choi, H.-I. Jung, J. Cho, I. Hwang, S. M. Kim, *J. Korean Assoc. Oral Maxillofac. Surg.* **2020**, *46*, 301.
- [63] L. Zhang, H. Xiao, S. Karlan, H. Zhou, J. Gross, D. Elashoff, D. Akin, X. Yan, D. Chia, B. Karlan, *PloS One* **2010**, *5*, e15573.
- [64] C. F. Streckfus, O. Mayorga-Wark, D. Arreola, C. Edwards, L. Bigler, W. P. Dubinsky, *Cancer Invest.* **2008**, *26*, 159.
- [65] E. C. Porto-Mascarenhas, D. X. Assad, H. Chardin, D. Gozal, G. D. L. Canto, A. C. Acevedo, E. N. S. Guerra, *Crit. Rev. Oncol. Hematol.* **2017**, *110*, 62.
- [66] H. Xiao, L. Zhang, H. Zhou, J. M. Lee, E. B. Garon, D. T. Wong, *Mol. Cell. Proteomics* **2012**, *11*, M111.

#### **Chapter 4. Detecting the PEX Like Domain of Matrix Metalloproteinase-14 (MMP-14) with Therapeutic Conjugated CNTs**

This chapter includes a published peer-reviewed paper. The bibliographic details of the coauthored paper, including all authors, are:

*Daniela Vieira, Jake Barralet, Edward J Harvey, Geraldine Merle*

Published: Biosensors 2022, 12(10), 884; <https://doi.org/10.3390/bios12100884>

My contributions to the paper involved: Experimental design, implementation, and performance; Data collection and analysis; Preparation of the manuscript.

Previous chapter III “*Stripping metalloprotein with bismuth nanomaterials tethered on carbon surface*” we showed how bismuth nanoparticles deposited on functionalized-carbon surface, with a flexible and conjugated spacer arm, could reach the buried redox center of carbonic anhydrase (CA), a zinc-containing protein. The present chapter IV also reveals an alternative way to the recognition bioelements by only applying non bio molecules on the detection of zinc-containing protein. In previous chapter II, the inhibition of CA by the  $SO_3^-$  showed a diminution of the current intensity as the concentration of CA increased. This synergistic interaction and the complex formation between the  $SO_3^-$  and CA initiated a new track of thought, where inhibitory molecules could interact with proteins giving current responses in function of the protein concentration. As mentioned before, the first approach towards the zinc-containing protein detection was achieved by aiming the well-known catalytic domain. In the following chapter IV “*Detecting the PEX Like Domain of Matrix Metalloproteinase-14 (MMP-14) with Therapeutic Conjugated CNTs*”, we designed a functionalized-carbon system with a MMP-14 inhibitory molecule, NSC-405020, that interacts with the hemopexin domain of MMP-14, an overexpressed cancerous zinc-related

biomarker. The inhibitor-loaded CNT system successfully detected and quantified MMP-14 using electrochemical impedance spectroscopy with a linear range of detection of 10 ng.mL<sup>-1</sup> to 100 ng.mL<sup>-1</sup>, and LOD of 7.5 ng.mL<sup>-1</sup>.

# Detecting the PEX Like Domain of Matrix Metalloproteinase-14 (MMP-14) with Therapeutic Conjugated CNTs

*D. Vieira*<sup>1</sup>, *J. Barralet*<sup>1,2</sup>, *E. Harvey*<sup>1,2</sup> and *G. Merle*<sup>1,3,\*</sup>

<sup>1</sup> Department of Experimental Surgery, Faculty of Medicine, McGill University, Montreal, H3G 2M1, Canada

daniela.vieira@mail.mcgill.ca (D.V.); jake.barralet@mcgill.ca (J.B.); edward.harvey@mcgill.ca (E.H.)

<sup>2</sup> Department of Surgery, McGill University, Montreal, H3G 1A4, Canada

<sup>3</sup> Department of Chemical Engineering, Polytechnique Montreal, Montreal, H3T 1J4, Canada

\*correspondence: [geraldine.merle@polymtl.ca](mailto:geraldine.merle@polymtl.ca)

**Abstract:** Matrix metalloproteinases (MMPs) are essential proteins acting directly in the breakdown of the extra cellular matrix and so in cancer invasion and metastasis. Given its impact on tumor angiogenesis, monitoring MMP-14 provides strategic insights on cancer severity and treatment. In this work, we report a new approach to improve the electrochemical interaction of the MMP-14 with the electrode surface while preserving high specificity. This is based on the detection of the hemopexin (PEX) domain of MMP-14, which has a greater availability with a stable and low-cost commercial molecule, as a recognition element. This molecule, called NSC-405020, is specific of the PEX domain of MMP-14 within the binding pocket. Through the covalent grafting of the NSC-405020 molecule on carbon nanotubes (CNTs), we were able to detect and quantify MMP-14 using electrochemical impedance spectroscopy with a linear range of detection of 10 ng.ml<sup>-1</sup> to 100 ng.ml<sup>-1</sup>, and LOD of 7.5 ng.ml<sup>-1</sup>. The specificity of the inhibitory small molecule was validated against the PEX domain of MMP-1. The inhibitor loaded CNTs

system showed as a desirable candidate to become an alternative to the conventional recognition bioelements for the detection of MMP-14.

**Keywords:** MMP-14; electrochemical detection; PEX domain; CNT; surface modification; cancer

## 1. Introduction

Matrix metalloproteinases (MMPs) are zinc family protein involved in the breakdown of various components of the extracellular matrix in normal physiological processes, such as embryonic development, reproduction, and tissue remodeling, as well as in disease processes such as arthritis and cancer <sup>[1-3]</sup>. To date, there are 23 MMPs identified in humans <sup>[2,3]</sup>. According to their function and substrate specificity, MMPs are divided in the following groups: collagenases (MMPs-1, 8, 13), gelatinases (MMPs-2 and 9), stromelysins (MMPs-3, 10 and 11), matrilysins (MMPs-7 and 26), membrane-type (MMPs-14, 15, 16, 17, 23, 24 and 25) and others (MMPs-12, 19, 20, 22, 27 and 28) <sup>[4,5]</sup>. MMPs are the major proteases involved in the degradation of extracellular matrix <sup>[4-6]</sup>. MMPs present a typical structure consisting of at least three domains: predomain, propeptide, catalytic and hemopexin <sup>[4,5]</sup>. The expression of MMPs is maintained in the body at a constant low level; however, their abnormal expression has been associated with numerous diseases, including cancer <sup>[4,7,8]</sup>. Excessive expression of MMPs is reported in and around tumors and is associated with cancer stage, progression, metastasis, and mortality <sup>[7-9]</sup>. Given their important role in both physiological and pathological processes, MMPs have become valuable biomarkers to various specific cancers. Current methods to detect MMPs include liquid chromatography-mass spectroscopy <sup>[10-12]</sup>, fluorescence resonance energy transfer <sup>[13-15]</sup>, surface plasmon resonance <sup>[16,17]</sup> and enzyme-linked immunosorbent assay (ELISA) <sup>[18,19]</sup>. Despite high specificity and limit of detection, these techniques require qualified personal and high costs of maintenance and performance <sup>[3,22,23]</sup>. Compared to these molecular approaches, electrochemical techniques are simpler, faster, low-cost, and user-friendly, which makes them a more appropriate tool for the rapid detection of proteins <sup>[20]</sup>. The electrochemical detection is usually facilitated by a recognition element that will bind specifically to the target molecules <sup>[20-22]</sup>. Most typically detections are

accomplished via biomolecules, such as antibody, enzymes, aptamers, nucleic acids, and peptides attached to gold/carbon substrates [20,22–24]; however, a crucial feature is not only the binding affinity but also the interfacial stability, where bioelements in terms of stability in terms of stability, are limited to physiological conditions and prone to irreversible denaturation and most of the case, expensive, affecting the activity of the sensors and limiting their use [25,29,30].

MMP-14, also known as MT1-MMP, is of particular interest in the field of oncology. It is an anchored membrane protein and has shown significant contribution in tumor angiogenesis by cleaving extra cellular matrix molecules as a matrix-degrading enzyme [4,10,11]. MMP-14 also coordinates key pro-angiogenic factors, such as VEGF, pro-TGF- $\beta$  and endoglin, suggesting crucial role in vessel maturation and formation [8,10,31]. Because of the elevated MMP-14 expression observed in breast [25,26], head and neck [26], fibrosarcoma [26,27], prostate [27], gastric [28], bladder [29], ovarian [30] and brain [31] cancer, the detection and measurement of MMP-14 has an essential role in the diagnostic and the treatment direction of cancer. The catalytic domain is usually the target domain for the electrochemical detection of MMPs because of communication between the redox active center (zinc) and the electrode surface. However, the proteolytic site is usually hidden within the insulating protein shell, making the electrochemical response very challenging to measure at the electrode [32]. An alternative to the catalytic approach is to use specific molecules that bind to the other domains, e.g., hemopexin (PEX). Except for MMPs-7, 23 and 26, all humans MMPs are expressed with a PEX-like domain [5,6]. PEX domain regulates key specific functions in different MMPs [33,34]; For example, PEX mediates the activation process of gelatinase (MMP-2) and collagenases (MMP-1 and 13); blocks the glycoproteins TIMPs (MMP-1, 2, 9 and 13) and clusterin (MMP-25), natural inhibitors of MMPs; assists on the homodimerization of MMP-1, 9 and 14; binds and cleavages different substrates, such as chemokines (MMP-2), C1q (MMP-14),

IGFBP-3 (MMP-19), fibrinogen (MMP-2), etc.; and is crucial for the attachment of MMPs to the cell surface <sup>[34]</sup>. PEX domain demonstrates easy access and abundance in the protein structure when compared to the hidden zinc ion on the catalytic core of the protein <sup>[35]</sup>.

Currently, only one approach has been employing inhibitory peptide to interact electrochemically with the PEX domain for the electrochemical detection of MMP-14 <sup>[36,37]</sup>. These peptides attached onto gold electrode exhibits a fairly good specificity towards MMP14 with a limit of detection (LOD) of  $7\text{ng}\cdot\text{L}^{-1}$  after 30 min, but some concerns associated with reduced shelf life (temperature sensitivity, denaturation, dependence on pH and ionic strength), complex synthesis and storage/operational procedure <sup>[28,44,45]</sup> exist. Given the importance and specificity of PEX domain in MMPs, enhancing response time and storage/operational stability while lowering cost and maintaining selectivity is highly attractive because reliable and cheap point-of-care testing diagnostics are needed to respond to cancer. In this work, we proposed a new avenue to detect MMP-14 by applying a synthetic chemical inhibitory chemical molecule as the recognition element. Our hypothesis was that a non biocomponent would bind specifically with the PEX domain of MMP-14, overcoming the limitations related to the use of unstable biomolecules and the inaccessible catalytic domain. A simple therapeutic would support low cost, reproducibility, resistance in less favorable microenvironments and stability in prolonged storage <sup>[38,39]</sup>.

In this work, we engineered a fast, precise, and specific electrochemical MMP-14 sensor by targeting the PEX like domain of MMP-14 using a therapeutic ligated onto multi-walled carbon nanotubes (CNTs). Among the different inhibitory therapeutic, a synthetic molecule, NSC-405020 (3,4-Dichloro-N-(pentan-2-yl) benzamide) was chosen because of its single action on the PEX domain of MMP-14. NSC-405020 is a specific noncatalytic inhibitor of MMP-14, that directly interacts with PEX domain, affecting protein homodimerization but not the catalytic activity <sup>[33,40]</sup>.

CNTs offer excellent intrinsic properties such as high surface area, chemical stability and high electrical conductivity ( $10^6$ – $10^7$  S/m) <sup>[41]</sup>, becoming one of the most attractive nanomaterials in electrochemical sensing <sup>[42–44]</sup>. Furthermore, CNTs act as signal amplifier due to their high specific area that allows multitude of proteins to be gathered <sup>[32]</sup>. The resultant inhibitor loaded CNT system was physiochemically characterized and tested in PBS (pH 7.40) to verify the ability to detect specifically MMP-14 and not other metalloproteinase.

## 2. Methodology

### *2.1 Functionalization of CNTs*

Multi walled carbon nanotubes (CNTs) were functionalized in 3 steps: (i) oxidation in an acid mixture <sup>[45]</sup>; (ii) generation of acyl chloride functional groups by suspension in a solution of  $\text{SOCl}_2$  <sup>[46]</sup>; and (iii) covalent grafting of the small molecule <sup>[47]</sup> (Figure 1). Briefly, in the first step, 50 mg of CNTs (Sigma-Aldrich, Ontario, Canada) were added to 50 mL of  $\text{H}_2\text{SO}_4$ : $\text{HNO}_3$  (3:1) (Fisher Scientific, Ontario, Canada) mixture, dispersed for 2 h in an ultrasound bath and then, upheld for 15 h. After, HCl (Fisher Scientific, Ontario, Canada) was added to the solution. Subsequently, ammonium hydroxide (Fisher Scientific, Ontario, Canada) was used to neutralize. Finally, oxidized CNTs were filtered using a 0.22  $\mu\text{m}$  nylon membrane (GVS, Fisher Scientific, Ontario, Canada), washed with ultra-pure water (Milli-Q, Merck, Darmstadt, Germany) until neutral pH and dried overnight in an oven at 40 °C. The second step consisted of the generation of the acyl chloride on CNTs surfaces. The oxidized CNTs were suspended in  $\text{SOCl}_2$  (0.1 g of CNT per 20 mL of  $\text{SOCl}_2$ ) (Fisher Scientific, Ontario Canada) and dispersed for 20 min in an ultrasound bath. The solution was stirred at 70 °C for 36 h. The resulting acylated CNTs were filtered, washed several times with anhydrous tetrahydrofuran (Fisher Scientific, Ontario, Canada) and dried

overnight at 40 °C. 3,4-Dichloro-N-(pentan-2-yl) benzamide, (MMP-14 Inhibitor- NSC-405020 (AmBeed, Illinois, USA)) was grafted onto acylated CNTs. The inhibitor molecule was mixed with 1 mL solution of DMF (Fisher Scientific, Ontario, Canada) and NaH (60%) (Fisher Scientific, Ontario, Canada) and then stirred for 1 h. The obtained acylated CNTs were then added to the suspension (molecule-to-CNTs weight ratio 15:1). The reaction was kept at 100 °C for 5 days. After, the inhibitor loaded CNTs were filtered, washed several times with ultra-pure water and dried overnight at 40 °C.

## *2.2 Materials Characterization*

The morphology of pristine CNTs, acylated CNTs, and inhibitor loaded CNTs was investigated by Scanning Electron Microscopy (SEM, Inspect F50, FEI Company, Hillsboro, OR, USA). Particle diameter was measured with ImageJ software taking the average of 10 CNTs. Fourier transform infrared spectroscopy (FT-IR–PerkinElmer) was carried out in the wavenumber range of 3500 to 500  $\text{cm}^{-1}$  to confirm the grafting of the molecule on CNTs. Cyclic voltammetry (CV) was performed to assure the modification of CNTs from  $-0.2$  V to  $+0.6$  V at scan rate of  $10 \text{ mV}\cdot\text{s}^{-1}$ . Electrochemical experiments were performed using a potentiostat (VersaSTAT 4, Princeton Applied Research, Oak Ridge, TN, USA) with a three-electrode system cell, where glassy carbon electrode (GCE), acylated CNTs and inhibitor loaded CNTs were used as work electrodes. Platinum wire was used as the counter electrode, and saturated calomel electrode (SCE) as the reference electrode. To prepare the acylated and inhibitor loaded CNTs electrodes, 50% of ethanol (Fisher Scientific, Ontario, Canada) aqueous solutions containing  $1 \text{ mg}\cdot\text{mL}^{-1}$  of acylated CNTs or inhibitor loaded CNTs were prepared and stored. GCE (5 mm, Alfa Aesar, Massachusetts, USA) were polished with  $0.05 \text{ }\mu\text{m}$   $\text{Al}_2\text{O}_3$  (Fisher Scientific, Ontario, Canada) suspension to achieve a shiny surface. GCEs were cleaned by sonication in 10%  $\text{H}_2\text{SO}_4$  (Fisher Scientific, Ontario,

Canada), 50% acetone (Fisher Scientific, Ontario, Canada), and ultra-pure water -each for 10 min successively. The electrodes were dried at room temperature. Finally, 20  $\mu\text{L}$  of the desired solution was dropped onto the cleaned GCE and dried at room temperature.

### *2.3 Detection of MMP-14*

The detection of the MMP-14 protein was performed via electrochemical impedance spectroscopy (EIS) within the frequency from 50 kHz to 500 Hz, 12 points per decade, applied potential of 50 mV, and direct potential of +0.20 V. All CVs and EIS spectra were obtained in PBS (pH 7.40) containing 10  $\text{mmol}\cdot\text{ml}^{-1}$  of  $\text{K}_4[\text{Fe}(\text{CN})_6]^-$  (Sigma-Aldrich, Ontario, Canada), 10  $\text{mmol}\cdot\text{ml}^{-1}$  of  $\text{K}_3[\text{Fe}(\text{CN})_6]^-$  (Sigma-Aldrich, Ontario, Canada) and 10  $\text{mmol}\cdot\text{ml}^{-1}$  of NaCl (Fisher Scientific, Ontario, Canada) [22]. MMP-14 and MMP-1 proteins were unfolded prior experiments. Briefly, 1  $\mu\text{g}\cdot\text{mL}^{-1}$  of protein was incubated for 1 h at 37 °C with 200  $\mu\text{M}$  EDTA (Fisher Scientific, Ontario, Canada) and 5 mM 2-Mercaptoethanol (Sigma-Aldrich, Ontario, Canada) to generate denatured MMPs [48]. Afterwards, solutions with the desired concentration (from 0 to 250  $\text{ng}\cdot\text{ml}^{-1}$ ) were prepared in PBS (pH 7.4), dropped onto electrodes surfaces (50  $\mu\text{L}$ ), and incubated at room temperature for 10 min. Electrodes were then extensively rinsed with ultra-pure water to remove any physically adsorbed MMP-14. EIS was performed in presence and absence of the proteins, applying the acylated and the inhibitor loaded CNTs electrodes. Circuit fit was performed using EC-Lab<sup>®</sup> software (Version 10.38, Biologic Science Instruments, France) (**Supporting information S4.1**). Resistance to charge ( $R_{ct}$ ) was extracted from the intercept on the real axis.

Limit of detection (LOD) was calculated according to the Formula (1):

$$LOD = 3 \times \left(\frac{SD}{S}\right) \quad (1)$$

where, SD is the standard error intercept and the S is the slope of the calibration curve (S), both extracted from origin software after linear regression.

#### 2.4 Statistics

The data were analyzed using OriginPro (OriginLab Corporation, version 2018G' Massachusetts, USA) and presented as mean  $\pm$  SD. A one-way ANOVA and Tukey test were performed to evaluate statistical significance. *p*-Value smaller than 0.05 denotes significant difference.

### 3. Results and Discussion

To overcome the challenging access to the catalytic core of the protein, we were interested to investigate and detect the PEX domain. Here, CNTs were chemically modified with PEX like domain inhibitory molecule to specifically bind one of MMP-14 domains. Pristine carbon materials are usually chemically inert, and require a prior surface treatment for activating and facilitating the immobilization of molecules of interest to offer a durable grafting and so a long term use<sup>[49]</sup>. CNTs were initially oxidized by a room temperature process in acid mixture of HNO<sub>3</sub> and H<sub>2</sub>SO<sub>4</sub>, with addition of HCl. Among the available methodologies to produce oxidized carbon structures, the designated for this work has been shown as the best to enable a high percentage of hydroxyl and carboxyl groups on CNTs surface<sup>[45]</sup>. The generated carboxylates were then further modified to more reactive acyl chloride groups after reacting with SOCl<sub>2</sub>. After acylation reaction, the inhibitory molecule NSC-405020 was covalently bounded to the acylated CNTs surface, via the addition-elimination process of the acyl group, resulting in the inhibitor loaded CNTs (**Figure**

4.1A). The covalent bond assures a more robust and stable connection between the organic compound and the CNTs in comparison to noncovalent procedures, generating a more effective electrode interface [50–53].

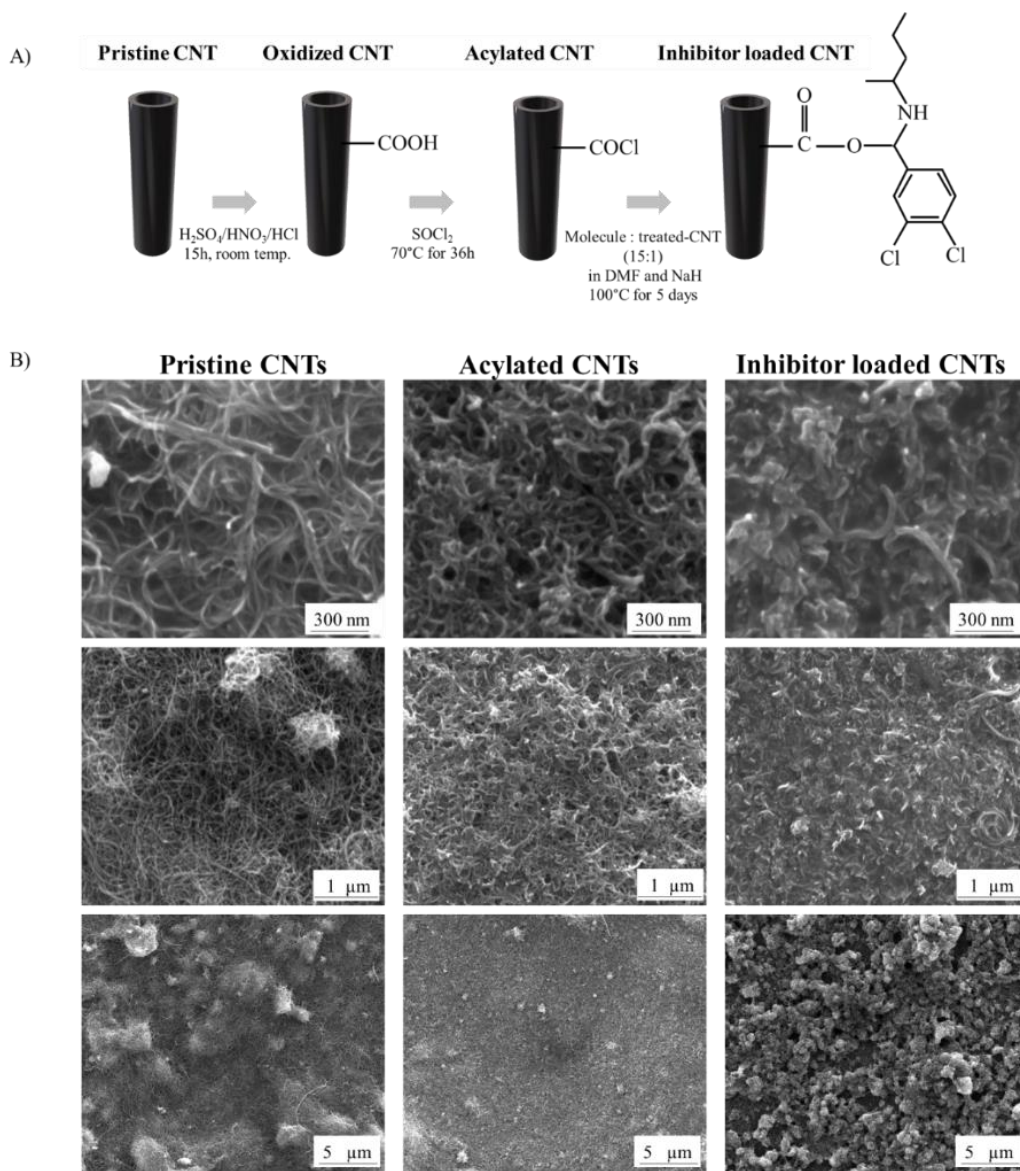


**Figure 4.1** - (A) Schematic representation of NSC-405020 molecule grafted onto CNTs surface followed by (B) SEM images for pristine, acylated, and inhibitor loaded CNTs (low and high magnification).

SEM images showed mild changes on the surface of CNTs after chemical treatment at high magnification (**Figure 4.1B**). Due to van der Waals' attraction causing significant agglomeration, the pristine CNTs show a longer length compared to the modified CNT [52,53]. As expected, after oxidation and generation of acyl groups the acylated CNTs showed a slight reduction in the length of the nanotubes [44,51]; however, they are denser and less aggregated due to the repulsion between CNTs with chemical groups attached to their surfaces—allowing a better dispersion [51,52]. The inhibitor loaded CNTs changed notably the dispersion with clearly more aggregated CNTs. The attachment of organic compounds on CNTs surface also increased the tube diameter ( $36.08 \pm 3.55$  nm compared to pristine  $18.05 \pm 1.11$  nm) [54,55].

Chemical grafting was confirmed with FT-IR analysis and cyclic voltammetry (CV). The FTIR spectra of pristine, acylated, and inhibitor loaded CNTs are shown in **Figure 4.2A**. As shown in **Figure 4.2A**, pristine CNTs did not show strong peaks when compared to the acylated and inhibitor loaded CNTs. Weak intensity could be observed at  $\sim 2105$ ,  $1500$ ,  $1267$  and  $1007$   $\text{cm}^{-1}$ , typical peaks related to the C=C bond from the hexagonal CNT structure [52]. After oxidation and generation of acyl groups, weak peaks were observed at  $\sim 1813$  and  $1700$   $\text{cm}^{-1}$ , that could be attributed to C=O bond stretching vibration as a result of carbon oxidation [53,54,59,63]; The peak at  $\sim 1388$  and  $1000$   $\text{cm}^{-1}$  is associated with C–O vibrations from acyl groups [52,56].

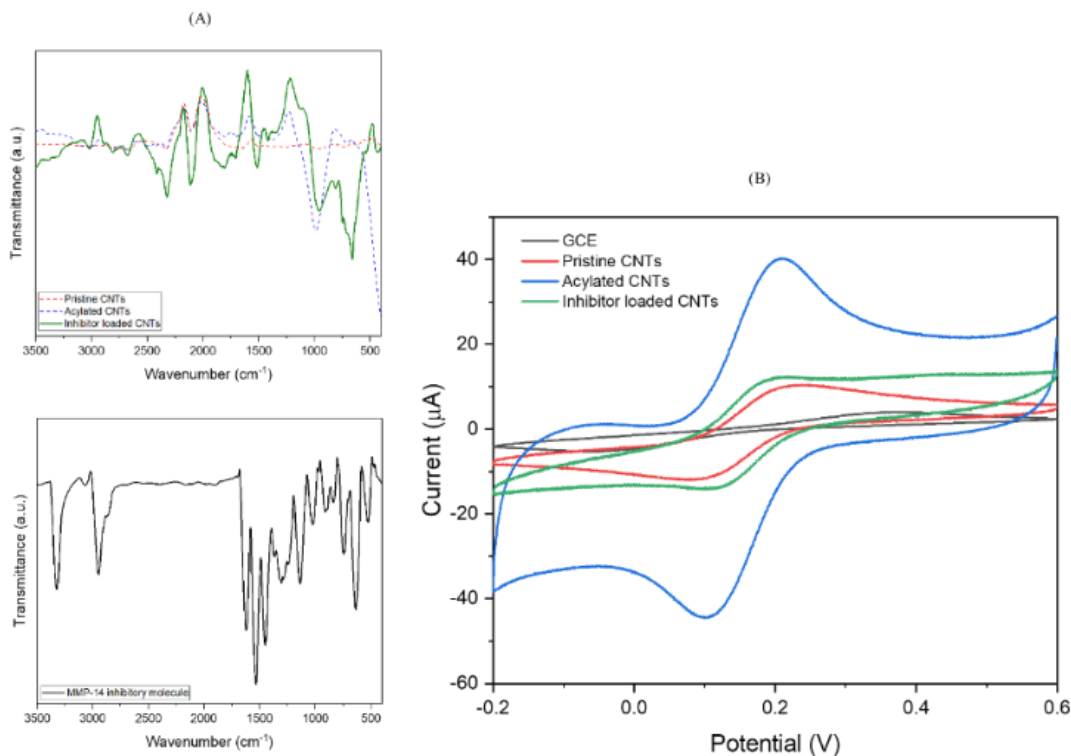


**Figure 4.2** - (A) FTIR spectrum (top) of pristine, acylated, and inhibitor loaded CNTs, respectively. The spectrum (down) of NSC-405020 molecule is also demonstrated. (B) CVs for GCE, pristine, acylated, and inhibitor loaded CNTs in PBS (pH 7.40) containing  $10 \text{ mmol}\cdot\text{mL}^{-1}$  of  $\text{K}_4[\text{Fe}(\text{CN})_6]^{3-}$ ,  $10 \text{ mmol}\cdot\text{mL}^{-1}$  of  $\text{K}_3[\text{Fe}(\text{CN})_6]^{2-}$  and  $10 \text{ mmol}\cdot\text{mL}^{-1}$  of NaCl, scan rate  $10 \text{ mV/s}$ .

After grafting the inhibitor on CNTs, additional peaks were observed at  $\sim 3012$ ,  $1513$  and  $1412 \text{ cm}^{-1}$ , assigned to C–C and C=C vibration of the benzene ring <sup>[57–59]</sup>. The strong peak at  $\sim 675 \text{ cm}^{-1}$  is characteristic of C–Cl bond present in the chlorobenzene <sup>[57,60]</sup>. The peak at  $\sim 1704 \text{ cm}^{-1}$  is associated with N–H stretching from the molecule structure <sup>[61]</sup>. Note that because of the grafting process leading to change in electronegativity of the neighboring atom, some peaks have shifted from the expected wavenumber, such as C–Cl ( $\sim 730 \text{ cm}^{-1}$ ) and N–H ( $\sim 1610 \text{ cm}^{-1}$ ). Cyclic voltammetry was carried out with ferrocyanide/ferricyanide redox couple ( $\text{Fe}(\text{CN})_6^{3-/4-}$ ) to confirm

the presence of inhibitor on CNTs (**Figure 4.2B**). An increase in peak current density ( $I_{pa} = \sim 10.30 \mu\text{A}$ ), and a decrease of peak width ( $\Delta E_p = \sim 134 \text{ mV}$ ) was observed in the  $\text{Fe}(\text{CN})_6^{3-/4-}$  voltammograms after deposition of CNTs on GCE because of the higher active surface area. Acylated CNT presented a significant improvement in the peak current density ( $I_{pa} = \sim 40.45 \mu\text{A}$ ), and a decrease of peak width ( $\Delta E_p = \sim 105 \text{ mV}$ ). It is known that the carbon oxidation and the generation of acyl groups improve the high electron transfer rate by introducing negative charges onto CNTs surface and increasing the number of active sites on electrode surface [44,53]. As expected, CNTs modified with the inhibitory molecule caused a significant drop of peak current density ( $I_{pa} = \sim 12.30 \mu\text{A}$ ), attributed to a loss of conductivity. These results were consistent with SEM and FTIR, confirming the successful grafting of molecule onto CNTs surface.

The efficacy of the inhibitor loaded CNTs towards the detection of MMP-14 was investigated using electrochemical impedance spectroscopy (EIS). **Figure 4.3A** shows the impedance spectra of the inhibitor loaded CNT electrode for the blank and MMP-14 in concentrations of 10, 50 and 100  $\text{ng}\cdot\text{ml}^{-1}$ , and its respective limit of detection (LOD) (Figure 4.3B). Note: logarithmic values were applied in **Supplementary information S4.2**.

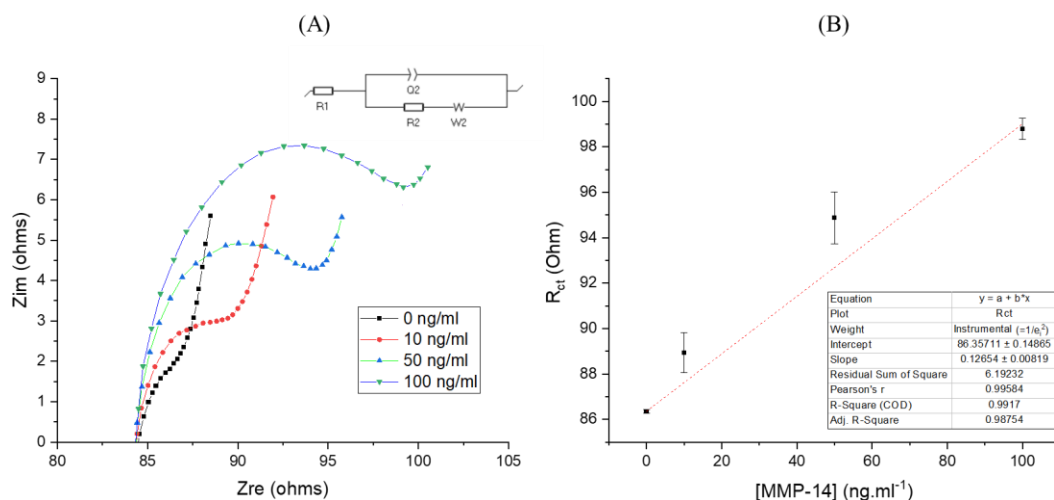


**Figure 4.3** - (A) Nyquist plots of inhibitor loaded CNTs before and after interaction with different concentrations of MMP-14 for 10 minutes in PBS (pH 7.40) containing 10 mmol.ml<sup>-1</sup> of K<sub>3</sub>[Fe(CN)<sub>6</sub>]<sup>-</sup> and 10 mmol.ml<sup>-1</sup> of NaCl. (B) Linear fit of EIS response for different concentrations of MMP-14, presenting LOD of 7.5 ng.ml<sup>-1</sup>. Significant difference between measurements was obtained at p-value < 0.05 (n = 2). Protein concentration varying from 10 ng.ml<sup>-1</sup> to 100 ng.ml<sup>-1</sup>, applied potential of +0.20 V, from 50 kHz to 500 Hz, amplitude 50 mV.

At high MMP-14 concentrations, the real and imaginary part of the impedance increased drastically; the electrochemical signal is reproducible and stable during each measurement for the same concentration of MMP-14. A linear relationship between MMP-14 concentration and the charge transfer resistance ( $R_{CT}$ ) values was observed. The inhibitor loaded CNT electrode achieve a high sensitivity of 2.83  $\mu\text{A} \cdot \log [\text{MMP-14}]^{-1}$  and a linear correlation of 0.99. The designed inhibitor loaded CNT system presented LOD of 7.5 ng.ml<sup>-1</sup>, and range of detection from 10 to 100 ng.ml<sup>-1</sup> (**Supplementary information S4.3**). Most common electrochemical systems applied to detect MMPs up to now have been using carbon and gold as substrate<sup>[32,49]</sup> combined with biomolecules, such as aptamers, antibodies, enzymes, or peptides as the recognition element <sup>[24]</sup>.

Carbon-Gold-Pb-Peptide sensor was applied for the detection of MMP-2 [62]. The sensor exhibited linear detection from  $1 \text{ pg.ml}^{-1}$  to  $1 \text{ }\mu\text{g.ml}^{-1}$ , high sensitivity of  $28.4 \text{ }\mu\text{A.log [MMP-2]}^{-1}$  and low LOD of  $0.40 \text{ pg.ml}^{-1}$  but was fabricated with peptides through several steps in a complex synthesis using polyaniline gel as substrate and C-AuNPs-Pb<sup>2+</sup> as impedance enhancer. In a recent study, silver nano particles were combined to peptides and receptor to allow the detection of MMP-2 by anodic stripping voltammetry [63]. The method offered a significant improvement when compared to the traditional ELISA assay, presenting range of detection from  $0.5 \text{ pg.ml}^{-1}$  to  $50 \text{ ng.ml}^{-1}$  and LOD of  $0.12 \text{ pg.ml}^{-1}$ . Besides innovative approach, the presence of bioelements is still a challenge to assure low cost and long stability. Vertically aligned single-wall CNTs were used as substrate to attach antibody and enzyme for the detection of MMP-3, presenting linear detection from  $0.4$  to  $40 \text{ ng.ml}^{-1}$ , sensitivity of  $77.6 \text{ nA.log [MMP-3]}^{-1}$  and LOD of  $4 \text{ pg.ml}^{-1}$  [64]. Despite great sensitivity, the labelling approach applied consumes time, involves complex sample handling and is expensive [65]. Peptide decorated gold-CNT electrode recognizes the MMP-7 protein, presenting linear detection from  $0.01$  to  $1000 \text{ ng.ml}^{-1}$  and LOD of  $6 \text{ pg.ml}^{-1}$  [66]. A screen-printed electrode was designed by grafting antibodies into 2D structures, graphene oxide and MoS<sub>2</sub>, aiming to amplify the analytical signal for the detection of MMP-7 [67]. Indeed, the 2D nanostructured immunosensor showed improvements and presented range of detection from  $10 \text{ pg.ml}^{-1}$  to  $75 \text{ ng.ml}^{-1}$  and LOD of  $7 \text{ pg.ml}^{-1}$ . 2D graphene structures were also employed to detect MMP-1 protein in an immunosensor based on a gold nanoparticle, polyethyleneimine and reduced graphene oxide [68]. The system showed great performance in different body fluids with range of detection from  $1 \text{ ng.ml}^{-1}$  to  $50 \text{ ng.ml}^{-1}$  and LOD of  $0.2 \text{ ng.ml}^{-1}$ . However, the graft of antibodies into 2D graphene structures in both works did not overcome the limitations of immunosensors, including high cost and issues with stability. Only one approach has explored the detection of

MMP-14 through the electrochemical interaction with hemopexin domain. In both works, inhibitory thiolated PEX-14 binding peptides (named ISC) were attached to gold electrodes exhibiting a fairly good specificity towards MMP-14, presenting linear detection from 0.4 pg.ml<sup>-1</sup> to 0.05 ng.ml<sup>-1</sup> with LOD of 7 pg.ml<sup>-1</sup> after 30 min; despite the ability of detect very low concentration of MMP-14, the challenges discussed previously, such as instability and complexity of bio elements, remains present. An important note to compare the present work to the ISC peptide is the limited concentration range of detection showed by the peptide system. The designed inhibitor loaded CNT system, presented in this work, revealed as an alternative to the conventional recognized bio elements, with ability to detect MMPs in a clinically relevant concentration range, presenting low cost, reproducibility, and stability in a real-world microenvironment (the loaded CNT system showed stability within 6 months of the study when stored at room temperature). The inhibitor loaded CNTs could be applicable for a variety of cancers as shown in **Table 4.1**. The LOD of 7.5 ng.ml<sup>-1</sup> includes the possibility of quantification of MMP-14 levels not only in the cancerous cells but also in different body samples, such as serum and tissues. Note: Cancerous tissue weight varies from ~10 mg to ~48 g depending on the anatomic site <sup>[69]</sup>. The present study showed the ability of the loaded CNTs in the detection and quantification of MMP-14 in a standard PBS solution, without interference of other biomolecules. Further analysis in biologic samples as such as tissue, serum and cells should be evaluated.

**Table 4.1** - Abnormal expression of MMP-14 for different types of cancer and body samples

Type of Cancer	Sample	MMP-14 Level	MMP-14 Level	Ref.
		(Healthy)	(Non-Healthy)	
<b>Breast</b>	Serum	$8.55 \pm 1.66 \text{ ng.ml}^{-1}$	$16.91 \pm 5.87 \text{ ng.ml}^{-1}$	[25,26]
	Cell	-	$\sim 26.7 \text{ ng.mg}^{-1*}$	
<b>Head &amp; Neck</b>	Tissue	$0.80 \pm 1.1 \text{ ng.ml}^{-1}$	$5.00 \pm 4.3 \text{ ng.mg}^{-1}$	[26]
	Cell	-	$\sim 14.5 \text{ ng.mg}^{-1*}$	
<b>Fibrosarcoma</b>	Tissue	$<0.01 \text{ ng.mg}^{-1*}$	$\sim 1.12 \text{ ng.mg}^{-1*}$	[26,27]
	Cell	-	$\sim 36.1 \text{ ng.mg}^{-1*}$	
<b>Prostate</b>	Tissue	$<0.01 \text{ ng.mg}^{-1*}$	$0.6 \pm 0.05 \text{ ng.mg}^{-1}$	[27]
<b>Gastric</b>	Tissue	$\sim 1.34 \text{ ng.mg}^{-1*}$	$\sim 3.57 \text{ ng.mg}^{-1*}$	[28]
<b>Bladder</b>	Tissue	$7.45 \pm 1.18 \text{ ng.mg}^{-1}$	$81.78 \pm 9.87 \text{ ng.mg}^{-1}$	[29]
<b>Ovarian</b>	Serum	$\sim 6 \text{ ng.ml}^{-1*}$	$\sim 12 \text{ ng.ml}^{-1*}$	[30]
<b>Brain</b>	Tissue	$\sim 1 \text{ ng.mg}^{-1*}$	$\sim 10 \text{ ng.mg}^{-1*}$	[31]

“-”: data not provided; “\*” Study did not provide the SD value.

Existing MMP inhibitors target the hidden active center in the catalytic domain and, as a result, impacts activity of many MMPs instead of MMP-14 alone [33]. The interest in detecting the PEX domain is not only because PEX domain is easily accessible but also for selectivity purpose. Indeed, the inhibitory molecule selected for this study has demonstrated specificity for MMP-14 PEX domain, not affecting the catalytic or other MMP PEX domains [33,40]. The small inhibitor interacts at the surface of proteins in a specific region named binding pocket, where small-molecules bind easily with little energetic cost [70]. The conformation changes associated with

inhibitor-protein binding is specific to every single protein. Few proteins present null (pre-formed pocket) to minor structural changes to reveal the binding pocket, easily allowing the interface with small inhibitors; while others exhibit extensive structural rearrangement in order to establish interactions with the inhibitors through the binding pocket <sup>[70]</sup>. In this work, we supposed that the exclusivity of inhibitor/protein interaction might be due to that the small molecule NSC-405020 is in the particular binding pocket of MMP-14, shaped by Met-328, Arg-330, Asp-376, Met-422, and Ser-470 <sup>[33]</sup> (**Figure 4.4A**). By taking advantage of the inhibitory molecule/protein binding interaction in the PEX domain of MMP-14, a layer of protein was accumulated around CNTs, hampering the electron transfer between the electrode surface and the analyte (**Figure 4.4B**). As a result, the resistance of the system increased linearly as a function of the protein concentration (**Figure 4.3B**).

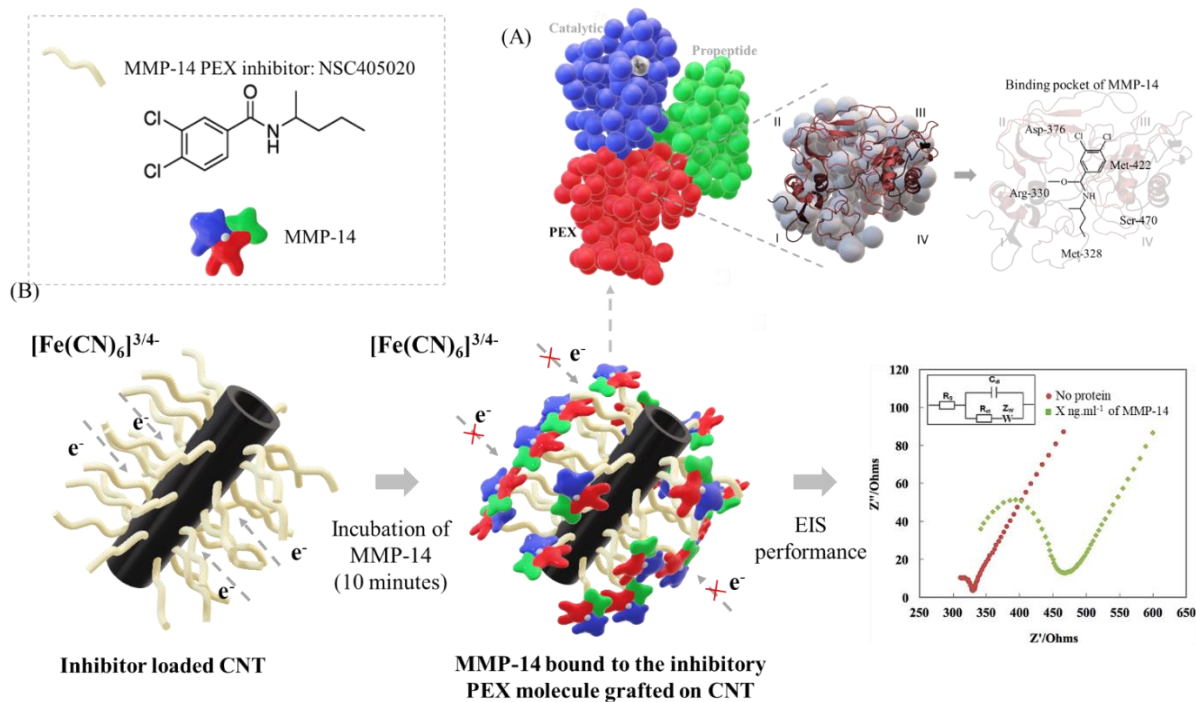


**Figure 4.4** - (A) The inhibitor/protein interaction between small molecule NSC-405020 and the binding pocket of MMP-14 and (B) Schematic of the MMP-14 detection through the binding mechanism of protein and inhibitory small molecule as the recognition element.

The specificity of the system was further confirmed in presence of MMP-1, another PEX domain based MMP which presents abnormal expression in different types of cancer [71,72]. The EIS response obtained in the presence of 50 ng.ml<sup>-1</sup> of protein is shown in **Figure 4.5**. Clearly, no noticeable change was observed, demonstrating the specificity of the selected molecule as the recognition element to interact to the binding pocket of MMP-14. Note that the performance of acylated CNTs without the molecule attached was also verified and no obvious resistance was observed (**Supplementary information S4.4**). The inhibitor loaded CNTs system demonstrated selectivity, microenvironmental stability (room temperature and PBS) and low cost when compared to the conventional biosensors.

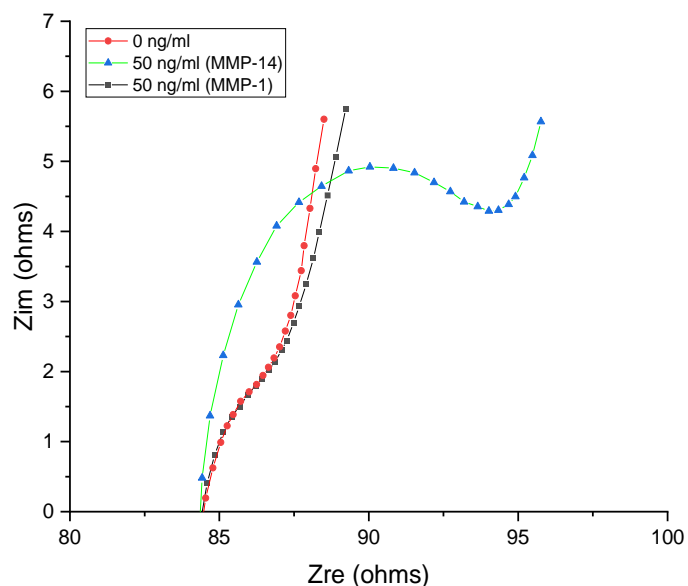


**Figure 4.5** - EIS response for the inhibitor loaded CNT after individual interaction with 50 ng.ml<sup>-1</sup> of MMP-1 and MMP-14 in PBS (pH 7.40) containing 10 mmol.ml<sup>-1</sup> of K<sub>4</sub>[Fe (CN)<sub>6</sub>]<sup>-</sup> 10 mmol.ml<sup>-1</sup> of K<sub>3</sub>[Fe (CN)<sub>6</sub>]<sup>-</sup> and 10 mmol.ml<sup>-1</sup> of NaCl. The inhibitor loaded CNT showed specificity to MMP-14 (applied potential of +0.20 V, from 50 kHz to 500 Hz, amplitude 50 mV).

#### 4. Conclusions

In this work, we focused on the detection of MMP-14 protein by targeting the PEX domain instead of the conventional catalytic domain. MMP-14 is overexpressed in a variety of diseases, including cancer. By taking advantage of the specificity and binding properties of an inhibitory small organic molecule, NSC-402050, an inhibitor loaded CNT system was designed. Pristine CNTs were modified by 3 steps: oxidation, addition of acyl groups and, molecule attachment. The successful grafting was well established by FT-IR, CV, and SEM analysis. The inhibitor loaded CNTs system performance was verified in MMP-14 (PBS, pH 7.4) and demonstrated LOD of 7.5 ng.ml<sup>-1</sup>. The

specificity was also demonstrated against MMP-1, a MMP type protein that contains PEX domain and is present in abnormal levels in different types of cancer. From our knowledge, this is the first time that an inhibitory small molecule was applied as the recognition element, overcoming the challenges offered by the regular bioelements, such as enzymes, peptides, aptamers, and antibodies. The inhibitor loaded CNT is a desirable candidate to become an alternative method to the complex and expensive diagnostic tools currently available for the detection of MMP-14. Further studies should be performed to conclude the interference with different biomolecules in a real clinical environment (body fluids, tissues, cells, etc.).

**Supplementary information:** Detecting the PEX Like Domain of Matrix Metalloproteinase-14 (MMP-14) with Therapeutic Conjugated CNTs

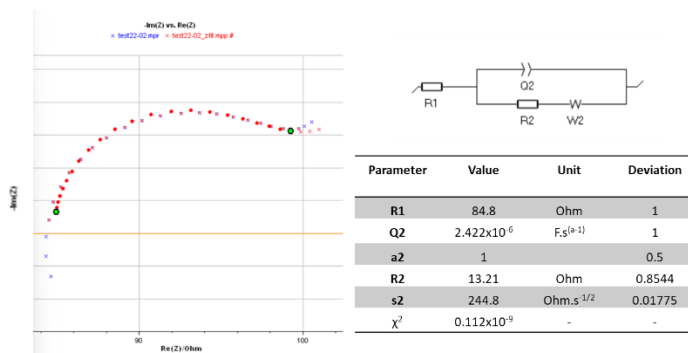


**Figure S 4.1** - Circuit fit for inhibitor loaded CNT electrode after interaction with  $50 \text{ ng.ml}^{-1}$  of MMP-14 in PBS (pH 7.40) containing  $10 \text{ mmol.ml}^{-1}$  of  $K_4[Fe(CN)_6]^-$ ,  $10 \text{ mmol.ml}^{-1}$  of  $K_3[Fe(CN)_6]^-$  and  $10 \text{ mmol.ml}^{-1}$  of NaCl, applied potential of +0.20V, from 50kHz to 500Hz, amplitude 50 mV.

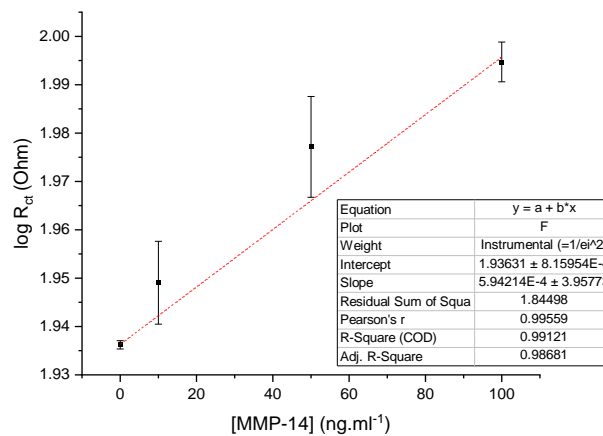


**Figure S 4.2** - Linear fit of log Rct response for different concentrations of MMP-14. Protein concentration varying from  $10 \text{ ng.ml}^{-1}$  to  $100 \text{ ng.ml}^{-1}$ , applied potential of +0.20V, from 50kHz to 500Hz, amplitude 50 mV.

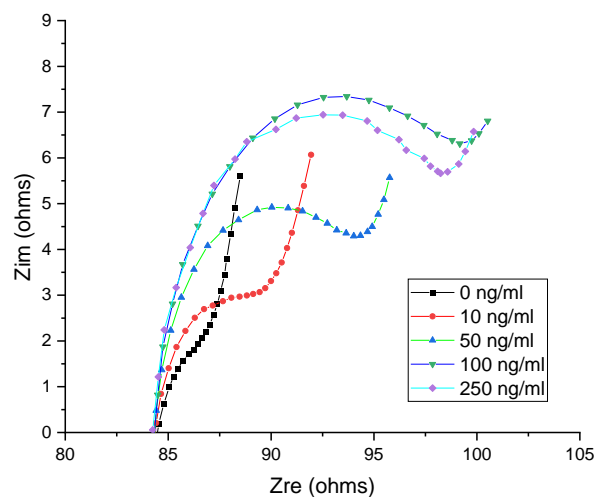


**Figure S 4.3** - EIS response of inhibitor loaded CNT after interaction with MMP-14, varying concentration from 0 to 250 ng.ml<sup>-1</sup>, in PBS (pH 7.40) containing 10 mmol.ml<sup>-1</sup> of K<sub>4</sub>[Fe (CN)<sub>6</sub>]<sup>-</sup>, 10 mmol.ml<sup>-1</sup> of K<sub>3</sub>[Fe (CN)<sub>6</sub>]<sup>-</sup> and 10 mmol.ml<sup>-1</sup> of NaCl (applied potential of +0.20V, from 50kHz to 500Hz, amplitude 50 mV).

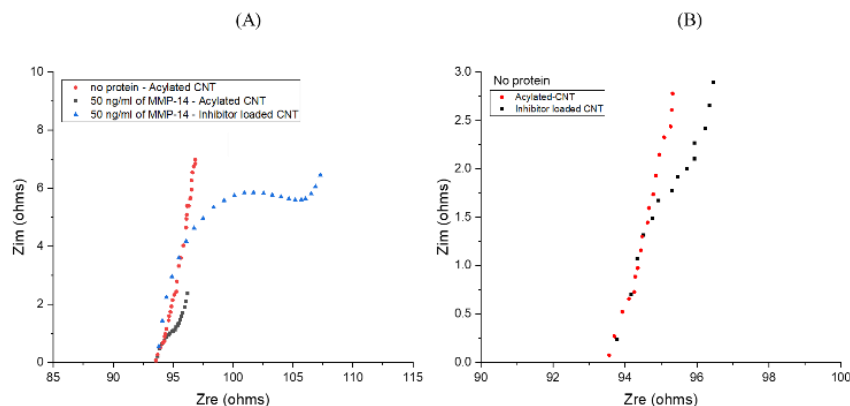


**Figure S 4.4** - (A) EIS response of acylated CNT after interaction with 50 ng.ml<sup>-1</sup> of MMP-14 and (B) EIS response in absence of protein for acylated and inhibitor loaded CNT in PBS (pH 7.40) containing 10 mmol.ml<sup>-1</sup> of K<sub>4</sub>[Fe (CN)<sub>6</sub>]<sup>-</sup>, 10 mmol.ml<sup>-1</sup> of NaCl, applied potential of +0.20V, from 50kHz to 500Hz, amplitude 50 mV.

## References

- [1] S. Mondal, N. Adhikari, S. Banerjee, S. A. Amin, T. Jha, *European journal of medicinal chemistry* **2020**, *194*, 112260.
- [2] M. Egeblad, Z. Werb, *Nature reviews cancer* **2002**, *2*, 161.
- [3] K. J. Isaacson, M. M. Jensen, N. B. Subrahmanyam, H. Ghandehari, *Journal of Controlled Release* **2017**, *259*, 62.
- [4] A. Jabłońska-Trypuć, M. Matejczyk, S. Rosochacki, *Journal of enzyme inhibition and medicinal chemistry* **2016**, *31*, 177.
- [5] R. Visse, H. Nagase, *Circulation research* **2003**, *92*, 827.
- [6] W. Bode, C. Fernandez-Catalan, H. Tschesche, F. Grams, H. Nagase, K. Maskos, *Cellular and Molecular Life Sciences CMLS* **1999**, *55*, 639.
- [7] F. Ren, R. Tang, X. Zhang, W. M. Madushi, D. Luo, Y. Dang, Z. Li, K. Wei, G. Chen, *PloS one* **2015**, *10*, e0135544.
- [8] S. Quintero-Fabián, R. Arreola, E. Becerril-Villanueva, J. C. Torres-Romero, V. Arana-Argáez, J. Lara-Riegos, M. A. Ramírez-Camacho, M. E. Alvarez-Sánchez, *Frontiers in oncology* **2019**, *9*, 1370.
- [9] M. Pytliak, V. Vargova, V. Mechirova, *Oncology Research and Treatment* **2012**, *35*, 49.
- [10] M. F. Ocaña, H. Neubert, *Analytical biochemistry* **2010**, *399*, 202.
- [11] R. Freije, T. Klein, B. Ooms, H. F. Kauffman, R. Bischoff, *Journal of Chromatography A* **2008**, *1189*, 417.
- [12] M. Golizeh, J. Abusarah, M. Benderdour, L. Sleno, *Chemical research in toxicology* **2014**, *27*, 1556.
- [13] Y. Wang, P. Shen, C. Li, Y. Wang, Z. Liu, *Analytical chemistry* **2012**, *84*, 1466.
- [14] H. Yao, Y. Zhang, F. Xiao, Z. Xia, J. Rao, *Angewandte Chemie* **2007**, *119*, 4424.
- [15] G. Xi, X. Wang, T. Chen, *International journal of nanomedicine* **2016**, *11*, 1537.
- [16] A. Tokarzewicz, L. Romanowicz, I. Sveklo, E. Gorodkiewicz, *Analytical Methods* **2016**, *8*, 6428.
- [17] A. Shoji, M. Kabeya, M. Sugawara, *Analytical biochemistry* **2011**, *419*, 53.
- [18] D. J. Leeming, Y. He, S. S. Veidal, Q. H. T. Nguyen, D. V. Larsen, M. Koizumi, T. Segovia-Silvestre, C. Zhang, Q. Zheng, S. Sun, *Biomarkers* **2011**, *16*, 616.

- [19] N. Barascuk, S. S. Veidal, L. Larsen, D. V. Larsen, M. R. Larsen, J. Wang, Q. Zheng, R. Xing, Y. Cao, L. M. Rasmussen, *Clinical biochemistry* **2010**, *43*, 899.
- [20] H. S. Magar, R. Y. Hassan, A. Mulchandani, *Sensors* **2021**, *21*, 6578.
- [21] V. Vanova, K. Mitrevska, V. Milosavljevic, D. Hynek, L. Richtera, V. Adam, *Biosensors and Bioelectronics* **2021**, *180*, 113087.
- [22] M. Negahdary, L. Angnes, *Microchimica Acta* **2022**, *189*, 1.
- [23] M. Labib, E. H. Sargent, S. O. Kelley, *Chemical reviews* **2016**, *116*, 9001.
- [24] S. N. Topkaya, M. Azimzadeh, M. Ozsoz, *Electroanalysis* **2016**, *28*, 1402.
- [25] P. Laudański, J. Swiatecka, L. Kozłowski, M. Leśniewska, M. Wojtukiewicz, S. Wołczyński, *Folia histochemica et cytobiologica* **2010**, *48*, 101.
- [26] T. Aoki, K. Yonezawa, E. Ohuchi, N. Fujimoto, K. Iwata, T. Shimada, T. Shiomi, Y. Okada, M. Seiki, *Journal of Immunoassay and Immunochemistry* **2002**, *23*, 49.
- [27] J. M. Atkinson, C. J. Pennington, S. W. Martin, V. A. Anikin, A. J. Mearns, P. M. Loadman, D. R. Edwards, J. H. Gill, *European journal of cancer* **2007**, *43*, 1764.
- [28] S. Ogawa, H. Kubo, Y. Murayama, T. Kubota, M. Yubakami, T. Matsumoto, T. Ohashi, K. Okamoto, Y. Kuriki, K. Hanaoka, *Photodiagnosis and Photodynamic Therapy* **2021**, *35*, 102420.
- [29] J. Kudelski, G. Młynarczyk, B. Darewicz, M. Bruczko-Goralewska, L. Romanowicz, *Medicine* **2020**, *99*.
- [30] R. Kaimal, R. Aljumaily, S. L. Tressel, R. V. Pradhan, L. Covic, A. Kuliopulos, C. Zarwan, Y. B. Kim, S. Sharifi, A. Agarwal, *Cancer research* **2013**, *73*, 2457.
- [31] Y. Ren, H. Hyakusoku, J. E. Sagers, L. D. Landegger, D. B. Welling, K. M. Stankovic, *Frontiers in cellular neuroscience* **2020**, 191.
- [32] M. Pacios, I. Martín-Fernández, R. Villa, P. Godignon, M. Del Valle, J. Bartrolí, M. J. Esplandiú, in *Carbon Nanotubes-Growth and Applications*, IntechOpen, **2011**.
- [33] A. G. Remacle, V. S. Golubkov, S. A. Shiryayev, R. Dahl, J. L. Stebbins, A. V. Chernov, A. V. Cheltsov, M. Pellicchia, A. Y. Strongin, *Cancer research* **2012**, *72*, 2339.
- [34] H. Piccard, P. E. Van den Steen, G. Opendakker, *Journal of leukocyte biology* **2007**, *81*, 870.
- [35] H. Laronha, J. Caldeira, *Cells* **2020**, *9*, 1076.
- [36] F. Ma, J. Yan, L. Sun, Y. Chen, *Talanta* **2019**, *205*, 120142.
- [37] F. Ma, Y. Zhu, Y. Chen, J. Liu, X. Zeng, *Talanta* **2019**, *194*, 548.

- [38] Y. Wang, H. Xu, J. Zhang, G. Li, *Sensors* **2008**, 8, 2043.
- [39] S. A. Piletsky, A. P. Turner, *Electroanalysis: An International Journal Devoted to Fundamental and Practical Aspects of Electroanalysis* **2002**, 14, 317.
- [40] “MT1-MMP Inhibitor, NSC405020 - Calbiochem | 444295,” can be found under [https://www.emdmillipore.com/CA/en/product/MT1-MMP-Inhibitor-NSC405020-Calbiochem,EMD\\_BIO-444295](https://www.emdmillipore.com/CA/en/product/MT1-MMP-Inhibitor-NSC405020-Calbiochem,EMD_BIO-444295), **n.d.**
- [41] B. Marinho, M. Ghislandi, E. Tkalya, C. E. Koning, G. de With, *Powder technology* **2012**, 221, 351.
- [42] X.-H. Zhang, Q.-Q. Tang, D. Yang, W.-M. Hua, Y.-H. Yue, B.-D. Wang, X.-H. Zhang, J.-H. Hu, *Materials Chemistry and Physics* **2011**, 126, 310.
- [43] Z. Zhu, *Nano-micro letters* **2017**, 9, 1.
- [44] C. Gao, Z. Guo, J.-H. Liu, X.-J. Huang, *Nanoscale* **2012**, 4, 1948.
- [45] A. G. Osorio, I. C. L. Silveira, V. L. Bueno, C. P. Bergmann, *Applied Surface Science* **2008**, 255, 2485.
- [46] X. H. Men, Z. Z. Zhang, H. J. Song, K. Wang, W. Jiang, *Composites Science and technology* **2008**, 68, 1042.
- [47] A. Khazaei, M. N. S. Rad, M. K. Borazjani, *International journal of nanomedicine* **2010**, 5, 639.
- [48] S. Tonello, F. Stradolini, G. Abate, D. Uberti, M. Serpelloni, S. Carrara, E. Sardini, *Scientific reports* **2019**, 9, 1.
- [49] T. Pasinszki, M. Krebsz, T. T. Tung, D. Losic, *Sensors* **2017**, 17, 1919.
- [50] X. Luo, J. J. Davis, *Chemical Society Reviews* **2013**, 42, 5944.
- [51] C. Klumpp, K. Kostarelos, M. Prato, A. Bianco, *Biochimica et Biophysica Acta (BBA)-Biomembranes* **2006**, 1758, 404.
- [52] V. Țucureanu, A. Matei, A. M. Avram, *Critical reviews in analytical chemistry* **2016**, 46, 502.
- [53] K. Balasubramanian, M. Burghard, *small* **2005**, 1, 180.
- [54] C. Gao, Y. Z. Jin, H. Kong, R. L. Whitby, S. F. Acquah, G. Y. Chen, H. Qian, A. Hartschuh, S. R. P. Silva, S. Henley, *The Journal of Physical Chemistry B* **2005**, 109, 11925.
- [55] M. Baibarac, I. Baltog, C. Godon, S. Lefrant, O. Chauvet, *Carbon* **2004**, 42, 3143.
- [56] J. Beauchamp, **2004**.

- [57] Y. Guo, Y. Li, J. Wang, T. Zhu, M. Ye, *Chemical Engineering Journal* **2014**, 236, 506.
- [58] Y. Liu, W. Wu, Y. Guan, P. Ying, C. Li, *Langmuir* **2002**, 18, 6229.
- [59] Z. Pei, L. Li, L. Sun, S. Zhang, X. Shan, S. Yang, B. Wen, *Carbon* **2013**, 51, 156.
- [60] S. Albert, K. Keppler, P. Lerch, M. Quack, A. Wokaun, *Journal of Molecular Spectroscopy* **2015**, 315, 92.
- [61] L.-F. Liao, C.-F. Lien, D.-L. Shieh, F.-C. Chen, J.-L. Lin, *Physical Chemistry Chemical Physics* **2002**, 4, 4584.
- [62] H. Wang, Z. Ma, H. Han, *Bioelectrochemistry* **2019**, 130, 107324.
- [63] W. Cheng, J. Ma, D. Kong, Z. Zhang, A. Khan, C. Yi, K. Hu, Y. Yi, J. Li, *Sensors and Actuators B: Chemical* **2021**, 330, 129379.
- [64] B. S. Munge, J. Fisher, L. N. Millord, C. E. Krause, R. S. Dowd, J. F. Rusling, *Analyst* **2010**, 135, 1345.
- [65] S. Menon, M. R. Mathew, S. Sam, K. Keerthi, K. G. Kumar, *Journal of Electroanalytical Chemistry* **2020**, 878, 114596.
- [66] Q. Palomar, X. Xu, R. Selegård, D. Aili, Z. Zhang, *Sensors and Actuators B: Chemical* **2020**, 325, 128789.
- [67] P. Yaiwong, N. Semakul, S. Bamrungsap, J. Jakmunee, K. Ounnunkad, *Bioelectrochemistry* **2021**, 142, 107944.
- [68] X. Liu, L.-Y. Lin, F.-Y. Tseng, Y.-C. Tan, J. Li, L. Feng, L. Song, C.-F. Lai, X. Li, J.-H. He, *Analyst* **2021**, 146, 4066.
- [69] D. G. Nohle, R. L. Mandt, M. E. Couce, A. V. Parwani, L. W. Ayers, *Biopreservation and Biobanking* **2018**, 16, 463.
- [70] D. K. Johnson, J. Karanicolas, *PLoS computational biology* **2013**, 9, e1002951.
- [71] C. E. Brinckerhoff, J. L. Rutter, U. Benbow, *Clinical Cancer Research* **2000**, 6, 4823.
- [72] R. Bendardaf, A. Buhmeida, R. Ristamäki, K. Syrjänen, S. Pyrhönen, *Scandinavian journal of gastroenterology* **2007**, 42, 1473.

## Conclusions and Future Perspective

This work explored the use of inorganic and organic molecules as recognition elements on the detection of zinc-related biomarkers, including mobile zinc and zinc-containing proteins (carbonic anhydrase and metalloproteinase-14). The relevance of these biomarkers on cancer development and progression was discussed along the previous chapters. Traditionally, bioelements, such as enzymes, peptides, nuclei acids and aptamers, have been widely applied on the design of electrochemical sensors for biomarkers detection due to their high specificity towards the target species, as such as proteins. However, as previously mentioned, their poor stability, complex synthesis, and high cost, limit further application as a clinical tool.

In this work, carbon nanostructures were functionalized with simple molecules as alternatives to the established recognition bio elements, aiming for more stable and accessible sensors. Non-surprisingly, carbon nanostructures showed their versatility, simplicity, and widely applicability as substrates for electrochemical systems. Functionalization of carbon nanostructures is usually performed via two strategies, non-covalent and covalent binding, through different techniques like adsorption of molecules by van der Waals force,  $\pi$ - $\pi$  interactions, hydrogen bonds, oxidation, end/defect, and side wall covalent functionalization. Among infinite possibilities of anchoring molecules onto carbon surface, we selected in our work to: i) functionalize sulfonated groups on carbon nanoparticles by a low-temperature procedure; and ii) covalent bind fasten molecules onto CNTs surface.

In the chapter 3, we discussed the low-temperature functionalization with auxiliary diazonium salts as alternative to the typical strong acids, which is less destructive to generate sulfonated groups, assuring a better surface and homogeneity of sulfonates ( $\text{SO}^{-3}$ ) groups in the final material. While

the covalent binding between CNTs and the molecules, employed in both chapter 2 and 4, enabled a strong interfacial interaction on CNTs and a better dispersion, facilitating the flow of electrons and enhancing the interface between the target specie and the electrode surface.

Non biological recognition elements were selected aiming the optimized interaction with the target species. For the mobile zinc, zincon was selected because of its selectivity towards zinc ions at specific pH range. In chapter 2, we clearly demonstrated its ability towards the detection of mobile zinc, even when other bio metallic elements are present (Ca, Cu, Co, Mg, Mn, and Fe). The well-defined peaks in SWV represented a linear current response as function of the concentration of the target zinc. Additionally, we tested the system with different zinc-containing proteins; but no current responses were recorded probably due to the lack of accessibility to the zinc center in the protein shell. The system was well evaluated in artificial urine and saliva. Zincon-CNTs showed as a good candidate for the detection of mobile zinc in a variety of cancerous samples, as it showed range of detection within the values described in the literature.

In chapter 3, we engineered a sulfonated-carbon bismuth nanoparticle system to detect carbonic anhydrase (CA), a zinc containing protein. Bismuth is a well known metal to form spontaneously “amalgam” with zinc, but without the high toxicity of the conventional metallic mercury. Bismuth has been widely applied in the electrochemical detection of mobile zinc; however, to date, there were not studies in the literature showing its ability to detect zinc-containing proteins (probably due to the isolated protein structure discussed several times in the previous chapters). Usually, the distance between the external and the redox center of a protein in the catalytic domain is  $\sim 20$  Å. We hypothesized that using nanostructure would bridge the gap between electrode surface and zinc center, thus facilitating the transfer of the electron. The sulfonated-carbon nanoparticle structure permitted a longer arm when compared to only carbon nanoparticles (as demonstrated in Figure

S3.8). In addition, we showed that the sulfonated structure allowed the electrodeposition of very small bismuth nanoparticles, ~2nm, which provided more active sites to enhance the electron transfer with the zinc core within the protein shell. A key element in this system was the sulfonated ( $\text{SO}^{-3}$ ) group, which complexed the carbonic anhydrase and so presented an inhibitory effect on the protein. In chapter 3, a comprehensive discussion described the findings. Indeed, we observed that the unique specificity of sulfonated-CN-bismuth system towards the electrochemical detection of carbonic anhydrase was possible because of the combined effects of i) the complex formation between  $\text{SO}^{-3}$  and CA, causing a decrease of the current response in function of CA concentration; ii) the higher affinity of zinc towards Bi; and iii) the length of linker of S-CN-Bi nanostructure that allow a better electron tunneling from CA to the electrode surface. The electrode was tested against MMP-1, a zinc-containing protein, and no signal was measured, demonstrating its specificity.

In chapter 4, a small chemical molecule NSC-405020 (3,4-Dichloro-N-(pentan-2-yl) benzamide), well known as a drug to inhibit matrix metalloproteinase-14 (MMP-14) was applied. NSC-405020 is a specific noncatalytic inhibitor of MMP-14, that directly interacts with its PEX domain, affecting protein homodimerization but not the catalytic activity. To date, this is the second work in the literature using PEX as the target domain to electrochemically detect MMP. The pioneer work studied the detection through peptides which provided specificity and sensitivity, but also all the limitations that recognition bioelement possesses. In chapter 4, the therapeutic conjugated CNTs showed great ability on the detection of MMP-14 using EIS with an incremental increase of resistance with increasing protein concentration. This result confirmed that the immobilized inhibitor can interact at the surface of proteins in a specific and unique region named binding pocket, where the small molecules bound easily with little energetic effort. Due to the exclusive binding pocket of MMP-14, designed by Met-328, Arg-330, Asp-376, Met-422, and Ser-470, the

system only showed capability of detection for MMP-14 and not for MMP-1, another PEX-based MMP which presents abnormal expression in different types of cancer.

The discoveries presented in chapters 2,3 and 4 confirmed the possibility of developing electrochemical sensors based on the grafted of simple molecules onto carbon surfaces, where the stability, cost, shelf-life, accessibility, and storage capability are significantly improved. The selected target species, mobile zinc, carbonic anhydrase, and MMP-14 are all of great interest in the field of oncology. Although more development using non biological strategies have been done in the direction of mobile zinc detection; there are still a considerable lack when applying these strategies in biofluids, where most of the studies focused on the environmental samples. In chapter 2, we could demonstrate the efficacy of zincon-CNT system in two artificial biofluids, urine and saliva; however, further studies should be performed in blinding manner with clinical samples from healthy and unhealthy patients.

This scenario is different when analysing electrochemical sensor for the detection of proteins, where the majority of them have been developed only applying bio elements, especially antibody and aptamers. Chapters 3 and 4 significantly contributed to understand the interaction of simple molecules with zinc-proteins; and how these interfaces could be translated to an electrical signal. The inhibitory effect of non bioelements when complexing and/or interacting with the selected proteins (carbonic anhydrase and MMP-14) showed linear current responses and demonstrated as an alternative approach of developing biosensing systems towards proteins.

Although the designed sensors showed great ability as diagnostic tools, further studies must be accomplished for the fully understanding of their applicability. Few suggestions include:

- Tests in real samples from unhealthy patients (urine, saliva, plasma, cells) and comparison with ELISA and mass spectrometry techniques in order to study the standard deviation between the methods.
- The miniaturization of the sensors, aiming for a disposable point-of-care (POC) device, providing instantaneous results, and supporting the treatment guidance.
- The design of a unique device where zinc, CA and MMP-14 could be simultaneously measured.

Despite the mentioned suggestions to effectively transfer the research finds into clinical scenario, we strongly believe that this work opened new avenues to the current literature. We successfully demonstrated the great ability of simple molecules as alternative choices to the bioelements on the detection and monitoring of relevant zinc-containing cancerous biomarkers. All the designed electrochemical systems demonstrated as simple, cost effective and assertive ways to support early detection of cancer, understand its development and stage, and in the future, assisting in the treatment guidance.